June 2019

Iron-Virus Interactions: Development and Testing of the Ferrojan Horse Hypothesis

Chelsea Bonnain
University of South Florida, cbonnain@mail.usf.edu

Iron-Virus Interactions: Development and Testing of the Ferrojan Horse Hypothesis

by

Chelsea Bonnain

A thesis submitted in partial fulfillment
of the requirements for the degree of
Master of Science
Department of Marine Science
College of Marine Science
University of South Florida

Co-Major Professor: Mya Breitbart, Ph.D.
Co-Major Professor: Kristen Buck, Ph.D.
Karyna Rosario, Ph.D.

Date of Approval:
June 28th, 2019

Keywords: Marine, bacteriophage, phage, ligand, colloidal, bacteria

DEDICATION

This thesis is dedicated to Connie Bonnain for her love and encouragement to follow my dreams. Even though she would say what I worked on was over her head, she would be so proud of this accomplishment. She was my constant cheerleader and I miss her dearly. I love you Nana!

ACKNOWLEDGEMENTS

I would like to thank my advisors Mya Breitbart and Kristen Buck for helping me navigate through this process and sharing their respective disciplines. I would also like to thank Karyna Rosario for her constant support and advice. Special thanks are due to Salvatore Caprara for his patience and guidance through the development of methods, Natalie Sawaya for her assistance with not only statistics but any question brought to her, and Makenzie Burrows for her management and assistance. I would like to extend a huge thank you to the Breitbart and Buck lab members past and present for their support and friendship. Without all of you none of this would have been possible. I would like to thank my husband for his patience and encouragement, and my family for always believing in me.

Thank you to Linton and Pauline Tibbetts, Mary & Russell Brandes, Senator & Mrs. Jeff Brandes & Mr. Dan Bowman for the Linton Tibbetts Fellowship. A special thank you to Mr. George Lorton for your support of my personal research goals. Thank you to the National Science Foundation for supporting this novel research with an EAGER grant. Further support for this project was provided by NSF grant OCE-1722761.

TABLE OF CONTENTS

LIST OF TABLES

LIST OF FIGURES

ABSTRACT

Iron is an essential micronutrient for phytoplankton metabolism that limits growth in many regions of the surface ocean. More than 99.9% of oceanic dissolved iron is organically complexed to an iron-binding ligand, many of which have yet to be characterized. This thesis puts forth the Ferrojan Horse Hypothesis, which predicts a role for marine phages in oceanic iron cycling. Based on evidence from non-marine model systems, the Ferrojan Horse Hypothesis suggests that some marine phages (short for bacteriophages, or viruses that infect bacteria) can use iron as a "Trojan Horse" to gain access to host siderophore-bound iron receptors for infection. After taking over the host bacterial cell, new phages are produced which potentially contain iron from host storages, thus decreasing the amount of dissolved iron available for remineralization upon lysis. *Escherichia coli* and its associated phages were used as a model system for method development to facilitate testing of aspects of the Ferrojan Horse Hypothesis. The stable isotope ^{57}Fe was used as a tracer to determine the quantity and source of iron to progeny phages. *E. coli* cells were grown in minimal media with ^{57}Fe as the sole iron source, infected with phage T4 or T5, and progeny phages were purified. After lysis, the ^{57}Fe content was quantified by inductively coupled plasma mass spectrometry (ICP-MS), and phage concentrations were quantified by nucleic acid staining and epifluorescence microscopy. The ^{57}Fe was significantly higher in purified T4 and T5 phage samples than in bacterial lysis controls, and samples contained 166-2,269 ^{57}Fe atoms per phage. Greater than 90% of the total ^{57}Fe in

each experiment pre-lysis was located within bacterial cells, as opposed to the external media, indicating the source of ^{57}Fe to progeny phages was likely from host storages. The methods developed in this study lay the groundwork for testing facets of the Ferrojan Horse Hypothesis in a marine phage-host system. If the principles demonstrated in this model phage-host system apply to marine phages as well, this research indicates a potentially significant role for viruses in oceanic iron cycling.

CHAPTER ONE:

INTRODUCTION

Iron in the Oceans

Iron is essential for all oceanic life forms. Iron readily changes oxidation state and mediates reactions with oxygen, making it an excellent redox mediator (Andrews, 1998). Multiple cellular functions involve iron, including nitrogen assimilation, photosynthesis, DNA synthesis, mitochondrial respiration, and reactive oxygen species scavenging (Hänsch and Mendel, 2009). Iron-sulfur proteins serve as regulator proteins, enzymes, and are essential for electron transfer (Lill, 2009).

Although a vital micronutrient for photosynthesis, iron limits phytoplankton growth in nearly 40% of open ocean surface waters (Martin et al., 1991; Liu and Millero, 2002; Morel and Price, 2003; Boyd et al., 2007). Nitrogen is commonly a limiting nutrient for oceanic primary productivity, but residual nitrate remains in large regions of the surface ocean where iron is the limiting nutrient. These areas are referred to as HNLC, or high nutrient, lower than expected chlorophyll regions due to the low bioavailability of iron for phytoplankton growth (Franck et al., 2003; Boyd et al., 2007). Iron bioavailability serves as a bottom-up control on primary productivity in the surface ocean, so a better understanding of iron chemistry is needed for improving understanding of the carbon cycle and ultimately global climate (Moore et al., 2001; Tagliabue et al., 2017).

Iron bioavailability for phytoplankton growth can be described by the ability to take up and metabolize different forms of iron from the environment (Morel et al., 2008; Shaked and Lis, 2012). Two of the main iron uptake mechanisms utilized by phytoplankton include the siderophore-bound iron pathway and the reductive pathway (Soria-Dengg et al., 2001; Shaked et al., 2005). Siderophores are small (<10 kD) iron-binding ligands secreted by autotrophic and heterotrophic bacteria to chelate Fe(III) from outside of the cell and bring it to the cell surface for uptake (Barbeau et al., 2003). The reductive pathway is also widely used, and it reduces the iron from an inorganic iron complex to transport the free iron into the cell (Atkinson and Guerinot, 2011; Shaked and Lis, 2012). Some aquatic cyanobacteria have also been shown to utilize the reductive pathway (Lis and Shaked, 2009; Kranzler et al., 2011).

The physicochemical properties of iron influence its accessibility to phytoplankton (Kuma et al., 1996). Inorganic iron (Fe') can be complexed to an iron-binding ligand or scavenged by bacteria, where it becomes part of the organic particulate (> 0.2 μm) iron pool (Jiang et al., 2013; Lin et al., 2018). The iron that passes through a 0.2 μm filter is considered dissolved and includes bioavailable forms of Fe(II) and Fe(III) (Lin et al., 2018). The dissolved fraction is separated further into a colloidal (0.02 μm-0.2 μm) and a soluble (<0.02 μm) fraction (Wu et al., 2001; Cullen et al., 2006; Bergquist et al., 2007; Fitzsimmons et al., 2015). Colloidal iron is not typically directly measured, but is calculated by taking the difference between the dissolved and the soluble fractions (Schlosser and Croot, 2008). In a recent study of surface waters in the Northern Atlantic Ocean, approximately 80% of the dissolved iron measured was colloidal in size (Fitzsimmons and Boyle, 2014).

More than 99.9% of dissolved iron is organically complexed (Gledhill and Van Den Berg, 1994; Rue and Bruland, 1995). Characterization of these organic iron-binding ligands aids

in forming a more complete picture of iron biogeochemical cycling (Hunter and Boyd, 2007; Gledhill and Buck, 2012). To date, siderophores are the most well characterized strong iron-binding ligands within the soluble fraction (Barbeau et al., 2003; Mawji et al., 2008; Bundy et al., 2014; Boiteau et al., 2016). Weaker iron-binding ligands within the colloidal fraction include humic substances, exopolysaccharides (EPS), and transparent exopolymers (TEP) (Mancuso Nichols et al., 2004; Laglera and van den Berg, 2009; Stolpe et al., 2010; Stolpe and Hassellov, 2010). However, the identities of most dissolved iron-binding ligands remain unknown. To date viruses, one of the most abundant biological entities collected in the colloidal size fraction, have yet to be considered for their potential contribution to dissolved organic iron pools.

Marine Viruses

Viruses are microscopic parasites that rely on a host to replicate. Nearly all living organisms from prokaryotes to plants, to insects and animals can be infected by one or more viruses. Viruses are the most abundant biological entities in the world, with an estimated 10^{30} viruses in the ocean alone (Suttle, 2005; Breitbart, 2012; Breitbart et al., 2018). A single milliliter of surface seawater contains ten million viruses on average (Bergh et al., 1989). A commonly used virus-to-bacteria ratio is 10, although measurements can vary over space and time (Wommack and Colwell, 2000; Parikka et al., 2017; Breitbart et al., 2018). A large proportion of these viruses are phages (short for bacteriophages), as their bacterial hosts comprise the second most abundant biological entities in the oceans (Wommack and Colwell, 2000).

Viruses have various morphologies, but commonly include a genome of nucleic acid (DNA or RNA) surrounded by a protein capsid structure (Luria and Anderson, 1942; Hershey and Chase, 1952). The vast majority of characterized phages have double-stranded (ds)DNA

genomes within an icosahedral capsid (Hendrix, 2002; Ackermann, 2007). Although recent studies have described abundant non-tailed viruses in the oceans (Brum et al., 2013; Kauffman et al., 2018b), most characterized dsDNA phages have tail proteins that are responsible for attachment and delivery of the phage genome into the host cell (Lindberg, 1973). Tailed phages within the family *Myoviridae* possess contractile tails, while phages within the family *Siphoviridae* have non-contractile tails, and members of the *Podoviridae* have short, stubby tails (Ackermann, 2009). In addition to a central tail tube, these phages have a varying number of thinner tail fibers that aid in attachment to the host cell. Once a phage adsorbs to a specific receptor on the bacterial host cell surface or punctures through the outer membrane, the release of the genome is initiated and the viral nucleic acid exits the capsid, travels through the central tail tube, and into the host bacterial cell cytoplasm (Rakhuba et al., 2010). In a lytic infection, the phage genome takes over host cellular mechanisms to produce new phage proteins and nucleic acid. The phage particles are assembled to produce the new phage progeny, and the host cell is lysed open to release the phage progeny into the environment to infect a new host.

Techniques used to enumerate viruses from the environment or in culture include transmission electron microscopy and nucleic acid staining (SYBR Gold or SYBR Green I) followed by epifluorescence microscopy or flow cytometry (Noble and Fuhrman, 1998; Wen et al., 2004; Brussaard, 2009; Breitbart et al., 2018). Transmission electron microscopy (TEM) was used to visualize the first phage structure, and many early counts of marine viruses were performed using TEM (Børsheim et al., 1990; Ackermann, 2012). Nucleic acid staining followed by epifluorescence microscopy or flow cytometry enables more efficient quantification of virus-like particles (VLPs); however, it can be difficult to detect small viruses above the background fluorescence and to differentiate small bacteria from large viruses (Noble and Fuhrman, 1998;

Dlusskaya et al., 2019). Double agar overlay plaque assay can also be used to quantify infectious phage by counting plaque-forming units (PFUs), but the method requires a phage to be in culture with a known host (Kropinski et al., 2009). This can be problematic for quantifying viruses from the marine environment, as many marine hosts are difficult to grow in culture (Staley and Konopka, 1985).

Influence of Marine Viruses on Iron Biogeochemistry

Various groups of marine bacteria perform roles essential for nutrient cycling and carbon export throughout the ocean. Autotrophic bacteria are primary producers that convert inorganic carbon (CO_2) into organic carbon via photosynthesis, in turn this organic carbon feeds into the marine food web and supports higher trophic levels. As particulate organic matter (POM, >0.2 µm size) is produced in the upper water column and sinks, some of it is broken down into dissolved organic matter (DOM, <0.2 µm size) which can be remineralized by heterotrophic bacteria, fueling the microbial loop (Azam et al., 1983). In iron-limited regions such as the subarctic Pacific, heterotrophic bacteria have been shown to account for half of the biogenic iron pool and are responsible for 20-45% of biological iron uptake (Tortell et al., 1996).

Grazing by protists and lysis by phages are the two main causes of bacterial mortality (Fuhrman, 1999). Grazing on bacteria and the subsequent packaging of organic matter into fecal pellets enhances the efficiency of carbon export via the biological pump by sinking POM out of the surface and into the deep ocean (Ducklow et al., 2001). Bacterial lysis by phage infection results in the release of dissolved organic matter (DOM, <0.2 µm in size) and nutrients for remineralization by heterotrophic bacteria (Wommack and Colwell, 2000). This process of recycling DOM from viral lysis of microbes within the microbial loop is referred to as the viral shunt (Wilhelm and Suttle, 1999; Wommack and Colwell, 2000; Brussaard, 2004). Conversely,

the viral shuttle has been suggested as a concept to describe the export of organic carbon into the deep ocean when viral lysis at the surface creates sticky lysates that aggregate and sink as POM (Weinbauer, 2004; Sullivan et al., 2017; Laber et al., 2018).

While many studies have examined the impact of viral lysis on nutrient cycling, few studies have examined the elemental contribution of viral particles to DOM. Although not truly dissolved, viruses are collected within the colloidal size fraction (0.02 μm – 0.2 μm). A theoretical analysis estimated that viral particles could account for 5% of the dissolved organic phosphorous pool and 7% of the dissolved organic nitrogen pool, depending on the system (Jover et al., 2014). To date however, no studies have investigated the influence of trace metal complexation to viral particles on marine metal cycles or the contribution of viral particles to dissolved trace metal pools. If viral particles contribute to nitrogen and phosphorus pools with concentrations measured in the micromolar range, then any viral contribution to trace element pools such as iron in the nanomolar range could be significant.

Thesis Overview

Given the abundance of marine viruses (10^7 VLP/mL), and the low concentrations of bioavailable iron in the oceans, this thesis aims to explore the potential roles of viruses in oceanic iron cycling. The Ferrojan Horse Hypothesis incorporates evidence from non-marine phage-host model systems to predict several ways in which viruses can affect oceanic iron cycling. Based on previous work showing that some phages contain iron in their structural proteins, we propose that if marine phages also contain iron, they would contribute substantially to the dissolved iron pool in the oceans (**Appendix A**). Prior research has also demonstrated that some *Escherichia coli* (*E. coli*) phages compete with siderophore-bound iron for cell surface receptors; we hypothesize that marine phages may use iron as a "Trojan Horse" mechanism to

gain access to host cell receptors that function for iron uptake. Finally, we propose that the iron present in phage structural proteins originates from host bacterial cell storages during phage replication, which reduces the amount of iron from cellular lysis products that is available for remineralization, with implications for models of global iron cycling.

Directly testing aspects of the Ferrojan Horse Hypothesis using a marine phage-host system presents several challenges. The presence of iron within the tail protein structures of phage has been shown for *E. coli* phage T4 using x-ray crystallography (Bartual et al., 2010), but the same structural evidence for protein structures of marine phages is not yet available. Additionally, *E. coli* phages were demonstrated to compete with siderophores for the bacterial host cell iron-siderophore receptor (Luckey et al., 1975), but the receptors remain unknown for most marine phage-host pairs (Silva et al., 2016; Breitbart et al., 2018). While some marine phages and their hosts have been cultured, the Great Plate Count Anomaly (Staley and Konopka, 1985) describes the difficulty in culturing many marine bacteria from the environment. Additionally, marine bacteria isolated from oligotrophic environments would be more sensitive to low concentrations of iron, making any iron contamination an added challenge.

Thus, prior to testing the Ferrojan Horse Hypothesis within a marine system, *E. coli* and two of its associated phages (T4 and T5) were used as a model system for the development of experimental methods. The goals of this study were to determine: *1.) How much iron is incorporated into progeny phages* and *2.) Whether the iron in progeny phages originates from within the bacterial host cell*. *E. coli* is a fast-growing, well-studied bacterial model system, and its associated phages are extremely well-characterized (Jessup et al., 2004; Calendar, 2012). *E. coli* cells were grown in a defined media with $^{57}FeSO_4$ as the sole iron source, then rinsed of excess ^{57}Fe. The cells were infected with one of the phages or lysed with chloroform, then the

phage fraction was purified using centrifugation, sucrose density-dependent ultracentrifugation, and dialysis. The purified phage fractions were analyzed for ^{57}Fe content using a mass spectrometer and the viral-like particles were quantified under epifluorescence microscopy to enable calculation of the number of iron atoms per phage. The methods established in this thesis can be applied to a marine phage-host system to test the Ferrojan Horse Hypothesis in the future.

CHAPTER TWO:

DETERMINING THE AMOUNT AND SOURCE OF IRON BOUND TO *E. COLI* PHAGES T4 & T5

Background

The Ferrojan Horse Hypothesis proposes marine viruses could contribute to the colloidal fraction of dissolved organic iron binding ligands. Additionally, the iron bound to phage tail fibers could outcompete siderophores for access to siderophore-bound iron receptors on the host cell. If iron is recycled from host storages into progeny phage, the amount of dissolved iron released following host lysis could be less than previously thought (**Appendix A**). In order to provide a proof-of-concept for aspects of the Ferrojan Horse Hypothesis, methods were developed using a well-studied phage-host laboratory model system.

This thesis used *E. coli* phages T4 and T5 for method development (**Figure 1**). Phage T4 is a member of the family *Myoviridae* and is a lytic double-stranded DNA (Group I) phage with a 169 kilobase (kb) genome (Baltimore, 1971). T4 has a 90 nm wide capsid and a 200 nm long central, contractile tail attached to a baseplate protein with six slender tail fibers (Leiman et al., 2003). Structural evidence exists for iron incorporation into phage T4 (Bartual et al., 2010) and it is one of the most well-studied phage in history (Kutter and Sulakvelidze, 2004). T4 adsorbs to the host OmpC receptor, which is a major outer membrane protein of *E. coli* used to transport a variety of small molecules into the cell (Osborn and Wu, 1980). Notably, in mammalian cells,

OmpC is able to transport lactoferrin, which is a bactericidal iron-binding glycoprotein found in secretory fluids as part of the innate immune system (Sallmann et al., 1999).

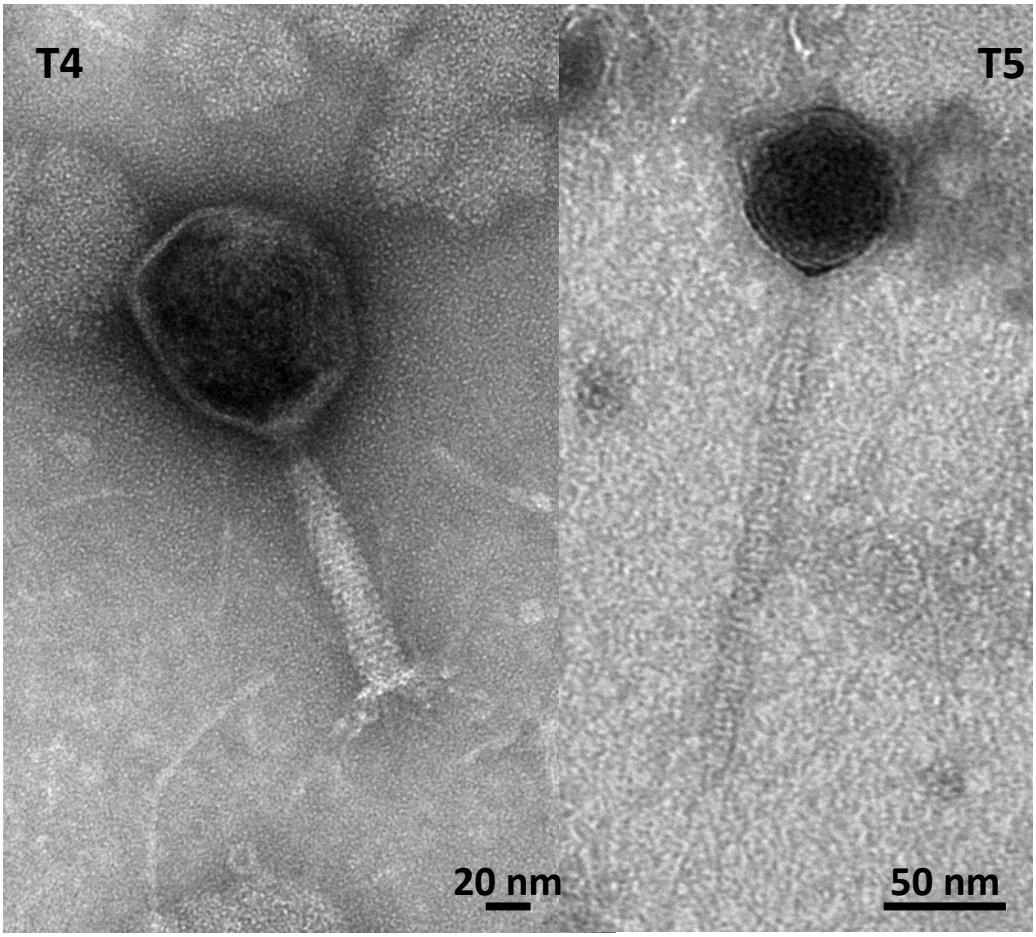

Figure 1: Transmission electron microscopy images of E. coli phages T4 and T5. Images by Anthony Greco.

E. coli phage T5 is a member of the family *Siphoviridae* and is a lytic double-stranded DNA (Group I) phage with a 122 kb genome (Baltimore, 1971). Phage T5 has a 90 nm capsid and a 250 nm long flexible, non-contractile tail and three L-shaped fibers surrounding a receptor binding tip (McCorquodale and Warner, 1988). T5 was shown to compete with the siderophore ferrichrome for access to a siderophore-bound iron uptake receptor FhuA in *E. coli* mutants (Hantke and Braun, 1978) but has not been shown to contain any structural iron.

Despite the lack of x-ray crystallography structural data of phage T5 tail fibers, protein sequences suggest this phage could also complex iron within its tail fiber proteins. In a study of the gpL tail tip protein of *E. coli* phage λ (also a member of the *Siphoviridae*), iron sulfur clusters were discovered to be bound by four highly conserved cysteine residues (Tam et al., 2013). The T5 pb3 tail protein (NCBI reference: YP_006966.1) was listed in Tam et al. (2013) as a gpL homologue and similarly contains four cysteines, however the study did not state the presence of iron in the pb3 tail protein.

Based on the direct structural evidence that the T4 tail fiber proteins contain iron and the detection of conserved iron-binding cysteine residues in T5, stable isotope tracing was used to determine the amount of iron incorporated into each of these phages and trace its origin back to cellular iron stocks. To accomplish this goal, *E. coli* cells were grown in minimal media with $^{57}FeSO_4$ as the predominant iron source, then rinsed in iron-free media to remove excess ^{57}Fe, before infection with either phage T4 or T5. A bacterial lysis control was included where bacterial cells were lysed using chloroform in place of phage infection. This control was necessary to account for any bacterial colloids that bound ^{57}Fe and co-purified with the phage fractions.

After multiple purification steps aimed to separate phage particles from cellular debris and other colloids, the purified phages were analyzed by mass spectrometry to quantify the ^{57}Fe in the purified phage particles. These results were then compared with epifluorescence microscopy counts to determine the number of phage particles in each sample, enabling calculation of the amount of ^{57}Fe bound to each phage. While the amount of iron incorporated into phage T4 can be extrapolated based on the iron binding proteins known in its tail fibers, there could be additional phage proteins that bind iron but are not yet known (Bartual et al.,

2010). We hypothesize that both phages T4 and T5 will have associated iron, but at potentially different abundances.

In addition, this experiment was designed to determine if the iron in phages originates from within its host, in this case the ^{57}Fe enriched *E. coli* cells. While it is known that phage T4 tail fiber proteins contain iron, the source of the iron (from within the host cell or from the outside environment) has not yet been determined. The process of phage replication inside of the host cytoplasm involves the production and assembly of phage proteins prior to lysis of the host. We thus hypothesize that the iron originates from within host storages and is incorporated into phage proteins during assembly and prior to lysis. Since the bacterial cells are highly enriched in ^{57}Fe compared to the unamended media, the presence of ^{57}Fe in the purified phage progeny would support the hypothesis that phage-bound iron originates from within the host's cellular reserves.

Methods

Media Development

Media Development Experiment I

The efficacy of using the stable isotope ^{57}Fe as a tracer of iron in these experiments is dependent on growing bacteria in media containing exclusively ^{57}Fe. Naturally occurring iron consists of 5.85% ^{54}Fe, 91.75% ^{56}Fe, 2.12% of ^{57}Fe and 0.29% ^{58}Fe (Dauphas and Rouxel, 2006). Excess iron contamination would make it difficult to reliably trace ^{57}Fe through a phage infection, as the *E. coli* cells may preferentially uptake other iron isotopes. Every effort was made to reduce iron contamination, including eliminating the use of materials that might introduce excess ^{56}Fe, such as glass flasks or metal scoopulas and sterilization methods such as

autoclaving. Instead, polycarbonate flasks were used for the experiments. All materials were cleaned by rinsing in reverse osmosis (RO) water, soaked in a soap bath for one week (1.5% Citrad in RO water, Decon Labs), rinsed in RO water, and soaked for 30 days in 10% trace metal grade (TMG) HCl (Fisher) in ultrapure water (Milli-Q, >18.2 MΩ cm). Materials were then rinsed with Milli-Q water, dried in an AirClean 400 laminar flow work station overnight, and double bagged in polyethylene bags until use to prevent contamination (Worsfold et al., 2014).

Several iterations of bacterial growth media were tested for both bacterial contaminant growth and iron contamination before the media for culturing was finalized. M9 minimal media for bacterial cultures was made according to Kutter and Sulakvelidze (2004). To prevent iron contamination, stock solutions of each component were made by pouring dry reagents directly into acid-cleaned Nalgene fluorinated high-density polyethylene (HDPE) bottles on a balance to weigh and Milli-Q water (18.2 MΩ cm) was added to desired concentration (**Table 1**). A 1 L volume of the media was then prepared by pouring stock solutions into an acid-cleaned HDPE bottle on a balance. The media contained final concentrations of 33.7 mM $Na_2HPO_4 \cdot 2H_2O$ (Sigma-Aldrich ≥99.0% Titration), 22 mM KH_2PO_4 (ACS Reagent ≥99% purity), 8.56 mM NaCl (Certified ACS ≥99.0% purity), 18.7 mM NH_4Cl (Fisher Scientific ≥99.0% purity FCC), 0.1 M $MgSO_4$ (Sigma-Aldrich ≥99.99% trace metal purity), 0.1 M $CaCl_2$ (Alfa Aesar from Fisher Scientific 99.99% metals basis purity), 1 µg/mL Thiamine HCl (Fisher Scientific 99% purity), and 0.5% Glucose (Fisher Scientific 99% purity) in a final volume of 1 L (Kutter and Sulakvelidze 2004, **Table 1**).

*Table 1: M9 minimal media composition from Kutter and Sulakvelidze (2004). A 1 L stock of 20X M9 Salts and 0.5 L of all stock solutions were weighed separately in acid-cleaned Nalgene fluorinated HDPE bottles and brought to desired concentrations using Milli-Q water (18.2 MΩ cm). A 1 L volume of liquid culture was prepared by adding all sterile stock solution components to 912.5 mL of Milli-Q water in an acid-cleaned HDPE bottle on a balance. *$FeSO_4$ added as $^{57}FeSO_4$ spike separately after all other components combined. Completed M9 minimal media was 0.02 µm filtered prior to use.*

Component	*20X M9 Salts (1 L)*	*Stock Concentration*	*Amount of Stock Added to 1 L Liquid*	*Final Concentration*
20X M9 Salts:				
$Na_2HPO_4 \cdot 2H_2O$	120 g	0.67 M		33.7 mM
KH_2PO_4	60 g	0.34 M		22 mM
NaCl	10 g	0.17 M		8.56 mM
NH_4Cl	20 g	0.37 M		18.7 mM
20X M9 Salts		20X	50 mL	1X
$MgSO_4$		0.1 M	10 mL	0.1 M
$CaCl_2$		0.1 M	1 mL	0.1 M
$FeSO_4$*		0.01 M	1 mL	10 µM
Thiamine HCl		2 mg/mL in 70% EtOH	500 µL	1 µg/mL
Glucose		20%	25 mL	0.5 %

Differences in the starting concentrations of ^{57}Fe between replicates were observed for the first attempts at making and sterilizing the M9 minimal media. It was hypothesized that this was due to the low solubility of iron forming precipitates at the neutral pH of the culture media. To optimize the media and gain consistency between the starting concentrations of the ^{57}Fe spike, an experiment was designed to monitor fluctuations in ^{57}Fe concentration pre- and post-incubation in the conditions used for *E. coli* growth.

M9 minimal media was amended with 10 µM $^{57}FeSO_4$ (95.06% enrichment, Isoflex) and triplicate samples of 100 mL volume were placed into acid-cleaned 250 mL polycarbonate Erlenmeyer flasks. Another triplicate set of 100 mL samples were 0.02 µm filtered using a Whatman Anotop syringe filter (GE Healthcare), after a pre-rinse with Milli-Q water (18.2 MΩ cm) and the first few drops of media discarded. To avoid metal contamination, the flasks were

individually placed upright into clean polyethylene bags left slightly open to vent, secured into flask clamps in an incubator, and left shaking (150 rpm) at 37 ˚C for 7 days.

Metal Analysis

Samples of 100 µL (by pipette with the first aspiration discarded to rinse the tip) were collected in acid-cleaned HDPE 7 mL scintillation vials (Fisher Scientific) pre-incubation (t=0) and at days 1, 3, and 7, placed in a rack, sealed within a clean polyethylene bag, and frozen at -20 ˚C until analysis.

To analyze the ^{57}Fe content of the samples, the 100 µL samples taken for metal analysis were thawed. A volume of 4.6 mL of Milli-Q (18.2 MΩ cm), water was added to each sample and the diluted sample was acidified with 250 µL HNO_3 (Fisher Scientific, Optima) for a final concentration of 5% nitric acid. A volume of 50 µL of rhodium (10 ppb final) was added as an internal standard. Six analysis blanks (4.7 mL Milli-Q water, no sample) were included, three for each of the calibration curves. External calibration curves of ^{56}Fe and ^{57}Fe contained the concentrations: 1.79 nM, 8.95 nM, 17.91 nM, 89.53 nM, 179.07 nM, and 358.13 nM. Samples were analyzed for ^{45}Sc, ^{56}Fe, ^{57}Fe, and ^{66}Zn on an Agilent 7500cx inductively coupled plasma mass spectrometer (ICP-MS).

The mass spectrometer data were corrected for the rhodium internal standard by dividing the metal counts per second of the sample by the rhodium counts per second. For ^{56}Fe and ^{57}Fe, the y-intercept of the ^{56}Fe or ^{57}Fe calibration curve was subtracted from the counts per second, divided by the slope of the calibration curve, and multiplied by the dilution factor (50). All results were reported in nanomolar (nM).

Media Development Experiment II

The second media experiment utilized chelexing in addition to 0.02 µm or 0.22 µm filtration to test the removal of ^{56}Fe contaminants from the media (Pai et al., 1988). The M9 minimal media was prepared (**Table 1**) in Milli-Q water (18.2 MΩ cm), and half was passed through a column of Chelex-100 (BioRad) resin (C; **Figure 2**), while the other half remained unchelexed (B; **Figure 2**). Half of each treatment was amended with 10 µM labeled $^{57}FeSO_4$ (2; **Figure 2**) while the other half remained un-amended (1; **Figure 2**). A volume of 25 mL of each sample was filtered through either a 0.22 µm Sterivex PVDF syringe filter (EMD Millipore) for the dissolved fraction (D; **Figure 2**), or a 0.02 µm Whatman Anotop syringe filter (GE Healthcare) for the soluble fraction (S; **Figure 2**). The filters were first rinsed with ~2 mL of Milli-Q water and the first few drops of sample were discarded. Samples were directly filtered into trace metal-clean polycarbonate Erlenmeyer flasks, placed in a clean polyethylene bag with a small opening to vent, and left shaking (150 rpm) in an incubator at 37 °C for one week.

Samples for analysis of ^{57}Fe content were taken and prepared as in Media Development Experiment I (see **Metal Analysis**). The samples were analyzed for ^{56}Fe, ^{57}Fe, ^{60}Ni, ^{63}Cu, ^{66}Zn, and ^{208}Pb on an ELEMENT XR HR-ICP-MS (Thermo Fisher Scientific). All data were corrected for the rhodium internal standard and the analytical blank value for ^{57}Fe was subtracted (see **Metal Analysis**).

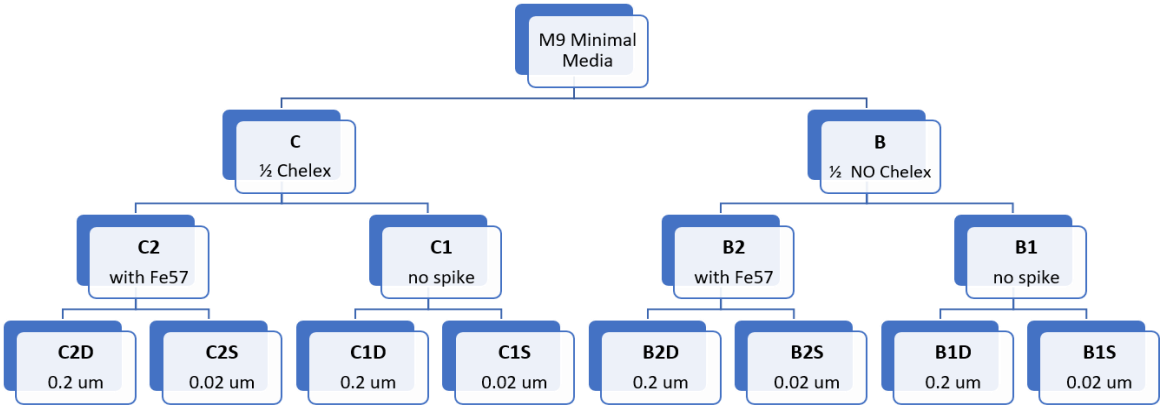

Figure 2: Treatments of M9 minimal media for the Media Development Experiment II. Half of the media was chelexed to remove metals (C), half was not chelexed (B). Half of each treatment was spiked with $^{57}FeSO_4$ (B2 & C2), while half remained un-spiked (B1 & C1). Lastly, half of each treatment was 0.2 µm filtered (B1D, B2D, C1D, C2D) and half was 0.02 µm filtered (B1S, B2S, C1S, C2S).

Tracing ^{57}Fe from *E. coli* to Phages T4 and T5

The methods developed for the tracing of ^{57}Fe from *E. coli* to phages T4 and T5 included the growth of *E. coli* cell cultures in M9 minimal media that contained ^{57}Fe as the sole iron source, then the rinsing of the cells to remove excess ^{57}Fe (see **Bacteria Preparation**), followed by infection with either phage T4 or T5 (see **Phage Infection**). Bacterial lysis control samples remained uninfected by phage and were instead lysed by treatment with chloroform, then subsequently taken through the same phage purification steps to account for any colloids that contained ^{57}Fe and co-purified with the phages (see **Chloroform Treatment**). A blank media control was not inoculated with bacteria or infected with either phage and was included to identify any sources of ^{56}Fe contamination through the phage purification steps. The phage lysates and controls were then purified through centrifugation to pellet bacterial debris, filtration of the supernatant through a 0.22 µm filter to collect the dissolved fraction, and subsequent

filtration of a subsample through a 0.02 µm filter to collect the soluble fraction. The difference in iron content between the dissolved and soluble fractions is the colloidal fraction (0.02 µm – 0.22 µm; see **Size Fractionation**). The dissolved fraction of each sample was then ultracentrifuged through a sucrose cushion, in which phages pellet but cellular debris does not (see **Sucrose Ultracentrifugation**). The pellets were then re-suspended and dialyzed over six buffer changes (see **Dialysis**). The starting cell culture samples and final purified phage samples were analyzed for bacterial cell or phage particle concentrations by SYBR Gold nucleic acid staining and epifluorescence microscopy (see **Bacterial and Phage Quantification**). For each experimental step, 100 µL samples were taken (by pipette with the first aspiration discarded to rinse the tip) to track the ^{57}Fe content pre-lysis and post-lysis during the subsequent phage purification steps. Metal content of the samples were quantified by XR ICP-MS (see **Trace Metal Quantification**).

These methods were repeated five times. The first iteration used only *E. coli* phage T4 (Experiment 1). The second (Experiment 2), third (Experiment 3), fourth (Experiment 4), and fifth (Experiment 5) iterations used both *E. coli* phages T4 and T5. In the fifth iteration (Experiment 5), all samples (including bacteria infected with both phages T4 and T5, the bacterial lysis control, and the media blank) were treated with chloroform, instead of only treating the bacterial lysis control with chloroform as in the previous four experiments).

Bacteria Preparation

In an acid-cleaned 2 L polycarbonate flask, 1 L of M9 minimal media was prepared (**Table 1**) without addition of ^{57}Fe and a 100 µL sample (see **Trace Metal Quantification**) was frozen at -20 ˚C for metal analysis by XR ICP-MS. A volume of 750 mL of the un-amended media (no added ^{57}Fe) was filtered through a 0.02 µm Whatman Anotop syringe filter (after a Milli-Q water (18.2 MΩ cm) pre-rinse and the first few drops of media discarded) and reserved

for bacteria pellet rinses. The remaining 250 mL of media was amended with $^{57}FeSO_4$ (final concentration: 10 µM, Kutter and Sulakvelidze, 2004) and filtered through a 0.02 µm Whatman Anotop syringe filter into a 250 mL polycarbonate flask.

For the bacterial stocks, *E. coli* strain ZK126 (provided by Betty Kutter, Evergreen State College) was grown over multiple generations exclusively on the media amended with $^{57}FeSO_4$. To do this, 50 mL of M9 minimal media (**Table 1**) amended with 10 µM $^{57}FeSO_4$ in an acid-cleaned polycarbonate flask was inoculated with 1% of ZK126 stock (stored in 50% glycerol at -80 ˚C) and incubated while shaking (150 rpm) at 37 ˚C. This first generation grew to mid-logarithmic phase measured by an optical density (OD_{600}) of 0.200 – 0.500 on a GENESYS 20 Thermo Spectronic spectrophotometer (**Figure 3**), and 1% was inoculated into a second 50 mL of media amended with 10 µM $^{57}FeSO_4$ in an acid-cleaned polycarbonate flask. The second generation was incubated while shaking (150 rpm) at 37 ˚C overnight (12-15 hours) and 1% of the culture was used to inoculate the third generation. This was repeated for a total of eight generations, and stored in 50% glycerol at -80 ˚C.

For the experiments, an initial culture was started by inoculating 20 mL of media (amended with 10 µM $^{57}FeSO_4$) with 1 mL of a thawed ZK126 *E. coli* ^{57}Fe glycerol stock aliquot in an acid-cleaned 125 mL polycarbonate flask. The culture flask was placed upright in a clean polyethylene bag left slightly open to vent, secured in a flask clamp within an incubator, and grown overnight at 37 ˚C while shaking (150 rpm) so that the culture could reach a high cell density.

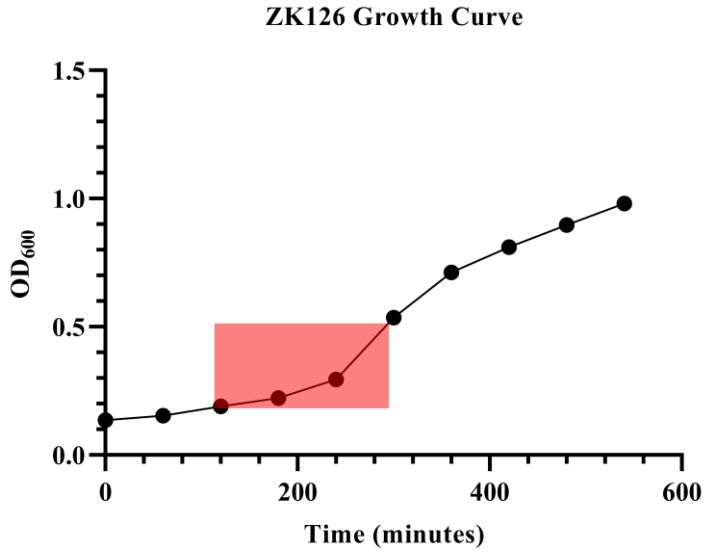

Figure 3: Growth curve for E. coli ZK126 measured on a spectrophotometer. Mid-logarithmic growth (indicated by shaded area) was an OD_{600}= 0.200-0.500.

After incubating for 12-15 hours, turbidity of the bacterial culture was observed visually, indicating late-logarithmic growth. Four 58.5 mL aliquots of media (amended with 10 µM $^{57}FeSO_4$) were measured by pouring into acid-cleaned 250 mL polycarbonate flasks on a balance (based on an approximate density of 1 g/mL) to prevent potential contamination using transfer pipettes (**Figure 4**). Each of the three media aliquots were inoculated with 10% (6.5 mL) of the overnight bacterial culture by pouring into acid-cleaned polycarbonate flasks on a balance, while the fourth served as the blank control and remained uninoculated with bacteria. The four flasks were placed upright into clean polyethylene bags that were left slightly open to vent, secured in flask clamps within an incubator, and grown at 37 ˚C while shaking (150 rpm). Once the cultures reached an OD_{600} of 0.200-0.500 (indicative of mid-logarithmic growth; **Figure 3**), the bacteria were poured into 20 mL aliquots in acid-cleaned 50 mL Falcon tubes (**Figure 4**).

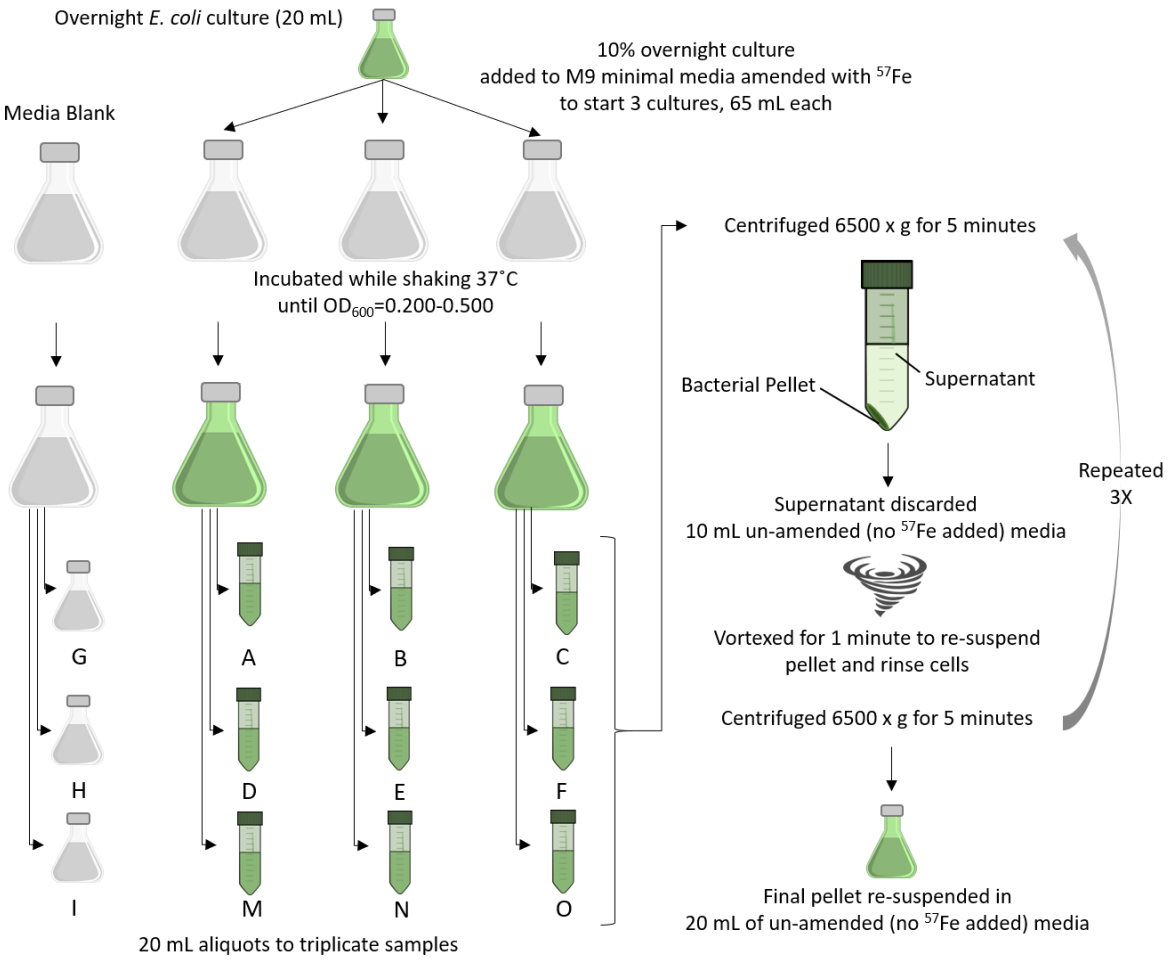

Figure 4: Flowchart of cell culture preparation. A culture of E. coli is grown overnight to start three 10% cultures which are grown to mid-logarithmic phase, or an OD_{600}= 0.200-0.500. The cultures are then divided across triplicate samples and centrifuged to pellet the bacterial cells. The supernatant containing excess ^{57}Fe in media is discarded, and the cells are re-suspended in un-amended media (no ^{57}Fe added). This is repeated three times and the final rinsed cell culture pellet is re-suspended in 20 mL of un-amended media.

Excess ^{57}Fe was rinsed from the surface of the bacterial cells by centrifuging the Falcon tubes containing the samples at a speed of 6,500 x g for 5 minutes (**Figure 4**). The bacterial cells pelleted to the bottom of the Falcon tube, and the supernatant was discarded. A volume of 10 mL of un-amended 0.02 µm filtered media (no $^{57}FeSO_4$ added) was added to each of the bacterial pellets, and the pellets were re-suspended by vortexing for 1 minute. The rinsed bacterial cells were centrifuged again for 5 minutes at 6,500 x g, and the cell rinsing procedure was repeated

three times. The final bacterial pellet was re-suspended in 20 mL of 0.02 µm filtered media that had no added $^{57}FeSO_4$.

Phage Infection

Figure 5 shows the experimental design for the phage infection experiments. Samples infected with *E. coli* phage T4 were designated **A**, **B**, and **C**. Samples infected with *E. coli* phage T5 were designated **M**, **N**, and **O**. The 20 mL of rinsed bacterial cells for each of the samples **A**, **B**, **C**, **M**, **N**, and **O** were poured from Falcon tubes into new acid-cleaned polycarbonate 125 mL flasks, and were infected with 5 µl of their respective phage from a stock (T4: provided by Betty Kutter, Evergreen State College, grown to a titer of 1.3 x 10^{11} phage/mL; T5: ATCC ® 11303-B5™, grown to a concentration of 8.2 x 10^{11} phage/mL). The flasks were placed upright into clean polyethylene bags left slightly open to vent, secured into flask clamps within an incubator, and left shaking (150 rpm) overnight (12-15 hours) at 37 ˚C. The bacterial lysis control samples (designated **D**, **E**, and **F**) and the blank control samples (designated **G**, **H**, and **I**) were not infected with phage and instead remained in Falcon tubes for storage overnight at 4 ˚C.

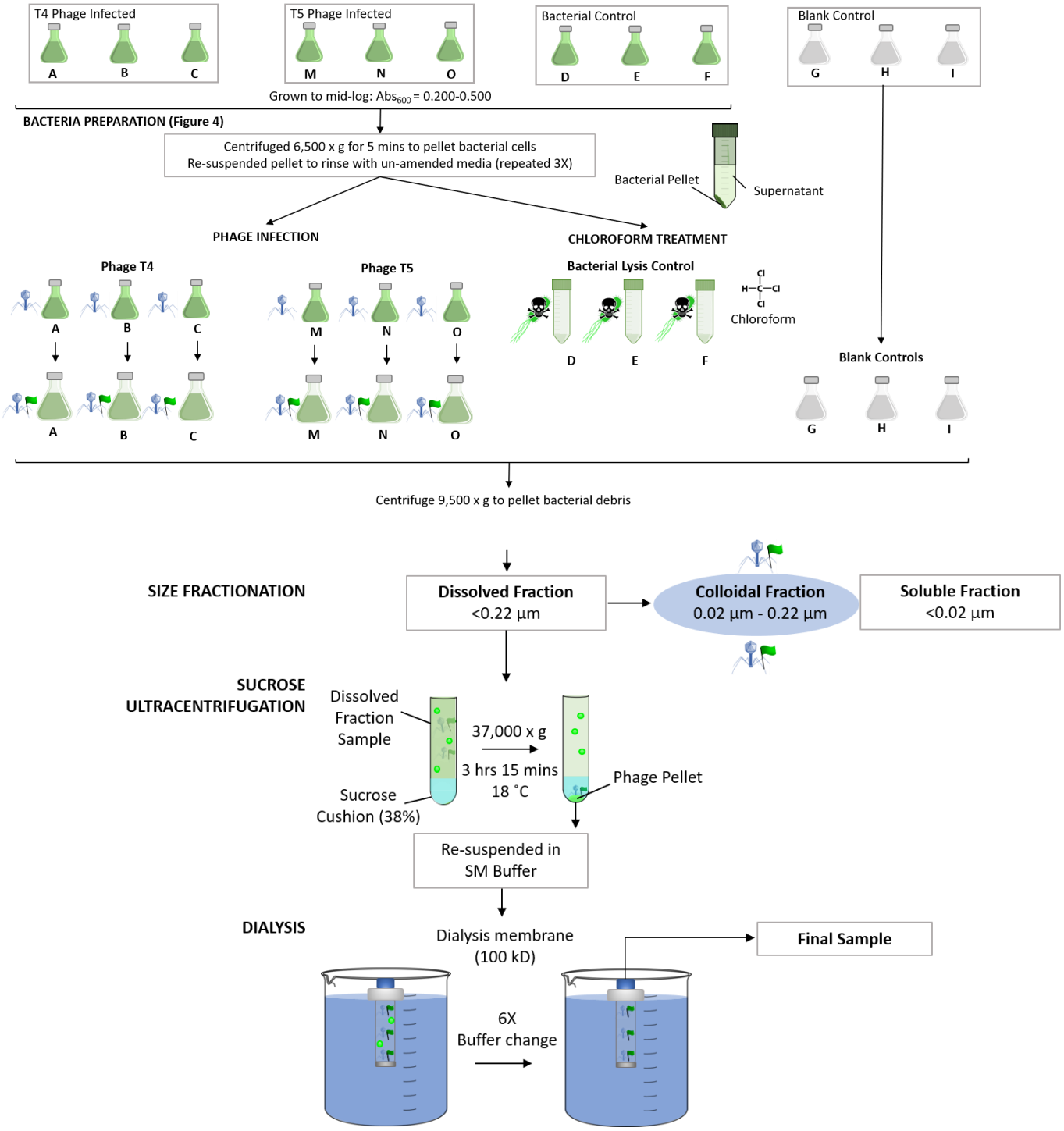

Figure 5: Flowchart of the Tracing ^{57}Fe to E. coli phages T4 & T5 Experimental method. First, cell cultures were grown and aliquoted into triplicate samples of each treatment: T4 infected (A, B, C), T5 infected (M, N, O), Bacterial Control (D, E, F), and Blank Control (G, H, I). Cell cultures were rinsed to remove excess ^{57}Fe, then lysed by phage T4 infection, phage T5 infection, or chloroform for the bacterial lysis control. The lysates are then purified for the phage by centrifugation, filtration, sucrose ultracentrifugation, and dialysis.

Chloroform Treatment

After storage overnight at 4 ˚C, all five experiments (Experiment 1-5) of the bacterial lysis control samples (**D**, **E**, and **F**) were treated with 20% chloroform (Fisher Scientific, for Molecular Biology applications ≥99% purity, 0.75% Ethanol as preservative) and vortexed for one minute to simulate the effect of viral lysis and burst open the bacterial cells (**Figure 5**). Due to concerns arising that chloroform would break down bacterial colloids differently in the bacterial lysis control sample than in the phage samples, chloroform treatment was performed on all samples in the fifth experiment (Experiment 5). In experiment 5, all samples (including T4 and T5 phage lysates (**A**, **B**, **C**, **M**, **N**, **O**), the blank control samples (**G**, **H**, **I**), and the bacterial lysis controls (**D**, **E**, **F**) were also treated with chloroform.

Size Fractionation

Phage T4 and T5 lysates (**A**, **B**, **C**, **M**, **N**, **O**), bacterial lysis controls (**D**, **E**, **F**) and blank control samples (**G**, **H**, **I**), were transferred to acid-cleaned 50 mL Falcon tubes by pouring and centrifuged at a speed of 9,500 x g for 5 minutes to pellet any remaining cellular debris (**Figure 5**). For chloroform-treated samples, centrifugation separates the chloroform organic phase (bottom layer) from the aqueous sample phase (top layer) so that the chloroform-treated sample could be removed by an acid-cleaned 10 mL polystyrene serological pipette (cotton plug removed prior to soap bath). The supernatant, which contained the T4 phage progeny for samples **A**, **B**, **C** and the T5 phage progeny for samples **M**, **N**, **O**, was then passed through a 0.22 µm Sterivex PVDF syringe filter (EMD Millipore) after the filter was pre-rinsed with Milli-Q water (18.2 MΩ cm) and the first few drops of sample were discarded. The filtrate was collected in an acid-cleaned 15 mL Falcon tube, and contained phage (for samples **A**, **B**, **C**, **M**, **N**, **O**) and any other soluble or colloidal-sized cellular debris bound to ^{57}Fe within the dissolved fraction (<0.22

μm). A 2 mL subsample from the dissolved fraction was subsequently filtered through a 0.02 μm Whatman Anotop syringe filter (with an Milli-Q water pre-rinse and the first few drops of sample discarded). The filtrate was collected in an acid-cleaned 1 mL microcentrifuge tube for measurement of ^{57}Fe in the soluble fraction (<0.02 μm). The ^{57}Fe content in the colloidal fraction (0.2 μm - 0.02 μm) was then calculated as the difference between ^{57}Fe content in the dissolved and the soluble fractions.

Sucrose Ultracentrifugation

Phage particles were concentrated and purified from the dissolved fraction of each sample by ultracentrifugation through a dense layer of sucrose (Hurwitz et al., 2013). A 2.5 mL layer of 38% D(+)-Sucrose (ACROS Organics™, 99.7% for biochemistry) in 0.02 μm filtered SM Buffer [100 mM NaCl (Fisher Chemical, ≥99.0% purity), 8 mM $MgSO_4$ (Sigma-Aldrich *Reagent Plus*®, ≥99.5% purity), 50 mM Tris-Cl (Fisher Bioreagents, ≥99% purity) in Milli-Q water (18.2 MΩ cm) pH of 7.5] was added to the bottom of an acid-cleaned ultracentrifuge tube (Beckman Coulter, ultra-clear 14 x 95 mm) after a pre-rinse with 1 mL of 0.02 μm filtered SM Buffer. The ultracentrifuge tube was tilted side-ways and 4 mL of each dissolved fraction sample were carefully dispensed above the sucrose cushion using an acid-cleaned 10 mL polystyrene serological pipette (cotton plug removed). Ultracentrifuge tubes were then gently filled to the top with 7.5 mL of 0.02 μm filtered SM Buffer to prevent collapse during high-speed centrifugation. Tubes were then carefully balanced in pairs and the samples were centrifuged in a swinging bucket rotor (Beckman Coulter, SW40Ti) for 3 hours and 15 minutes at a speed of 175,000 x g (37,200 rpm) and 18 ˚C. The supernatant was poured out, and any remaining liquid was removed using a 1 mL pipette kept along the side of the tube so as not to disturb the phage pellet. The

tubes were dried in an AirClean laminar flow clean hood for 20 minutes, then phage pellets were re-suspended in 1.2 mL of 0.02 µm filtered SM Buffer (**Figure 5**).

Dialysis

The dialysis devices (Spectrum™ Spectra/Por™ Float-A-Lyzer™ G2) consisted of a cellulose ester membrane tubing with 100 kD pore sizes and a 1 mL capacity. To prepare for dialysis, 10% ethanol (Fisher Bioreagents, Molecular Biology grade) was added to the dialysis tubing, which was submerged in 10% ethanol for 10 minutes. The ethanol was poured out, and the dialysis tubing was rinsed with Milli-Q water (18.2 MΩ cm). The tubing was then filled with Milli-Q water and submerged in Milli-Q water for 20 minutes. The water was then poured out, and 1 mL of re-suspended pellet samples were added to individual dialysis tubing and placed into a 1 L tank of dialysis buffer (10 mM NaCl, 50 mM Tris-Cl pH 8.0, 10 mM $MgCl_2$ (Spectrum Spectra/Por™ Float-A-Lyzer™ G2 manual). The dialysis buffer was replaced every 8-15 hours over 4 days for a total of 6 buffer changes (**Figure 5**). This timeline was determined from the first iteration of the experiment, which showed diminishing amounts of ^{57}Fe per buffer change until the 6^{th} which contained less than 1 nmol ^{57}Fe for a 1 L reservoir, as determined by XR ICP-MS.

Trace Metal Quantification

Samples for trace metal quantification were taken during each experimental step, preserved (-20 ˚C), and prepared for analysis on the ELEMENT XR ICP-MS as per the methods outlined in the Media Development Experiment I (**Metal Analysis**). The natural abundances of each iron isotope had to be accounted for as well, because any iron contamination would be 91.7% ^{56}Fe and 2.119% ^{57}Fe (Dauphas and Rouxel, 2006). Additionally, the $^{57}FeSO_4$ stock from

the manufacturer (Isoflex) contains 95.06% ^{57}Fe and 3.04% ^{56}Fe. The measured values of ^{56}Fe concentration were therefore adjusted using a correction ratio, which was calculated using the iron isotope concentrations of the un-amended 0.02 µm filtered M9 minimal media (pre-spike with 10 µM $^{57}FeSO_4$) and the amended 0.02 µm filtered media for each experimental round. The ^{56}Fe background concentration of the media prior to any addition of ^{57}Fe (Media) was subtracted from the concentration of ^{56}Fe added to the media through the 10 µM $^{57}FeSO_4$ spike (Media + ^{57}Fe), then divided by the concentration of ^{57}Fe added to the media after the $^{57}FeSO_4$ spike (^{57}Fe Measured).

$$Correction\,ratio = \frac{(Media + {}^{57}Fe) - Media}{{}^{57}Fe\ \mathrm{Measured}}$$

For each sample, the correction ratio was then multiplied by the ^{57}Fe concentration measured (^{57}Fe Measured) for that sample and subtracted from the measured ^{56}Fe (^{56}Fe Measured) concentration in that sample, resulting in the fully corrected ^{56}Fe concentration.

$$Corrected\ {}^{56}Fe = {}^{56}Fe\ \mathrm{Measured} - (Correction\,ratio \cdot {}^{57}Fe\ \mathrm{Measured})$$

To correct for ^{57}Fe for that could have been added to a sample through ^{56}Fe contamination, the corrected value for ^{56}Fe (Corrected [^{56}Fe]) was multiplied by the naturally occurring isotopic ratio of ^{57}Fe: ^{56}Fe (2.119%) and subtracted from the ^{57}Fe measured (Measured [^{57}Fe]) for that sample.

$$Corrected\ {}^{57}Fe = Corrected\ {}^{56}Fe \cdot 0.02119$$

Lastly, all values were converted from nanomolar to nanomoles by multiplying by the volume (in liters) that the sample was taken from.

Bacterial and Phage Quantification

For microscopy, 99 µL of bacterial and viral samples were fixed with 1% formalin for storage at 4 ˚C in sterile microcentrifuge tubes (Chen et al., 2001). Slides of bacterial cells were prepared by adding 10 µL of fixed bacteria to 990 µL of 0.22 µm filtered SM Buffer for a ratio of 1:100. Phage samples need a higher dilution, so 5 µL of fixed phage were pipetted into 5 mL of 0.22 µm filtered SM Buffer for a ratio of 1:1000. A Millipore Mixed-ester membrane filter (EMD Millipore, 25 mm, 0.8 µm pore size) was placed on the filter platform, followed by a 0.02 µm Whatman Anodisc filter (25 mm). The bacterial and phage sample dilutions were vortexed, and 1 mL of sample was pipetted directly onto the filter, with one sample per filter (Noble and Fuhrman, 1998). Once all the sample passed through, the filter was placed onto a 100 µL drop of 20X SYBR™ Gold Nucleic Acid Stain (Life Technologies) in deionized (DI) water in a petri dish in the dark. After eight minutes, the filter was then placed on a 98 µL drop of DI water to rinse excess stain. The stained filter was then placed onto a glass slide, and 28 µL of antifade mounting solution (antifade solution was prepared fresh each time: 990 µL 50:50 PBS/ Glycerin with 10 µl 10% w/v p-phenylenediamine hydrochloride) was pipetted onto it. A cover slip was placed over the filter and the slides were imaged under a Zeiss Axio Scope.A1 epifluorescence microscope. For each slide, ten frames were counted and averaged using Media Cybernetics Image-Pro software. The average counts were multiplied by the dilution factor (100, 1,000, or 10,000), and then multiplied by the conversion factor (31,915), which accounts for the area of the counting frame relative to the surface area the sample was filtered onto.

Results & Discussion

Media Development

For the Media Development I Experiment, triplicate samples of unfiltered and 0.02 µm filtered M9 minimal media amended with 10 µM $^{57}FeSO_4$ were monitored over seven days in a shaking (150 rpm) incubator at 37 ˚C. Metal analysis by inductively coupled mass spectrometry (ICP-MS) revealed a starting ^{57}Fe concentration of 11.18 ± 0.15 µM for unfiltered samples. After incubating for 24 hours, the ^{57}Fe concentration for the unfiltered media decreased to 8.59 ± 1.10 µM, and 6.22 ± 1.40 µM after seven days (**Figure 6**). The 0.02 µm filtered media had a starting concentration of 5.57 ± 0.12 µM, which was relatively stable at 5.52 ± 0.12 µM after incubating for 24 hours and decreased slightly to 4.94 ± 0.24 µM after incubating for seven days. Thus, filtration through a 0.02 µm filter reduced the initial concentration of the ^{57}Fe spike by roughly half (from 11.18 ± 0.15 µM in unfiltered media to 5.57 ± 0.12 µM in 0.02 µm filtered media), while the 0.02 µm filtered media maintained a more constant ^{57}Fe concentration than unfiltered media over the seven days of the experiment (**Figure 6**).

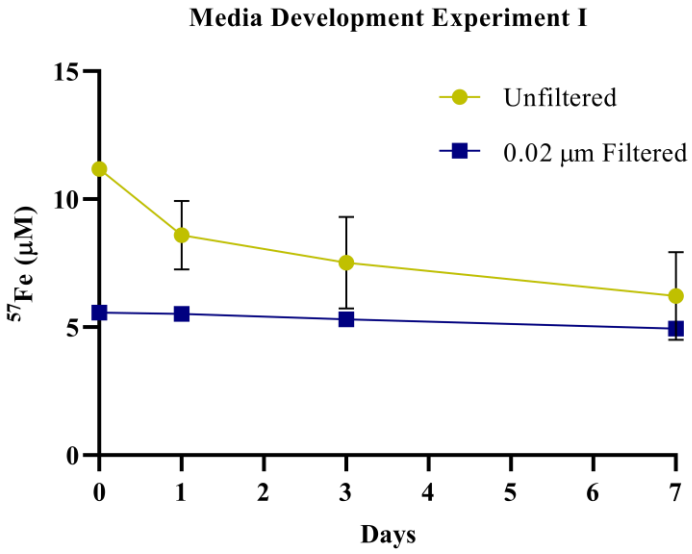

Figure 6: Media Development Experiment I. ^{57}Fe concentrations of unfiltered (yellow) and 0.02 µm filtered (blue) M9 minimal media after 10 µM spike with $^{57}FeSO_4$ incubated while shaking (150 rpm) at 37 ˚C for seven days. Metals were quantified by ICP-MS. Error bars represent standard deviation between triplicate samples.

The decrease in ^{57}Fe concentrations for unfiltered M9 minimal media was predicted to be the result of precipitation of iron and loss to the walls of the polycarbonate flask (Fischer et al., 2007). The Media Development Experiment I demonstrated this apparent loss in iron at variable magnitudes across triplicate samples after incubating at 37 ˚C while shaking (150 rpm) for 24 hours (conditions used for overnight *E. coli* culture growth). Samples that were 0.02 µm filtered maintained a more constant concentration of ^{57}Fe over 24 hours and throughout the seven-day incubation with less variability between triplicate samples, making filtration a more consistent media preparation for culture growth (**Figure 6**).

Concentrations of ^{56}Fe were also measured by ICP-MS for all samples to monitor metal contamination. Starting concentrations of ^{56}Fe for unfiltered samples were 0.8 ± 0.01 µM with a final concentration of 0.5 ± 0.09 µM. Samples that were 0.02 µm filtered had a starting ^{56}Fe concentration of 0.4 ± 0.03 µM and a final concentration of 0.4 ± 0.01 µM. While the ^{57}Fe

concentrations are in excess of ^{56}Fe, any preferential uptake of the lighter ^{56}Fe isotope by bacteria could affect the ^{57}Fe-labeling of phages. To further remove excess metals, the Media Development Experiment II used Chelex-100 resin and filtration of the M9 minimal media.

For the Media Development Experiment II, the unfiltered chelexed (C2) and unchelexed (B2) samples spiked with 10 µM $^{57}FeSO_4$ had starting concentrations of 10.6 µM and 8.8 µM, respectively (**Figure 7**). Over a seven-day incubation at 37 ˚C while shaking (150 rpm) the ^{57}Fe concentrations varied, decreasing to 8.5 µM for the unfiltered chelexed sample (C2) and increasing to 10.6 µM for the unfiltered unchelexed sample (B2), likely due to contamination. Filtered samples had less variable starting concentrations, with 7.5 µM for the unchelexed dissolved sample (0.2 µm filtered; B2D), 7.1 µM for the unchelexed soluble sample (0.02 µm filtered; B2S), 7.3 µM for the chelexed dissolved sample (C2D), and 7.0 µM for the chelexed soluble sample (C2S). Over the seven-day incubation the filtered samples remained more constant than the unfiltered samples, with a final average ^{57}Fe concentration of 7.1 ± 3.6 µM across all four treatments (**Figure 7**).

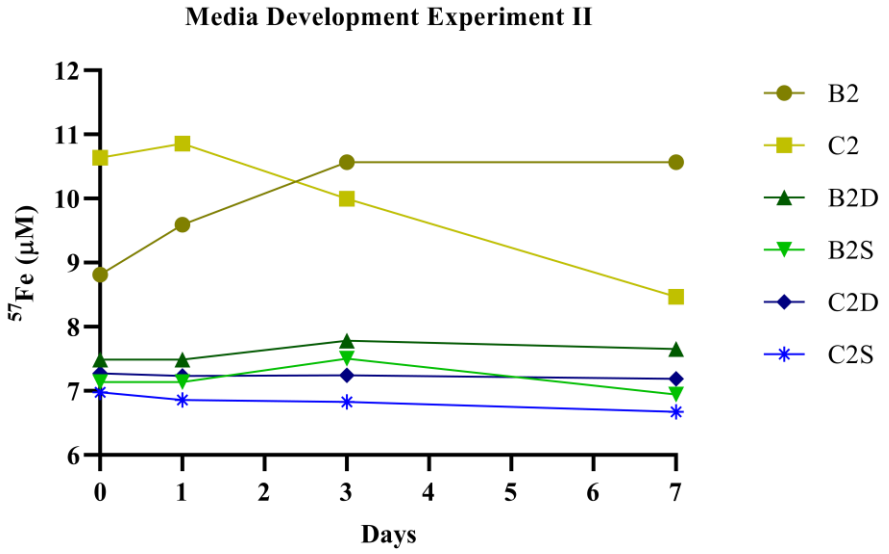

Figure 7: Media Development Experiment II. All M9 minimal media samples were spiked with 10 µM $^{57}FeSO_4$, chelexed or filtered, and left incubating while shaking (150 rpm) for seven days. Samples were either chelexed unfiltered (C2), chelexed and 0.2 µm filtered (C2D), or chelexed and 0.02 µm filtered (C2S). Unchelexed samples were either unfiltered (B2), unchelexed and 0.2 µm filtered (B2D), or unchelexed and 0.02 µm filtered (B2S).

As in the Media Development Experiment I, unfiltered M9 minimal media samples had variable concentrations of ^{57}Fe over the seven-day incubation. While the unfiltered chelexed (C2) sample had a similar starting concentration (10.6 µM) and decreased over the seven-day incubation, the unfiltered unchelexed sample (B2) had a lower starting concentration (8.8 µM) but increased over the incubation. Filtered samples were comparatively stable and had less variability in ^{57}Fe concentration, demonstrating that filtration is a necessary step to produce media that is less variable in starting ^{57}Fe concentration.

The purpose of using Chelex-100 resin was to remove any excess ^{56}Fe contamination from the media in the event the bacteria cultures had preferential uptake of the lighter ^{56}Fe isotope over the ^{57}Fe tracer. Starting concentrations of ^{56}Fe were not much lower for the filtered chelexed media, with 0.3 ± 0.04 µM, comparable to 0.4 ± 0.02 µM in the filtered unchelexed

media. Furthermore, when inoculated with an *E. coli* culture, the filtered chelexed media did not support bacterial growth. This may be due to the removal of other metals essential for bacterial growth such as magnesium and calcium by the Chelex-100 resin. Due to similar starting concentrations of both the ^{57}Fe and background ^{56}Fe in filtered media regardless of whether it was chelexed, the filtered not chelexed media was decidedly the best choice.

When comparing filtered medias, the concentrations of ^{57}Fe and ^{56}Fe in the 0.2 µm filtered "dissolved" media and in the 0.02 µm filtered "soluble" media were not significantly different (**Figure 7**). After incubating 24 hours, the ^{57}Fe concentration in the 0.2 µm filtered media was 7.4 µM while the 0.02 µm filtered media contained 7.1 µM. Due to the potential for iron contamination through autoclaving, polycarbonate flasks were instead acid-cleaned, dried, and double-bagged. Media sterilization was maintained by ultrafiltration (0.02 µm) to prevent contamination by small bacteria or any viruses in the absence of autoclaving.

Tracing ^{57}Fe from *E. coli* to Phages T4 and T5

The Tracing ^{57}Fe from *E. coli* to Phages T4 and T5 experiment was repeated for a total of five iterations, with Experiment 1 utilizing only phage T4 and Experiments 2, 3, 4, and 5 using both phages T4 and T5. Experiment 5 was the only iteration to treat phage samples as well as the bacterial control samples with chloroform. Experiments 2, 3, and 4 have two analytical datasets from analyzing the experimental samples twice on the XR-ICP-MS; these results are designated 2.1, 3.1, and 4.1 for the first mass spectrometry analysis, and 2.2, 3.2, and 4.2 for the second analysis. During the first analytical run for Experiment 2, the calibration curve had to be re-made due to contaminated HCl. During Experiments 3 and 4, it is hypothesized that a sample with a different density clogged the nebulizer introduction system. The data from the second analysis would have replaced the first, however the higher blank values for ^{56}Fe from contaminating

samples on the second ICP-MS run meant a higher blank value had to be subtracted for those samples. Instead, the values for samples from Experiments 2, 3, and 4 were calculated from the average of the six measurements made (two analyses of the triplicate samples).

Metal Analysis

Samples were analyzed for trace metals ^{56}Fe, ^{57}Fe, ^{60}Ni, ^{63}Cu, ^{66}Zn, and ^{208}Pb on an ELEMENT XR HR-ICP-MS (**Appendix B**). Analytical blanks for each mass spectrometry run consisted of Milli-Q water (18.2 MΩ cm) acidified in 5% nitric acid with rhodium internal standard (10 ppb) and were analyzed throughout the run (**Table 2**). Blank samples were analyzed throughout the mass spectrometer run to monitor for drift, and blank measurements were spaced between every ten samples. The number of blank values used to calculate the average and standard deviation are provided as "*n*" (**Table 2**). Due to re-running the samples from Experiments 2, 3, and 4 on the XR-ICP-MS, the blank values were higher for the second analysis due to contamination but could be corrected for in the datasets.

Table 2: Analytical blank values for ^{56}Fe and ^{57}Fe after rhodium correction as measured on ELEMENT XR ICP-MS. "Expt" refers to experimental and analytical dataset; e.g. Expt 2.1 is experiment 2, first analytical dataset, while Expt 2.2 is experiment 2, second analytical dataset. The number of blank measurements used to calculate the average and standard deviation for each round is "n".

Expt	**1**	**2.1**	**2.2**	**3.1**	**3.2**	**4.1**	**4.2**	**5**
^{56}Fe (nM)	0.545 ± 0.074 *n= 5*	0.82 ± 0.32 *n= 5*	5.85 ± 0.26 *n= 6*	0.73 ± 0.2 *n= 5*	5.30 ± 0.53 *n= 6*	1.02 ± 0.18 *n= 4*	4.61 ± 0.51 *n= 6*	0.38 ± 0.099 *n= 5*
^{57}Fe (nM)	0.014 ± 0.002 *n= 5*	0.03 ± 0.01 *n= 4*	0.13 ± 0.01 *n= 6*	0.02 ± 0.006 *n= 5*	0.12 ± 0.02 *n= 6*	0.03 ± 0.004 *n= 5*	0.09 ± 0.01 *n= 6*	0.018 ± 0.006 *n= 5*

The starting ^{57}Fe content measured for the M9 minimal media (amended with 10 µM $^{57}FeSO_4$ and 0.02 µm filtered) ranged from 1.9 ± 0.05 µM to 6.0 ± 0.3 µM for all iterations of the experiment (**Table 3**).

Table 3: Starting ^{57}Fe content in M9 minimal media after amendment with 10 µM $^{57}FeSO_4$ and 0.02 µm filtration for each iteration of the experiment. Experiments 2, 3, and 4 are provided as the average of the two analytical values measured by XR ICP-MS.

Expt	1	2	3	4	5
^{56}Fe (µM)	0.05	0.3 ± 0.2	0.3 ± 0.09	0.05 ± 0.007	0.1
^{56}Fe (nmol)	7.0	51.4 ± 28.6	44.3 ± 12.8	7.5 ± 1.0	19.4
^{57}Fe (µM)	4.9	1.9 ± 0.05	6.0 ± 0.3	4.7 ± 0.4	5.7
^{57}Fe (nmol)	736.1	278.5 ± 7.6	894.4 ±46.2	698.0 ± 62.4	856.7

^{57}Fe in Experimental Samples

The values for ^{57}Fe measured for Rounds 1 and 5 are the average of triplicate experimental samples. Samples from Rounds 2, 3, and 4 were analyzed twice; both sets of ^{57}Fe measurements for the triplicate experimental samples were averaged (six values total) and the standard deviations provided (**Table 4**). To allow for the direct comparison of ^{57}Fe content in samples with different volumes along the culturing and purification process, all ^{57}Fe data were provided in nanomoles (nmol) instead of nanomolar (nM). The percentage of ^{57}Fe retained through each of the phage purification steps is included between each sample step. There is a higher percentage of ^{57}Fe retained for phage T4 and T5 samples across most purification steps than for the bacterial control samples (**Table 4**).

Table 4: Amount of ^{57}Fe (nmol) measured in nanomoles (nmol) by XR ICP-MS for cell culture (pre-lysis) and subsequent phage purification steps (post-lysis) in each experiment (Expt). T4 and T5 refer to phage-infected samples, the bacterial lysis control (Bact Control) was lysed by chloroform treatment, and the Blank refers to the media blank. Values for ^{57}Fe are the average of triplicate samples with standard deviation. ^{57}Fe content for experiments 2, 3, and 4 are the average of the six analytical values measured between the two XR ICP-MS runs. Percent of ^{57}Fe retained between each purification step is included. Missing values are where the percentage of ^{57}Fe retained between purification steps was greater than 100%.

Expt	Sample	Cell Culture Pre-lysis (nmol)	Post- lysis Unfiltered (nmol)	Dissolved (< 0.2 μm) (nmol)	Colloidal (0.02- 0.2 μm) (nmol)	Sucrose Pellet (nmol)	Post-dialysis (nmol)
1	**T4**	22.25 ± 0.63	10.85 ± 0.93	9.87 ± 1.23	9.56 ± 1.23	0.34 ± 0.11	0.16 ± .04
% ^{57}Fe Retained		*48.8%*	*90.9%*	*96.9%*	*3.6%*		*46.2%*
1	**Bact Control**	22.31 ± 3.79	3.80 ± 0.17	3.40 ± 0.09	3.20 ± 0.10	0.008 ± .0007	0.002 ± 0.0005
% ^{57}Fe Retained		*17.0%*	*89.6%*	*94.0%*	*0.22%*		*26.4%*
1	**Blank**	0.031 ± 0.003	0.031 ± 0.02	0.40 ± 0.40	0.40 ± 0.40	0.001 ± 0.0005	0.001 ± 0.001
2	**T4**	14.48 ± 2.36	7.79 ± 0.92	6.63 ± 0.92	6.58 ± 0.90	0.28 ± 0.10	0.16 ± 0.01
% ^{57}Fe Retained		*53.8%*	*85.1%*	*99.3%*	*4.2%*		*56.6%*
2	**T5**	14.88 ± 0.79	8.74 ± 0.50	7.86 ± 0.53	7.84 ± 0.53	0.18 ± 0.06	0.10 ± 0.009
% ^{57}Fe Retained		*58.7%*	*89.9%*	*99.8%*	*2.3%*		*52.0%*
2	**Bact Control**	14.37 ± 0.74	4.36 ± 1.31	2.87 ± 0.12	2.66 ± 0.11	0.10 ± 0.01	0.006 ± 0.003
% ^{57}Fe Retained		*30.4%*	*65.7%*	*92.7%*	*3.6%*		*6.2%*
2	**Blank**	0.17 ± 0.05	0.13 ± 0.02	0.15 ± 0.02	0.15 ± 0.02	0.008 ± 0.002	0.007 ± 0.002
3	**T4**	12.95 ± 1.04	7.24 ± 0.40	5.36 ± 0.56	5.34 ± 0.56	0.71 ± 0.11	0.37 ±.0.53
% ^{57}Fe Retained		55.9%	74.1%	99.7%	13.3%		52.2%
3	**T5**	12.94 ± 1.25	7.34 ± 0.82	6.53 ± 0.74	6.52 ± 0.74	0.85 ± 0.06	0.45 ± 0.03
% ^{57}Fe Retained		56.7%	89.03%	99.9%	13.0%		53.5%
3	**Bact Control**	12.88 ± 1.85	2.86 ± 0.22	2.69 ± 0.30	2.54 ± 0.28	0.03 ± 0.002	0.008 ± 0.005
% ^{57}Fe Retained		22.2%	93.8%	94.4%	1.1%		26.8%
3	**Blank**	0.11 ± 0.03	0.08 ± 0.03	0.11 ± 0.11	0.11 ± 0.11	0.002 ± 0.0006	0.003 ± 0.003
4	**T4**	18.36 ± 2.03	10.67 ± 1.95	9.16 ± 1.01	8.75 ± 1.04	0.24 ± 0.04	0.05 ± 0.006.
% ^{57}Fe Retained		58.1%	85.9%	95.5%	2.7%		19.6%
4	**T5**	17.10 ± 2.13	12.00 ± 2.04	11.33 ± 1.67	11.31 ± 1.66	0.19 ± 0.02	0.09 ± 0.025
% ^{57}Fe Retained		70.2%	94.4%	99.8%	1.7%		44.9%
4	**Bact Control**	17.60 ± 1.81	3.09 ± 0.47	3.29 ± 0.27	3.07 ± 0.29	0.18 ± 0.03	0.005.± 0.0005
% ^{57}Fe Retained		17.5%	-	93.2%	5.5%		2.6%
4	**Blank**	0.03 ± 0.02	0.02 ± 0.01	0.02 ± 0.02	0.02 ± 0.01	0.001 ± 0.0006	0.0005 ± 0.0003
5	**T4**	12.98 ± 0.72	2.92 ± 0.13	3.02 ± 0.12	2.92 ± 0.11	0.01 ± 0.008	0.005 ± 0.003
% ^{57}Fe Retained		22.5%	-	96.7%	0.4%		39.0%
5	**T5**	12.25 ± 1.04	4.30 ± 1.09	4.70 ± 0.42	4.59 ± 0.41	0.02 ± 0.005	0.01 ± 0.001
% ^{57}Fe Retained		35.1%	-	97.8%	0.5%		44.2%
5	**Bact Control**	13.04 ± 0.68	5.04 ± 0.52	2.06 ± 0.27	1.89 ± 0.29	0.02 ± 0.003	0.003 ± 0.0001
% ^{57}Fe Retained		38.6%	40.9%	91.8%	0.8%		16.9%
5	**Blank**	0.06 ± 0.01	0.04 ± 0.007	0.05 ± 0.003	0.05 ± 0.002	0.004 ± 0.0003	0.002 ± 0.0001

Statistical Analyses

The significance of differences between ^{57}Fe content measured in samples for the starting cell culture samples and phage T4 or T5 for each successive purification step were determined by t-test using RStudio (**Table 5**). Individual t-tests were conducted to compare phage T4 vs. the bacterial lysis control (Bact), phage T5 vs. the bacterial lysis control (Bact), and T4 vs. T5. The normality of the data were tested to ensure the assumptions were met. The Shapiro-Wilk test was used to determine whether the data were normally distributed, and an F-test of equality of variances was employed to determine whether or not the variances were equal and to adjust the t-test accordingly (Shapiro and Wilk, 1965; Brown and Forsythe, 1974).

When compared by t-test with a significance cut-off set to 0.01, the ^{57}Fe content in all the cell culture samples pre-lysis were not significantly different from each other ($p \geq 0.01$; **Table 5**). This is as expected, because prior to lysis all bacterial cell cultures should have been homogenous. Post-lysis and over the subsequent purification steps the ^{57}Fe content measured in the bacterial lysis control samples, when compared to either phage T4 or T5 samples, became significantly different ($p < 0.01$) for most experiments (**Table 5**). This is consistent with the hypothesis that ^{57}Fe from the bacterial cells is incorporated into phage. As excess ^{57}Fe is removed from the samples with each purification step, the phage T4 or T5 samples stay enriched in ^{57}Fe while the bacterial lysis control samples continuously lose the signal. For the T4 vs. T5 t-tests, ^{57}Fe values were not significantly different from each other, indicating the association of iron to phage T5 at an abundance comparable to the iron associated with phage T4 (**Table 5**).

Table 5: T-tests of ^{57}Fe (nmol) content measured by XR-ICP-MS for samples or phage T4 or T5 compared to the bacterial lysis control (Bact) as well as samples of phage T4 and T5 compared to each other. A significance cut-off was set to 0.01. Values in black are not significantly different ($p \geq 0.01$), values in blue are significantly different ($p < 0.01$). T-tests performed using RStudio.

Expt	Experiment Step	T4 vs. Bact	T5 vs. Bact	T4 vs. T5
1	Cell Culture (pre-lysis)	0.985268	-	-
	Unfiltered Lysate	0.000467	-	-
	Dissolved	0.017133	-	-
	Colloidal	0.055564	-	-
	Sucrose Pellet	0.051696	-	-
	Dialyzed	0.024704	-	-
2	Cell Culture (pre-lysis)	0.922281	0.313037	0.731375
	Unfiltered Lysate	0.000738	0.000038	0.068772
	Dissolved	0.000224	0.000002	0.026514
	Colloidal	0.000170	0.000002	0.021602
	Sucrose Pellet	0.010353	0.020993	0.091361
	Dialyzed	0.000486	0.000927	0.018726
3	Cell Culture (pre-lysis)	0.941454	0.955251	0.984998
	Unfiltered Lysate	0.000269	0.000031	0.289884
	Dissolved	0.000003	0.000001	0.017828
	Colloidal	0.000002	0.000001	0.017400
	Sucrose Pellet	0.000016	0.000199	0.028944
	Dialyzed	0.000019	0.000199	0.647380
4	Cell Culture (pre-lysis)	0.278726	0.693535	0.203055
	Unfiltered Lysate	0.000220	0.000125	0.313596
	Dissolved	0.000022	0.000093	0.032335
	Colloidal	0.493097	0.000076	0.139446
	Sucrose Pellet	0.017522	0.537462	0.028186
	Dialyzed	0.004906	0.000329	0.203075
5	Cell Culture (pre-lysis)	0.929046	0.414670	0.458230
	Unfiltered Lysate	0.005046	0.433805	0.213752
	Dissolved	0.010181	0.001716	0.005679
	Colloidal	0.009321	0.001622	0.005297
	Sucrose Pellet	0.574282	0.117514	0.131213
	Dialyzed	0.401970	0.008179	0.042204

Phage T4 & T5 Samples Enriched in ^{57}Fe

The ^{57}Fe content of the bacterial cells pre-lysis ranged from 12.9 ± 1.3 nmol ^{57}Fe to 22.3 ± 3.8 nmol, with consistent amounts of ^{57}Fe across cell culture samples within each experiment (**Figure 8A**). For each purification step post-lysis, the ^{57}Fe content diminished across all samples but was retained at higher quantities for phage T4 and T5 samples than for the bacterial lysis control samples or the blank samples. By the final dialysis purification step, the ^{57}Fe content in the T4 and T5 samples exceeded that of the bacterial lysis control samples for most experiments (**Figure 8B**).

The pre-lysis cell culture samples did not contain significantly different amounts of ^{57}Fe for samples to be lysed with phage T4, T5, or the bacterial lysis control. However, post-lysis the ^{57}Fe content declined by a greater magnitude for the bacterial lysis control samples (Bact) than for the phage T4 or T5 samples (**Figure 9A**, **C**, **E**, **G**, **I** & **Table 4**). Experimental media blank samples remained relatively low in ^{57}Fe throughout each experiment. For the final purification steps (sucrose and dialysis purified), phages T4 and T5 maintained an excess of ^{57}Fe (> 0.01 nmol) compared to that of the bacterial lysis control samples (^{57}Fe content < 0.0076 nmol; **Figure 9B**, **D**, **F**, **H**, **J** & **Table 4**). This indicates that phages T4 and T5 have iron associated with their virion that is maintained following the removal of bacterial colloids.

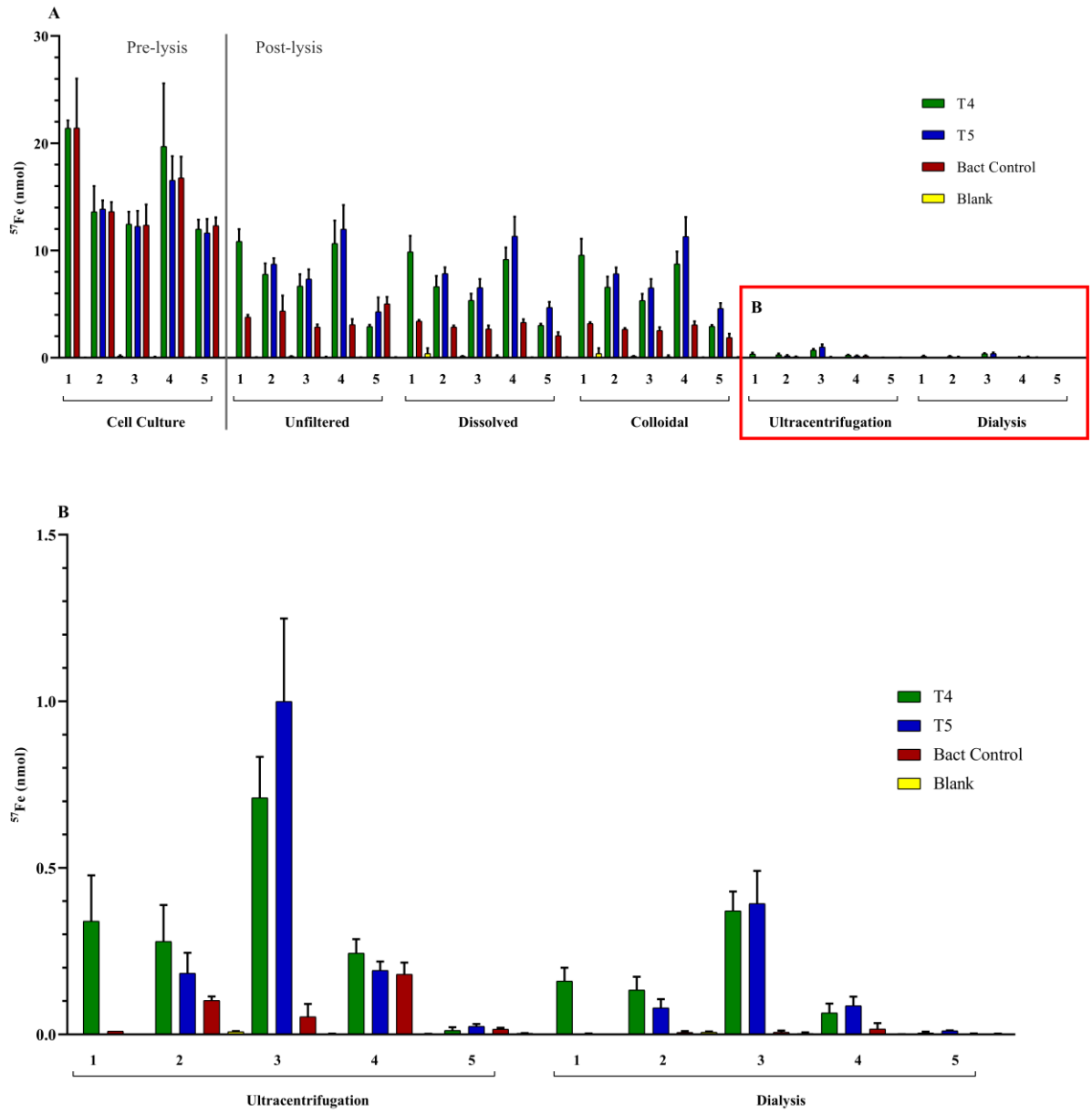

*Figure 8: ^{57}Fe (nmol) content pre-lysis and post-lysis through each phage purification step of all experimental iterations (**Part A**). Green represents the average of triplicate samples infected with phage T4, blue is the average of triplicate T5 samples, red is the average of triplicate bacterial lysis control samples (Bact Control), and yellow is the average of triplicate media blank samples. **Part B**: Enlarged view of the last two phage purification steps (red box in Part A): the re-suspended sucrose ultracentrifugation pellet and post-dialysis fractions. Error bars represent standard deviation between triplicate samples. Values for rounds 2, 3, and 4 are the average of six samples (two analytical datasets of triplicate samples).*

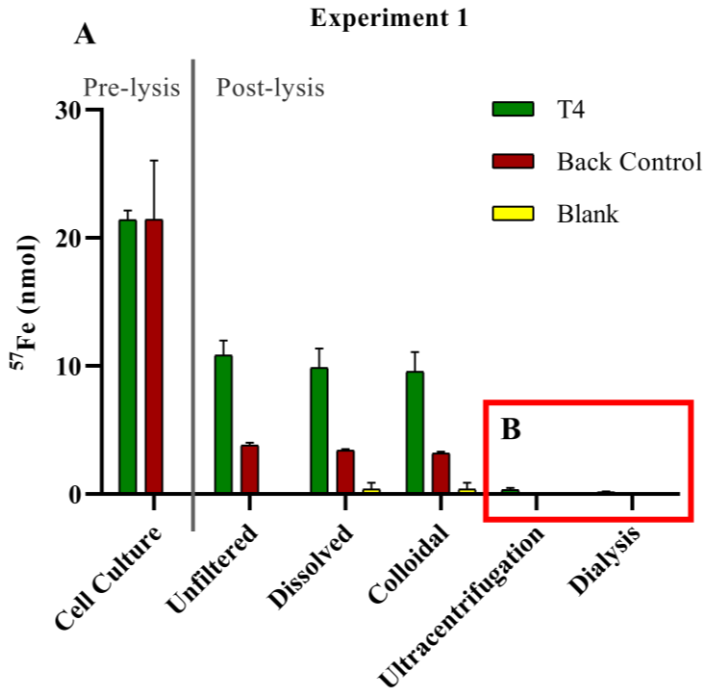
A
Experiment 1
Pre-lysis
Post-lysis
T4
Back Control
Blank
^{57}Fe (nmol)
30
20
10
0
B
Cell Culture
Unfiltered
Dissolved
Colloidal
Ultracentrifugation
Dialysis

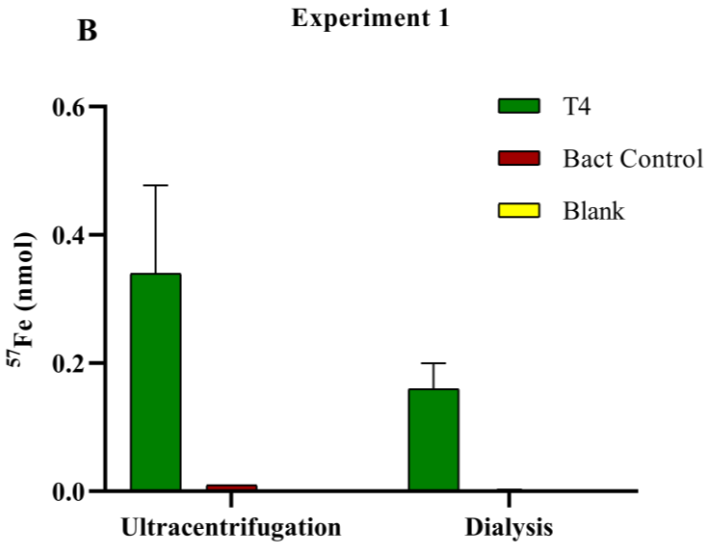
B
Experiment 1
T4
Bact Control
Blank
^{57}Fe (nmol)
0.6
0.4
0.2
0.0
Ultracentrifugation
Dialysis

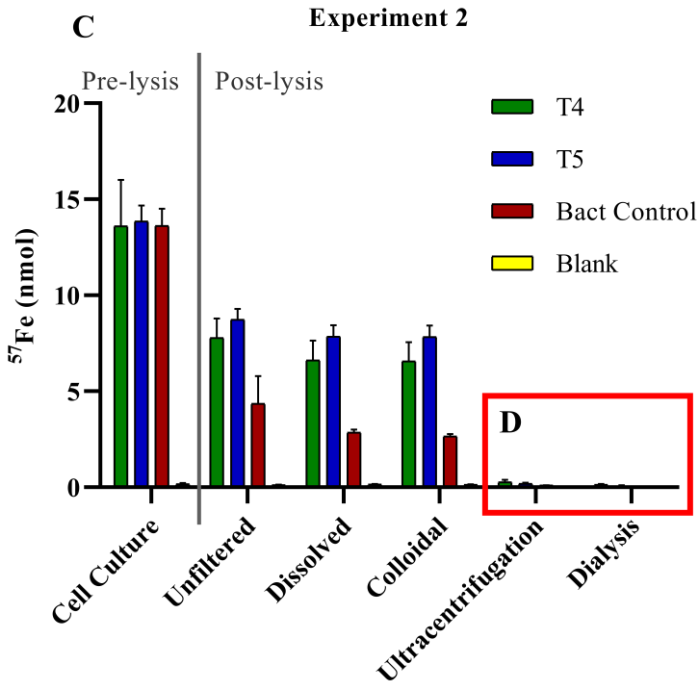
C
Experiment 2
Pre-lysis
Post-lysis
T4
T5
Bact Control
Blank
^{57}Fe (nmol)
20
15
10
5
0
D
Cell Culture
Unfiltered
Dissolved
Colloidal
Ultracentrifugation
Dialysis

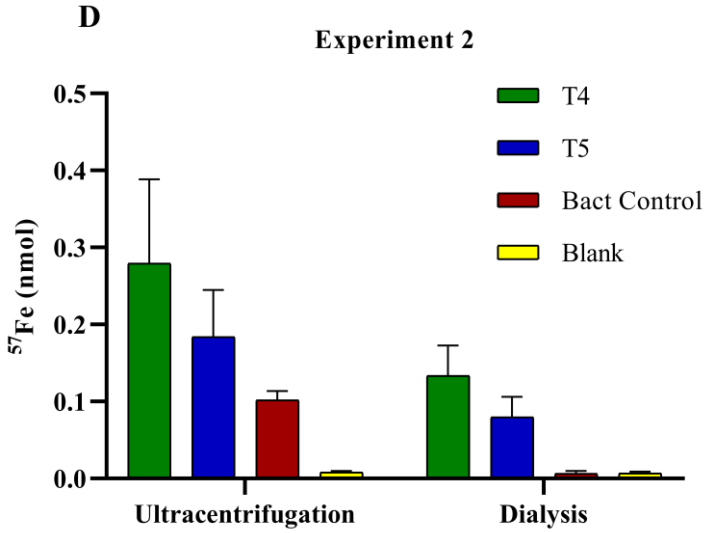
D
Experiment 2
T4
T5
Bact Control
Blank
^{57}Fe (nmol)
0.5
0.4
0.3
0.2
0.1
0.0
Ultracentrifugation
Dialysis

FIGURE 9 CONTINUED

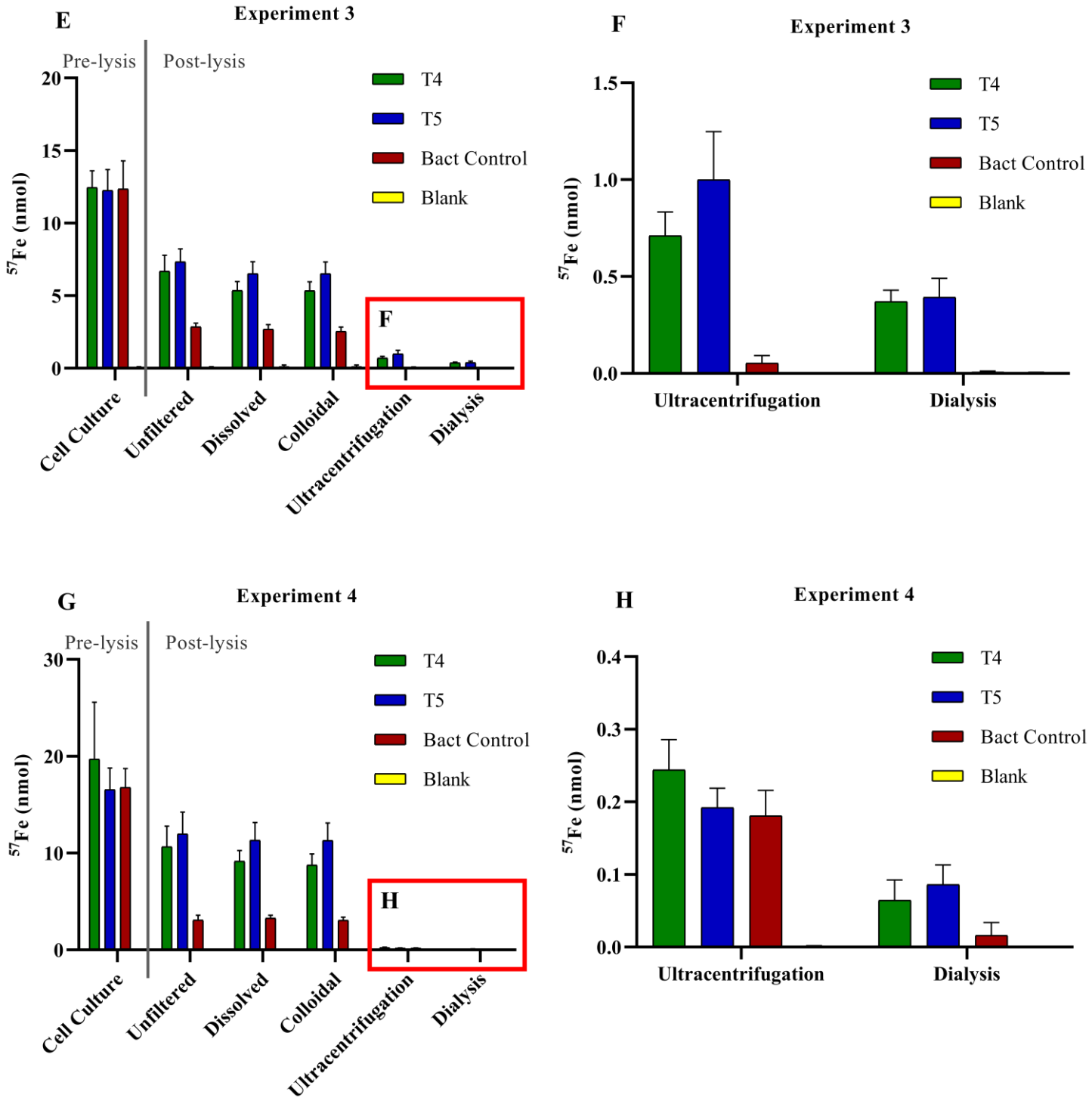

FIGURE 9 CONTINUED

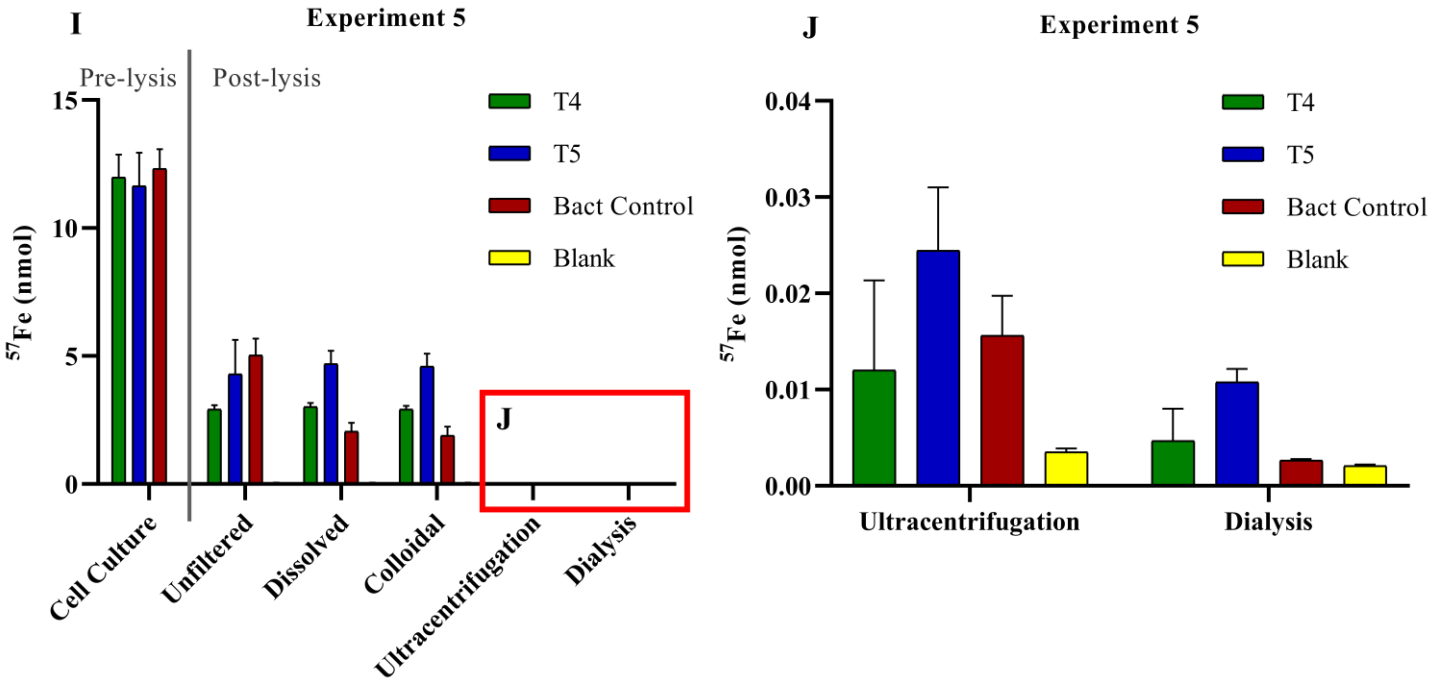

Figure 9: ^{57}Fe (nmol) content pre-lysis (prior to phage infection or chloroform treatment) and post-lysis through each phage purification step separated by experimental round. Green represents the average of triplicate samples infected with phage T4, blue is the average of triplicate T5 samples, red is the average of triplicate bacterial lysis control samples, and yellow is the average of triplicate experimental blank samples for Experiments 1 & 5. Experiments 2, 3, and 4 are the average of triplicate samples from both analytical datasets (6 values total). Parts A, C, E, G, I: ^{57}Fe content of each purification step for experiments 1-5; Parts B, D, F, H, J: Enlarged view of the last two phage purification steps (red box in Part A, C, E, G, I), the re-suspended sucrose ultracentrifugation pellet and post-dialysis fractions. Error bars represent standard deviation between triplicate samples.

Bacterial and Phage Quantification

SYBR Gold counts of bacterial cell density pre-lysis ranged from 1.7 x 10^7 bacteria/mL to 3.5 x 10^8 bacteria/mL for all five rounds of the experiment (**Figure 10**). SYBR Gold counts of fully purified phage samples post-dialysis ranged in abundance from 1.72 x 10^{10} to 3.2 x 10^{11} viral-like particles (VLPs) per sample for all five rounds of the experiment (**Figure 11**). While

viral lysis releases multiple progeny phage per infected host cell, sucrose ultracentrifugation both purifies and concentrates the progeny phage. Both processes increase the number of phage per bacterial cell, resulting in VLP counts greater than one order of magnitude higher than the number of bacterial cells that were infected.

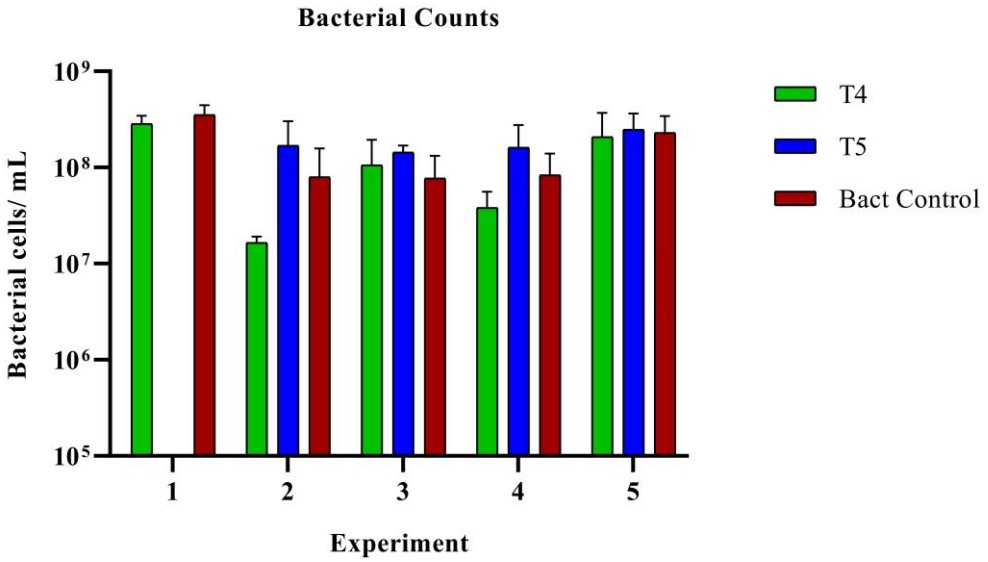

Figure 10: Bacterial concentrations for all iterations of the experiment pre-lysis (prior to phage infection or chloroform treatment). Bacterial cells were quantified after being stained by SYBR Gold nucleic acid stain and counted using an epifluorescence microscope. Bacterial concentrations were calculated in bacterial cells per milliliter of sample. Error bars represent standard deviation between triplicate samples.

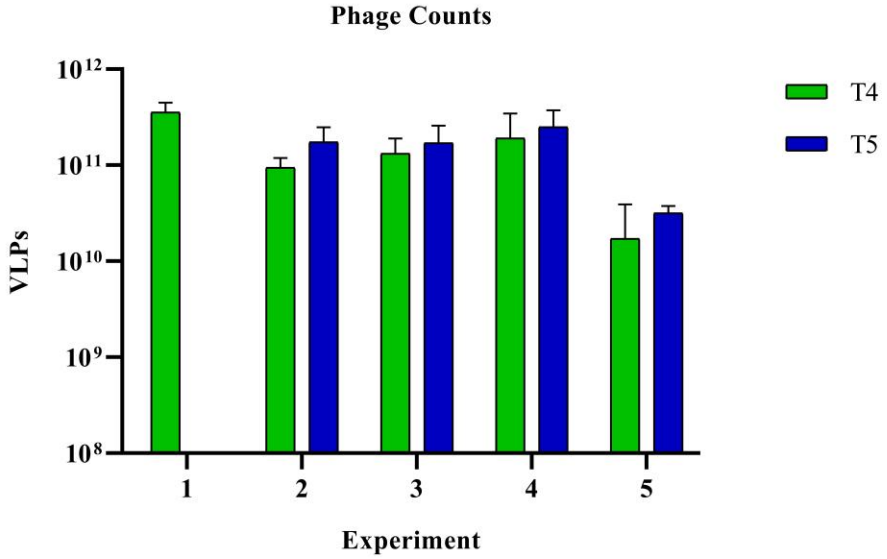

Figure 11: Phage counts for all iterations of the experiment after final dialysis purification step. Phages T4 and T5 were quantified as viral-like particles (VLPs) after being stained with SYBR Gold nucleic acid stain and counted using an epifluorescence microscope. Error bars represent standard deviation between triplicate samples.

Fluctuations in bacterial and phage concentrations calculated for samples within the same experiment could be due to the SYBR Gold method for quantification. A sample is diluted 1:100 times for bacterial cells or 1:1000 (even 1:10,000 for highly concentrated samples) for phage samples, and filtered onto a 0.02 µm filter then stained with SYBR Gold (see **Bacterial and Phage Quantification**). Under an epifluorescence microscope, ten frames are taken and counted for bacterial cells or VLPs. The average of the counts is then multiplied by a conversion factor (31,915), which accounts for the area of the counting frame relative to the surface area the sample was filtered onto, and then multiplied by the dilution factor (100 for bacteria, and 1,000 or 10,000 for phage). Therefore, small differences in the number of cells or VLPs counted per frame between triplicate samples can result in a relatively large range in concentrations.

Phages preserved in 1% formalin for longer than one week before quantification were tested for degradation (Parvathi et al., 2011). Samples of phage T4 from Experiment 1 and 2 that

were stored in 4 ˚C for one and three months, respectively, were then diluted, filtered, and stained with SYBR Gold for epifluorescence microcopy. The number of VLPs quantified for phage T4 samples from Experiment 1 and 2 were slightly lower after storage for 1-3 months but were within the same order of magnitude as freshly quantified samples (**Figure 12**). Following concentration by sucrose ultracentrifugation, the phage samples contained high concentrations of VLPs, perhaps contributing to the stability of the phage particles over long-term storage in 4 ˚C (Bonilla et al., 2016).

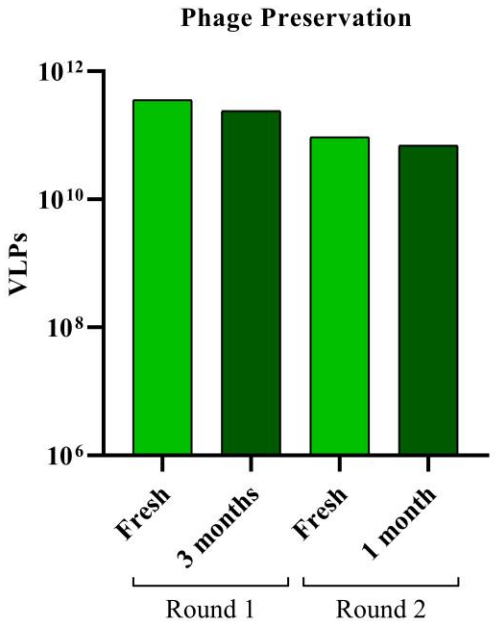

Figure 12: Phage counts before and after long-term storage in 1% formalin at 4 ˚C. Phage T4 from Experiment 1 was quantified by SYBR gold nucleic acid stain and counted using an epifluorescence microscope less than one week after purification (fresh) and 1-3 months after storage.

^{57}Fe per Bacterial Cell or Phage

The number of ^{57}Fe atoms per *E. coli* cell was calculated by multiplying the amount of ^{57}Fe (nmol) measured in the pre-lysis bacterial samples using the XR-ICP-MS by Avogadro's constant (6.022×10^{23} atoms/mol, and dividing by the number of bacteria counted using SYBR Gold nucleic acid stain and

epifluorescence microscopy (**Figure 13**). The number of ^{57}Fe atoms per *E. coli* cell ranged from 2.65 x 10^7 ± 4.96 x 10^6 to 4.83 x 10^8 ± 4.05 x 10^7 ^{57}Fe atoms/ cell for all rounds of the experiment (**Table 6**).

The number of ^{57}Fe atoms per phage was calculated by multiplying the amount of ^{57}Fe measured in the final dialyzed phage T4 or T5 fractions by Avogadro's constant, and dividing by the number of viral-like particles counted in that sample (**Figure 14**). The resulting number ^{57}Fe atoms per phage ranged from 166 to 2,269 ^{57}Fe atoms per phage (**Table 6**).

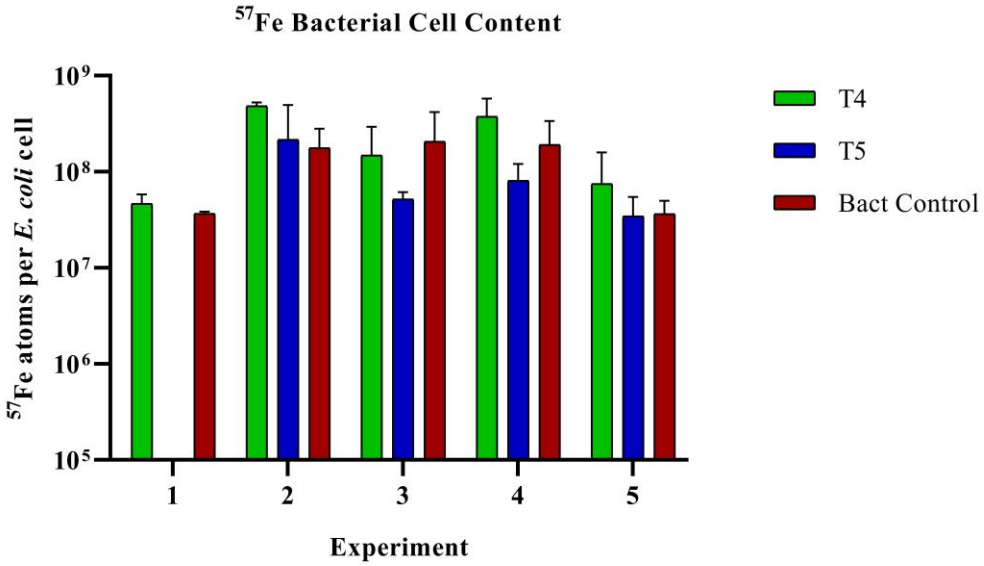

Figure 13: ^{57}Fe atom content per E. coli cell (pre-lysis) for each of the rounds of experimentation. Bacterial counts determined by SYBR Gold nucleic acid stain and epifluorescence microscopy. ^{57}Fe values determined by ICP-MS. Error bars represent standard deviation between triplicate samples.

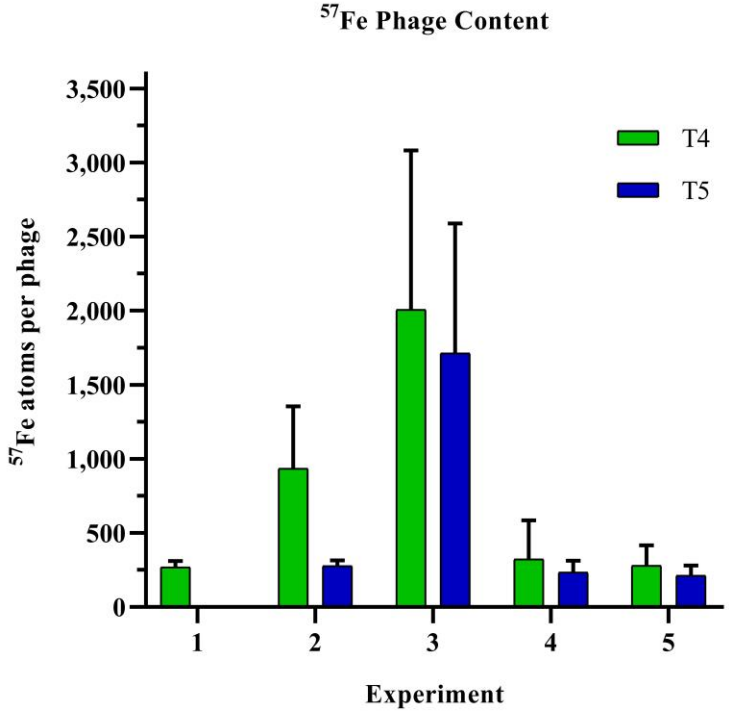

Figure 14: ^{57}Fe atom content per phage (final dialyzed) for each of the rounds of experimentation. Viral-like particles were quantified by SYBR Gold nucleic acid stain and epifluorescence microscopy. ^{57}Fe values determined by ICP-MS. Error bars represent standard deviation between triplicate samples.

Table 6: ^{57}Fe atom content per E. coli cell (pre-lysis) or phage (final dialyzed) for each of the rounds of experimentation. Bacterial cells and viral-like particles were quantified by SYBR Gold nucleic acid stain and epifluorescence microscopy. ^{57}Fe values determined by XR ICP-MS.

Round	Bacterial Sample	^{57}Fe atoms/ bacterial cell	Phage	^{57}Fe atoms/phage
1	T4	$4.68 \times 10^7 \pm 9.29 \times 10^6$	T4	270 ± 34
	Bact. Control	$3.68 \times 10^7 \pm 1.32 \times 10^6$	-	-
2	T4	$4.38 \times 10^8 \pm 4.05 \times 10^7$	T4	1195 ± 135
	T5	$3.47 \times 10^7 \pm 7.92 \times 10^5$	T5	278 ±34
	Bact. Control	$2.44 \times 10^8 \pm 1.25 \times 10^7$	-	-
3	T4	$5.73 \times 10^7 \pm 2.23 \times 10^7$	T4	1320 ± 114
	T5	$5.21 \times 10^7 \pm 8.65 \times 10^6$	T5	2269 ± 177
	Bact. Control	$6.98 \times 10^7 \pm 6.99 \times 10^6$	-	-
4	T4	$3.76 \times 10^8 \pm 1.83 \times 10^8$	T4	166 ± 90
	T5	$8.08 \times 10^7 \pm 3.64 \times 10^7$	T5	234 ±71
	Bact. Control	$1.90 \times 10^8 \pm 1.47 \times 10^8$	-	-
5	T4	$2.65 \times 10^7 \pm 4.96 \times 10^6$	T4	279 ± 112
	T5	$3.46 \times 10^7 \pm 1.64 \times 10^7$	T5	214 ±54
	Bact. Control	$3.65 \times 10^7 \pm 1.09 \times 10^7$	-	-

Expected quantities of iron atoms found within an *E. coli* cell are 10^5-10^6 iron atoms per cell, depending on growth conditions (Andrews et al., 2003; Semsey et al., 2006). The *E. coli* cell cultures were not iron-limited for these experiments. Iron limitation for *E. coli* is below sub-micromolar concentrations, while the M9 minimal media used contained between 1.9 ± 0.05 µM to 6.0 ± 0.3 µM ^{57}Fe for all iterations (Hartmann and Braun, 1981). The higher number of iron atoms measured in these experiments (10^7- 10^8 ^{57}Fe atoms per cell) could be due to the iron replete media conditions.

The first goal of this study was to quantify *the amount of iron incorporated into progeny phages*. Forty-two iron atoms are expected in each T4 virion based on the seven paired histidine iron-binding motifs found in each of the six phage tail fibers (Bartual et al. 2010). This total presumes that there are no other iron-binding motifs in the various proteins that make up the rest of the phage tail or capsid, and that there is not any iron sticking to the outside of the phage particle. Phage T4 samples had a range of 166 ± 90 to 1320 ± 114 ^{57}Fe atoms per phage, and T5 had an average of 214 ± 54 to 2269 ± 177 ^{57}Fe atoms per phage for all samples (**Figure 13, Table 5**). Across all iterations of the experiment there was not a consistent difference in the number of ^{57}Fe atoms between phages T4 and T5 (**Table 5**).

Individual Samples from Round 5

An equipment malfunction during Experiment 5 of the experiment provided interesting results. During the sucrose purification step, the ultracentrifuge rose in temperature causing some of the ultracentrifuge tubes containing phage T4 or T5 to partially collapse. The pelleted phage T4 particles for samples A, B, and C were still able to be re-suspended and dialyzed, however samples A and B resulted in an order of magnitude lower phage abundance (4.49 x 10^9 & 4.76 x 10^9 VLPs, respectively) than sample C (4.24 x 10^{10} VLPs; **Table 7**). Samples of phage T5 (M, N,

and O) had better recovery with an average of $3.16 \times 10^{10} \pm 4.78 \times 10^{9}$ VLPs. Higher standard deviations for phage T4 samples (**Figure 9J & Table 7**) warranted a closer look at those individual samples.

When comparing the Experiment 5 final dialyzed samples of phage T4 individually (**Figure 15**), the ^{57}Fe content of the samples with the lower recovered phage abundance (A and B) have less ^{57}Fe measured than the sample from which more phage was recovered (C). Although this was an error, it is notable that the lower phage titers of samples A & B had correspondingly low amounts of ^{57}Fe when compared to sample C. The number of ^{57}Fe atoms per phage for sample C is about half that of sample A or B, but that is likely due to the order of magnitude higher number of phage quantified by SYBR Gold staining and epifluorescence. Being a much less precise method for quantification, it is difficult to directly compare SYBR Gold counts for phages to that of the XR ICP-MS analyses for trace metal concentrations.

Table 7: Phage counts for individual final dialyzed samples from Round 5. Phages T4 and T5 were quantified as viral-like particles (VLPs) after being stained by SYBR Gold nucleic acid stain and counted using an epifluorescence microscope.

Phage	**Sample**	**Phage Titer (VLPs)**	**^{57}Fe atoms per phage**
T4	A	4.49×10^{9}	376
	B	4.76×10^{9}	340
	C	4.24×10^{10}	122
T5	M	2.54×10^{10}	290
	N	3.25×10^{10}	177
	O	3.70×10^{10}	174

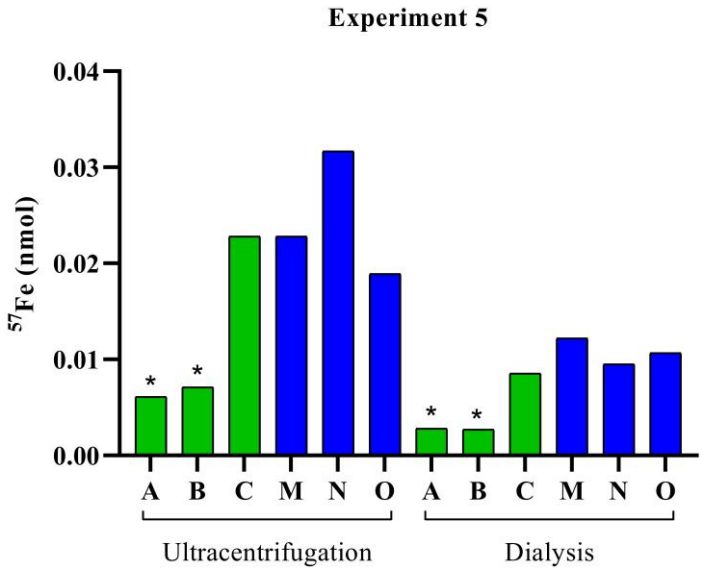

Figure 15: The ^{57}Fe content in Experiment 5 phage T4 and T5 individual samples after the sucrose and dialysis purification steps. Samples A & B with lower phage recovery from sucrose ultracentrifugation are indicated by (*).

Source of ^{57}Fe to Progeny Phage

After growing to mid-logarithmic phase and before lysing by phage infection or chloroform treatment, the repeatedly rinsed bacterial cells were centrifuged a final time to pellet. The ^{57}Fe content re-suspended bacterial cell pellet constitutes the $^{57}Fe_{TOTAL}$, while the supernatant refers to the excess media above the cell culture pellet after centrifugation. The cell culture pellet is calculated by taking the difference between the re-suspended pellet and the supernatant. The ^{57}Fe content within the cell culture pellet comprised approximately >93% of the $^{57}Fe_{TOTAL}$ across all experimental rounds while the supernatant comprised 7% or less of the $^{57}Fe_{TOTAL}$ for all samples (**Figure 16**).

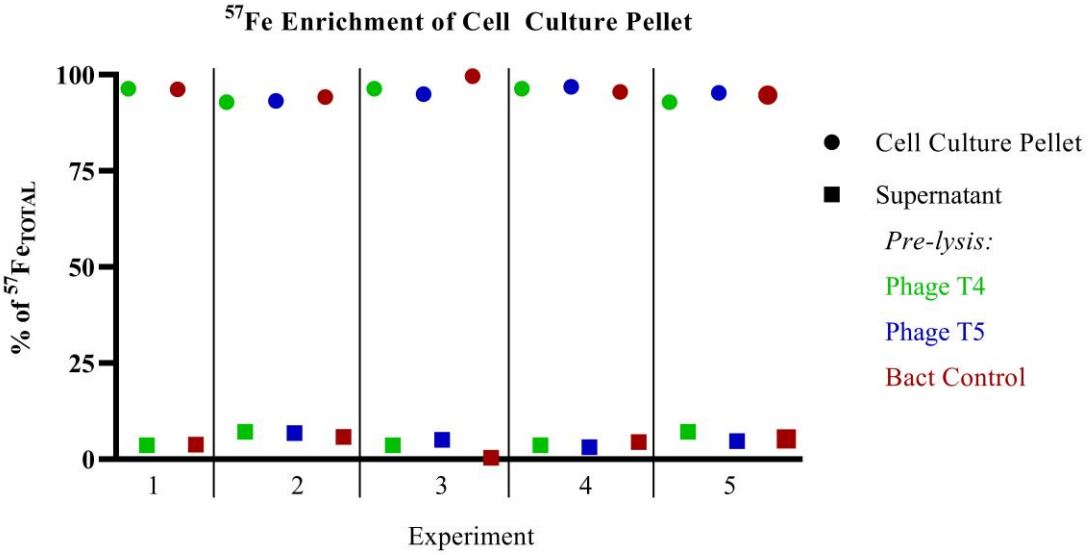

Figure 16: The percentage of ^{57}Fe within the bacterial pellet or supernatant compared to the $^{57}Fe_{TOTAL}$ (^{57}Fe measured in re-suspended cell culture pellet) for rinsed bacterial cells in all experiments. Supernatant refers to any excess ^{57}Fe remaining in the media after centrifugation and pelleting of bacterial cells. Cell culture pellet refers to the ^{57}Fe content of the re-suspended cell culture pellet minus that of the supernatant.

The second goal of this study was to determine *whether the iron in progeny phages originates from within the bacterial host cell.* The proportion of ^{57}Fe in the bacterial pellet or in the media supernatant following centrifugation was compared to the total amount of ^{57}Fe ($^{57}Fe_{TOTAL}$) in the bacterial pellet re-suspended in the media (**Figure 16**). For all rounds of the experiment, greater than 93% of the $^{57}Fe_{TOTAL}$ was accounted for by the bacterial cells, indicating the source of the ^{57}Fe to the progeny phage was likely from inside of the bacterial cell and not from the surrounding media, which accounted for less than 7% of the $^{57}Fe_{TOTAL}$. Phage assembly takes place within the cytoplasm of the host bacterial cell (Aksyuk and Rossmann, 2011) and the folding of proteins would likely incorporate iron from host storages into tail fiber proteins at this time, as the surrounding environment could contain much lower concentrations of bioavailable iron.

Table 8: Proportion of ^{57}Fe from cell culture to each of the size fractions and final dialyzed phage samples. Average and standard deviations calculated across all experimental iterations, with the exclusion of Experiment 5 values for the T4 and T5 samples.

Sample	Dissolved	Colloidal	Soluble	Dialyzed
T4	45.5 ± 2.37%	45.7 ± 2.35%	0.85 ± 0.62%	1.26 ± 1.01%
T5	59.6 ± 6.33%	59.5 ± 6.30%	0.57 ± 0.68%	1.43 ± 1.25%
Bact Control	19.8 ± 2.17 %	18.5 ± 2.03%	1.27 ± 0.20%	0.04 ± 0.03%

The proportion of ^{57}Fe from the host cells that remained in each size fraction was calculated by dividing the starting cell culture ^{57}Fe content by the ^{57}Fe content measured in the dissolved, colloidal, and soluble fractions (**Table 8**). For phages T4 and T5, ~45% of the ^{57}Fe in the original cell culture was retained in the dissolved fraction and the majority is colloidal in size, while <1% was retained in the soluble fraction. For the bacterial control, ~20% of the original cell culture was retained in in the dissolved fraction, while ~19% was colloidal and ~1.5% was soluble (**Table 8**).

The proportion of ^{57}Fe from the original cell culture samples that was associated with purified progeny phages was calculated by dividing the ^{57}Fe content measured in final dialyzed phage T4 or T5 samples by the ^{57}Fe measured in their respective bacterial cell culture samples pre-lysis. For all phage T4 infections (except for Experiment 5), the amount of ^{57}Fe incorporated into progeny phage was 1.26 ± 1.01% of the iron released from host cell lysis and 1.43 ± 1.25% for phage T5. Experiment 5 values were excluded from these averages due to inconsistencies in the amount of phage recovered (**Table 7**).

In the Ferrojan Horse Hypothesis, calculations based on average marine phage abundances with 42 iron atoms per phage and average iron quotas for marine heterotrophic bacterial cells, it was estimated that marine progeny phages could account for up to 14% of iron released from the bacterial host after lysis (**Appendix A**). However, these estimates were based on the iron quota of 7,518 iron atoms per marine heterotrophic bacterial cell, which grows in an

iron-limited environment (Ducklow, 2000). *E. coli* cells grown in iron-replete media are not limited by iron, and can accumulate orders of magnitude more iron atoms than a marine bacterium (Andrews et al., 2003). Therefore, if marine viral lysis releases new progeny phage with hundreds to thousands of iron atoms associated with each virion, then phages could have a significant impact on the amount of dissolved iron released for remineralization.

CHAPTER THREE:

CONCLUSIONS AND FUTURE DIRECTIONS

Conclusions

The Ferrojan Horse Hypothesis proposes that viruses comprise a proportion of the organic iron-binding ligands within the dissolved fraction of seawater. Additionally, iron in phages could be used to gain access to siderophore-bound iron uptake receptors on the cell surface of bacterial hosts, serving as a "Trojan horse" for infection. Once infected, the host cell replicates new progeny phage within the cytoplasm. If iron from host storages is packaged into progeny phage tail fibers, then lysis would release less bioavailable iron than previously thought. Since viruses are the most abundant biological entities in the ocean, such interactions with iron could have a significant impact on oceanic iron-cycling.

The evidence for iron associated with phages came from studies of non-marine model systems, which made *E. coli* and its associated phages the ideal system to develop methods to test aspects of the Ferrojan Horse Hypothesis. Cultures of *E. coli* grown in media with ^{57}Fe were infected with phage T4 or T5 and the phages were purified by centrifugation, filtration, sucrose ultracentrifugation, and dialysis. Controls of bacteria lysed by chloroform treatment instead of phage infection were included to account for other colloidal ^{57}Fe from the bacterial cells that could co-purify with phage particles. Bacteria pre-lysis and phages post-purification were quantified by nucleic acid staining and microscopy, while trace metals were quantified by ICP-MS.

The methods developed in this thesis revealed the incorporation of ^{57}Fe into both T4 and T5 progeny phages. Following each purification step post-lysis, T4 and T5 samples contained significantly more ^{57}Fe (as determined by t-test) than the bacterial controls. This demonstrates the association of ^{57}Fe atoms with progeny phage. Between phages T4 and T5, the ^{57}Fe content in final dialyzed samples was not significantly different for all rounds of the experiment. Although phage T5 does not contain the paired histidine iron-binding motifs known to bind iron in phage T4 tail fibers, these results suggest that similar quantities of iron are associated with phage T5 despite the lack of analogous structural evidence.

The number of ^{57}Fe atoms per progeny phage was calculated to be between 100-300 iron atoms per phage in 6 out of 9 of the T4 and T5 purified phage samples for all iterations of the experiment. In the other 3 experiments the T4 and T5 samples contained between 1,000-3,000 ^{57}Fe atoms per phage. While higher than the 42 iron atoms predicted per phage based on the paired histidine iron-binding motifs in T4 tail fibers, there could be additional iron-binding motifs that have yet to be characterized or iron that is associated with various phage surfaces. The iron associated with progeny phages was likely to have originated from within the bacterial host cell, as bacterial cells comprised greater than 91% of the total ^{57}Fe in pre-lysis bacterial suspensions. These tracing of ^{57}Fe from the bacterial host to phage experiments require further repetitions to generate more robust results.

Future Directions

This thesis lays the foundation towards future testing of the Ferrojan Horse Hypothesis in a marine phage-host system. Culturable marine bacteria are generally more slow-growing than enteric bacteria and marine phage-host systems that have been cultured comprise only a small portion of the overall bacterial and viral diversity in the oceans. Applying the ^{57}Fe tracing to

progeny phage experimental methods developed here for *E. coli* to a marine bacterial system would require a defined seawater minimal media prepared with ^{57}Fe as the sole iron source. Bacterial growth and infection times could vary, but the rinsing of bacterial cells and subsequent post-lysis purification steps could likely remain the same.

Vibrio are a genus of fast-growing, well-characterized, ubiquitous, marine bacterial pathogens and are ideal for a host model system from the ocean. Recently, 251 *Vibrio* phage genome annotations were published (Kauffman et al., 2018a). Selecting a few phages and a sensitive *Vibrio* strain would be the logical next step in applying the methods put forth in this thesis to test the Ferrojan Horse Hypothesis. The *Vibrio* phage collection could even be screened for both phages that contain and do not contain paired histidine or cysteine iron-binding motifs for comparison. Additionally, the use of a non-tailed phage would provide insight into whether the ^{57}Fe measured in phage fractions is due solely to tail proteins or if there are other ^{57}Fe-associated phage proteins contributing to the ^{57}Fe enrichment.

If marine *Vibrio* phages provide similar results to that of the Tracing of ^{57}Fe from *E. coli* to Phages T4 and T5 experiments, then perhaps other marine phages complex iron as well. As suggested in the Ferrojan Horse Hypothesis, phage-bound iron falls within the colloidal size fraction (0.02-0.2 μm) of dissolved iron and organic iron-binding ligands, most of which remain largely uncharacterized (**Appendix A**). It is unknown whether the iron bound to phages could be exchanged with well-characterized iron-binding ligands like siderophores, but this could be tested experimentally. In a recent study by Caputi et al. (2018), metagenomes from *Tara Oceans* were mined for tail proteins and baseplate assembly proteins containing HxH motifs, as well as tail tip proteins containing iron-sulfur cluster proteins. The paired histidine motifs were found in 87% of marine viral tail proteins, 47% of baseplate assembly proteins, and 12% of tail tip

proteins (Caputi et al., 2018). It is promising that phage iron-binding proteins are widely conserved across the oceans and suggests that viruses may significantly contribute to colloidal iron pools.

The source of phage-associated iron has implications for oceanic iron biogeochemical cycling as well. If *Vibrio* phages are shown to acquire iron from host storages as evidenced with phages T4 and T5, then a portion of the dissolved iron released from the host after phage lysis would be incorporated in phage particles instead of available for remineralization. Additionally, the iron associated with phages collected in this size fraction would still contribute to the colloidal dissolved iron pool. In this study, less than 1.5% of the iron from host storages was recycled into new phage progeny for either phage T4 or T5. However, in these experiments the *E. coli* cultures were not limited by iron as many marine bacteria can be, therefore the recycling of iron into progeny marine phage could comprise a much larger proportion of the dissolved iron released into the ocean through viral lysis.

REFERENCES

Ackermann, H.-W. (2007). 5500 Phages examined in the electron microscope. Archives of Virology *152*, 227-243.

Ackermann, H.-W. (2009). Phage classification and characterization. In Bacteriophages (Springer), pp. 127-140.

Ackermann, H.-W. (2012). Bacteriophage electron microscopy. In Advances in Virus Research (Elsevier), pp. 1-32.

Aksyuk, A.A., and Rossmann, M.G. (2011). Bacteriophage assembly. Viruses *3*, 172-203.

Andrews, S.C. (1998). Iron storage in bacteria. In Advances in Microbial Physiology (Elsevier), pp. 281-351.

Andrews, S.C., Robinson, A.K., and Rodríguez-Quiñones, F. (2003). Bacterial iron homeostasis. FEMS Microbiology Reviews *27*, 215-237.

Atkinson, A., and Guerinot, M.L. (2011). Metal transport. In The Plant Plasma Membrane (Springer), pp. 303-330.

Azam, F., Fenchel, T., Field, J.G., Gray, J., Meyer-Reil, L., and Thingstad, F. (1983). The ecological role of water-column microbes in the sea. Marine Ecology Progress Series *10*, 257-263.

Baltimore, D. (1971). Expression of animal virus genomes. Bacteriological Reviews *35*, 235.

Barbeau, K., Rue, E.L., Trick, C.G., Bruland, K.T., and Butler, A. (2003). Photochemical reactivity of siderophores produced by marine heterotrophic bacteria and cyanobacteria based on characteristic Fe (III) binding groups. Limnology and Oceanography *48*, 1069-1078.

Bartual, S.G., Otero, J.M., Garcia-Doval, C., Llamas-Saiz, A.L., Kahn, R., Fox, G.C., and van Raaij, M.J. (2010). Structure of the bacteriophage T4 long tail fiber receptor-binding tip. Proceedings of the National Academy of Sciences *107*, 20287-20292.

Bergh, Ø., BØrsheim, K.Y., Bratbak, G., and Heldal, M. (1989). High abundance of viruses found in aquatic environments. Nature *340*, 467.

Bergquist, B.A., Wu, J., and Boyle, E.A. (2007). Variability in oceanic dissolved iron is dominated by the colloidal fraction. Geochimica Et Cosmochimica Acta *71*, 2960-2974.

Boiteau, R.M., Mende, D.R., Hawco, N.J., McIlvin, M.R., Fitzsimmons, J.N., Saito, M.A., Sedwick, P.N., DeLong, E.F., and Repeta, D.J. (2016). Siderophore-based microbial adaptations to iron scarcity across the eastern Pacific Ocean. Proceedings of the National Academy of Sciences *113*, 14237-14242.

Bonilla, N., Rojas, M.I., Cruz, G.N.F., Hung, S.-H., Rohwer, F., and Barr, J.J. (2016). Phage on tap–a quick and efficient protocol for the preparation of bacteriophage laboratory stocks. PeerJ *4*, e2261.

Børsheim, K., Bratbak, G., and Heldal, M. (1990). Enumeration and biomass estimation of planktonic bacteria and viruses by transmission electron microscopy. Applied and Environmental Microbiology *56*, 352-356.

Boyd, P.W., Jickells, T., Law, C., Blain, S., Boyle, E., Buesseler, K., Coale, K., Cullen, J., De Baar, H.J., and Follows, M. (2007). Mesoscale iron enrichment experiments 1993-2005: synthesis and future directions. Science *315*, 612-617.

Breitbart, M. (2012). Marine viruses: Truth or dare. Annual Review of Marine Science *4*, 425-448.

Breitbart, M., Bonnain, C., Malki, K., and Sawaya, N.A. (2018). Phage puppet masters of the marine microbial realm. Nature Microbiology *3*, 754-766.

Brown, M.B., and Forsythe, A.B. (1974). Robust tests for the equality of variances. Journal of the American Statistical Association *69*, 364-367.

Brum, J.R., Schenck, R.O., and Sullivan, M.B. (2013). Global morphological analysis of marine viruses shows minimal regional variation and dominance of non-tailed viruses. ISME Journal *7*, 1738-1751.

Brussaard, C.P. (2004). Viral control of phytoplankton populations—A review. Journal of Eukaryotic Microbiology *51*, 125-138.

Brussaard, C.P. (2009). Enumeration of bacteriophages using flow cytometry. In Bacteriophages (Springer), pp. 97-111.

Bundy, R.M., Biller, D.V., Buck, K.N., Bruland, K.W., and Barbeau, K.A. (2014). Distinct pools of dissolved iron-binding ligands in the surface and benthic boundary layer of the California Current. Limnology and Oceanography *59*, 769-787.

Calendar, R. (2012). The Bacteriophages, Vol 1 (Springer Science & Business Media).

Caputi, L., Carradec, Q., Eveillard, D., Kirilovsky, A., Pelletier, E., Pierella Karlusich, J.J., Rocha Jimenez Vieira, F., Villar, E., Chaffron, S., and Malviya, S. (2018). Community-level responses to iron availability in open ocean planktonic ecosystems. Global Biogeochemical Cycles, 391-419.

Chen, F., Lu, J.-r., Binder, B.J., Liu, Y.-c., and Hodson, R.E. (2001). Application of digital image analysis and flow cytometry to enumerate marine viruses stained with SYBR Gold. Applied and Environmental Microbiology *67*, 539-545.

Cullen, J.T., Bergquist, B.A., and Moffett, J.W. (2006). Thermodynamic characterization of the partitioning of iron between soluble and colloidal species in the Atlantic Ocean. Marine Chemistry *98*, 295-303.

Dauphas, N., and Rouxel, O. (2006). Mass spectrometry and natural variations of iron isotopes. Mass Spectrometry Reviews *25*, 515-550.

Dlusskaya, E.A., Atrazhev, A.M., and Ashbolt, N.J. (2019). Colloid chemistry pitfall for flow cytometric enumeration of viruses in water. Water Research X, 100025.

Ducklow, H. (2000). Bacterial production and biomass in the oceans. In Microbial Ecology of the Oceans, D.L. Kirchman, ed. (New York: Wiley-Liss Inc.), pp. 85-120.

Ducklow, H.W., Steinberg, D.K., and Buesseler, K.O. (2001). Upper ocean carbon export and the biological pump. Oceanography Society *14*, 50-58.

Fischer, A., Kroon, J., Verburg, T., Teunissen, T., and Wolterbeek, H.T. (2007). On the relevance of iron adsorption to container materials in small-volume experiments on iron marine chemistry: 55Fe-aided assessment of capacity, affinity and kinetics. Marine Chemistry *107*, 533-546.

Fitzsimmons, J.N., and Boyle, E.A. (2014). Both soluble and colloidal iron phases control dissolved iron variability in the tropical North Atlantic Ocean. Geochimica Et Cosmochimica Acta *125*, 539-550.

Fitzsimmons, J.N., Bundy, R.M., Al-Subiai, S.N., Barbeau, K.A., and Boyle, E.A. (2015). The composition of dissolved iron in the dusty surface ocean: An exploration using size-fractionated iron-binding ligands. Marine Chemistry *173*, 125-135.

Franck, V.M., Bruland, K.W., Hutchins, D.A., and Brzezinski, M.A. (2003). Iron and zinc effects on silicic acid and nitrate uptake kinetics in three high-nutrient, low-chlorophyll (HNLC) regions. Marine Ecology Progress Series *252*, 15-33.

Fuhrman, J.A. (1999). Marine viruses and their biogeochemical and ecological effects. Nature *399*, 541-548.

Gledhill, M., and Buck, K.N. (2012). The organic complexation of iron in the marine environment: a review. Frontiers in Microbiology *3*, 69.

Gledhill, M., and Van Den Berg, C.M.G. (1994). Determination of complexation of iron (III) with natural organic complexing ligands in seawater using cathodic stripping voltammetry. Marine Chemistry *47*, 41-54.

Hänsch, R., and Mendel, R.R. (2009). Physiological functions of mineral micronutrients (Cu, Zn, Mn, Fe, Ni, Mo, B, Cl). Current Opinion in Plant Biology *12*, 259-266.

Hantke, K., and Braun, V. (1978). Functional interaction of TonA-TonB receptor system in *Escherichia-coli*. Journal of Bacteriology *135*, 190-197.

Hartmann, A., and Braun, V. (1981). Iron uptake and iron limited growth of *Escherichia coli* K-12. Archives of Microbiology *130*, 353-356.

Hendrix, R.W. (2002). Bacteriophages: evolution of the majority. Theoretical Population Biology *61*, 471-480.

Hershey, A.D., and Chase, M. (1952). Independent functions of viral protein and nucleic acid in growth of bacteriophage. Journal of General Physiology *36*, 39-56.

Hunter, K.A., and Boyd, P.W. (2007). Iron-binding ligands and their role in the ocean biogeochemistry of iron. Environmental Chemistry *4*, 221-232.

Hurwitz, B.L., Deng, L., Poulos, B.T., and Sullivan, M.B. (2013). Evaluation of methods to concentrate and purify ocean virus communities through comparative, replicated metagenomics. Environmental Microbiology *15*, 1428-1440.

Jessup, C.M., Kassen, R., Forde, S.E., Kerr, B., Buckling, A., Rainey, P.B., and Bohannan, B.J. (2004). Big questions, small worlds: microbial model systems in ecology. Trends in Ecology & Evolution *19*, 189-197.

Jiang, M., Barbeau, K.A., Selph, K.E., Measures, C.I., Buck, K.N., Azam, F., Mitchell, B.G., and Zhou, M. (2013). The role of organic ligands in iron cycling and primary productivity in the Antarctic Peninsula: A modeling study. Deep Sea Research Part II: Topical Studies in Oceanography *90*, 112-133.

Jover, L.F., Effler, T.C., Buchan, A., Wilhelm, S.W., and Weitz, J.S. (2014). The elemental composition of virus particles: implications for marine biogeochemical cycles. Nature Reviews Microbiology *12*, 519-528.

Kauffman, K.M., Brown, J.M., Sharma, R.S., VanInsberghe, D., Elsherbini, J., Polz, M., and Kelly, L. (2018a). Viruses of the Nahant Collection, characterization of 251 marine Vibrionaceae viruses. Scientific Data *5*.

Kauffman, K.M., Hussain, F.A., Yang, J., Arevalo, P., Brown, J.M., Chang, W.K., VanInsberghe, D., Elsherbini, J., Sharma, R.S., and Cutler, M.B. (2018b). A major lineage of non-tailed dsDNA viruses as unrecognized killers of marine bacteria. Nature *554*, 118.

Kranzler, C., Lis, H., Shaked, Y., and Keren, N. (2011). The role of reduction in iron uptake processes in a unicellular, planktonic cyanobacterium. Environmental Microbiology *13*, 2990-2999.

Kropinski, A.M., Mazzocco, A., Waddell, T.E., Lingohr, E., and Johnson, R.P. (2009). Enumeration of bacteriophages by double agar overlay plaque assay. In Bacteriophages (Springer), pp. 69-76.

Kuma, K., Nishioka, J., and Matsunaga, K. (1996). Controls on iron(III) hydroxide solubility in seawater: The influence of pH and natural organic chelators. Limnology and Oceanography *41*, 396-407.

Kutter, E., and Sulakvelidze, A. (2004). Bacteriophages: biology and applications (CRC Press).

Laber, C.P., Hunter, J.E., Carvalho, F., Collins, J.R., Hunter, E.J., Schieler, B.M., Boss, E., More, K., Frada, M., and Thamatrakoln, K. (2018). Coccolithovirus facilitation of carbon export in the North Atlantic. Nature Microbiology *3*, 537-547.

Laglera, L.M., and van den Berg, C.M.G. (2009). Evidence for geochemical control of iron by humic substances in seawater. Limnology and Oceanography *54*, 610-619.

Leiman, P., Kanamaru, S., Mesyanzhinov, V., Arisaka, F., and Rossmann, M. (2003). Structure and morphogenesis of bacteriophage T4. Cellular and Molecular Life Sciences *60*, 2356-2370.

Lill, R. (2009). Function and biogenesis of iron–sulphur proteins. Nature *460*, 831.

Lin, M., Hu, X., Pan, D., and Han, H. (2018). Determination of iron in seawater: from the laboratory to in situ measurements. Talanta *188*, 135-144.

Lindberg, A.A. (1973). Bacteriophage receptors. Annual Reviews in Microbiology *27*, 205-241.

Lis, H., and Shaked, Y. (2009). Probing the bioavailability of organically bound iron: a case study in the *Synechococcus*-rich waters of the Gulf of Aqaba. Aquatic Microbial Ecology *56*, 241-253.

Liu, X., and Millero, F.J. (2002). The solubility of iron in seawater. Marine Chemistry *77*, 43-54.

Luckey, M., Wayne, R., and Neilands, J.B. (1975). In vitro competition between ferrichrome and phage for outer membrane T5 receptor complex of *Escherichia coli*. Biochemical and Biophysical Research Communications *64*, 687-693.

Luria, S.E., and Anderson, T.F. (1942). The identification and characterization of bacteriophages with the electron microscope. Proceedings of the National Academy of Sciences *28*, 127.

Mancuso Nichols, C.A., Garon, S., Bowman, J.P., Raguenes, G., and Guezennec, J. (2004). Production of exopolysaccharides by Antarctic marine bacterial isolates. Journal of Applied Microbiology *96*, 1057-1066.

Martin, J.H., Gordon, M., and Fitzwater, S.E. (1991). The case for iron. Limnology and Oceanography *36*, 1793-1802.

Mawji, E., Gledhill, M., Milton, J.A., Tarran, G.A., Ussher, S., Thompson, A., Wolff, G.A., Worsfold, P.J., and Achterberg, E.P. (2008). Hydroxamate siderophores: occurrence and importance in the Atlantic Ocean. Environmental Science & Technology *42*, 8675-8680.

McCorquodale, D.J., and Warner, H.R. (1988). Bacteriophage T5 and related phages. In The Bacteriophages (Springer), pp. 439-475.

Moore, J.K., Doney, S.C., Glover, D.M., and Fung, I.Y. (2001). Iron cycling and nutrient-limitation patterns in surface waters of the World Ocean. Deep Sea Research Part II: Topical Studies in Oceanography *49*, 463-507.

Morel, F.M.M., Kustka, A.B., and Shaked, Y. (2008). The role of unchelated Fe in the iron nutrition of phytoplankton. Limnology and Oceanography *53*, 400-404.

Morel, F.M.M., and Price, N.M. (2003). The biogeochemical cycles of trace metals in the oceans. Science *300*, 944-947.

Noble, R.T., and Fuhrman, J.A. (1998). Use of SYBR Green I for rapid epifluorescence counts of marine viruses and bacteria. Aquatic Microbial Ecology *14*, 113-118.

Osborn, M.J., and Wu, H.C.P. (1980). Proteins of the outer-membrane of gram-negative bacteria. Annual Review of Microbiology *34*, 369-422.

Parikka, K.J., Le Romancer, M., Wauters, N., and Jacquet, S. (2017). Deciphering the virus-to-prokaryote ratio (VPR): insights into virus–host relationships in a variety of ecosystems. Biological Reviews *92*, 1081-1100.

Parvathi, A., Radhakrishnan, S., Sajila, M., and Jacob, B. (2011). Study of changes in bacterial and viral abundance in formaldehyde-fixed water samples by epifluorescence microscopy. Environment Monitoring and Assessment *177*, 227-231.

Rakhuba, D., Kolomiets, E., Dey, E.S., and Novik, G. (2010). Bacteriophage receptors, mechanisms of phage adsorption and penetration into host cell. Polish Journal of Microbiology *59*, 145-155.

Rue, E.L., and Bruland, K.W. (1995). Complexation of iron(III) by natural organic-ligands in the central north Pacific as determined by a new competitive ligand equilibration adsorptive cathodic stripping voltammetric method. Marine Chemistry *50*, 117-138.

Sallmann, F.R., Baveye-Descamps, S., Pattus, F., Salmon, V., Branza, N., Spik, G., and Legrand, D. (1999). Porins OmpC and PhoE of Escherichia coli as specific cell-surface targets of human lactoferrin - Binding characteristics and biological effects. Journal of Biological Chemistry *274*, 16107-16114.

Schlosser, C., and Croot, P.L. (2008). Application of cross-flow filtration for determining the solubility of iron species in open ocean seawater. Limnology and Oceanography-Methods *6*, 630-642.

Semsey, S., Andersson, A.M., Krishna, S., Jensen, M.H., Masse, E., and Sneppen, K. (2006). Genetic regulation of fluxes: iron homeostasis of *Escherichia coli*. Nucleic Acids Research *34*, 4960-4967.

Shaked, Y., Kustka, A.B., and Morel, F.M. (2005). A general kinetic model for iron acquisition by eukaryotic phytoplankton. Limnology and Oceanography *50*, 872-882.

Shaked, Y., and Lis, H. (2012). Disassembling iron availability to phytoplankton. Frontiers in Microbiology *3*, 123.

Shapiro, S.S., and Wilk, M.B. (1965). An analysis of variance test for normality (complete samples). Biometrika *52*, 591-611.

Silva, J.B., Storms, Z., and Sauvageau, D. (2016). Host receptors for bacteriophage adsorption. FEMS Microbiology Letters *363*, FNW002.

Soria-Dengg, S., Reissbrodt, R., and Horstmann, U. (2001). Siderophores in marine coastal waters and their relevance for iron uptake by phytoplankton: experiments with the diatom *Phaeodactylum tricornutum*. Marine Ecology Progress Series *220*, 73-82.

Staley, J.T., and Konopka, A. (1985). Measurement of in situ activities of nonphotosynthetic microorganisms in aquatic and terrestrial habitats. Annual Review of Microbiology *39*, 321-346.

Stolpe, B., Guo, L., Shiller, A.M., and Hassellov, M. (2010). Size and composition of colloidal organic matter and trace elements in the Mississippi River, Pearl River and the northern Gulf of Mexico, as characterized by flow field-flow fractionation. Marine Chemistry *118*, 119-128.

Stolpe, B., and Hassellov, M. (2010). Nanofibrils and other colloidal biopolymers binding trace elements in coastal seawater: Significance for variations in element size distributions. Limnology and Oceanography *55*, 187-202.

Sullivan, M., Weitz, J., and Wilhelm, S. (2017). Viral ecology comes of age. Environmental Microbiology Reports *9*, 33.

Suttle, C.A. (2005). Viruses in the sea. Nature *437*, 356-361.

Tagliabue, A., Bowie, A.R., Boyd, P.W., Buck, K.N., Johnson, K.S., and Saito, M.A. (2017). The integral role of iron in ocean biogeochemistry. Nature *543*, 51.

Tam, W., Pell, L.G., Bona, D., Tsai, A., Dai, X.X., Edwards, A.M., Hendrix, R.W., Maxwell, K.L., and Davidson, A.R. (2013). Tail tip proteins related to bacteriophage

lambda gpL coordinate an iron-sulfur cluster. Journal of Molecular Biology *425*, 2450-2462.

Tortell, P.D., Maldonado, M.T., and Price, N.M. (1996). The role of heterotrophic bacteria in iron-limited ocean ecosystems. Nature *383*, 330-332.

Weinbauer, M.G. (2004). Ecology of prokaryotic viruses. FEMS Microbiology Reviews *28*, 127-181.

Wen, K., Ortmann, A.C., and Suttle, C.A. (2004). Accurate estimation of viral abundance by epifluorescence microscopy. Applied and Environmental Microbiology *70*, 3862-3867.

Wilhelm, S.W., and Suttle, C.A. (1999). Viruses and Nutrient Cycles in the Sea - Viruses play critical roles in the structure and function of aquatic food webs. Bioscience *49*, 781-788.

Wommack, K.E., and Colwell, R.R. (2000). Virioplankton: Viruses in aquatic ecosystems. Microbiology and Molecular Biology Reviews *64*, 69-114.

Worsfold, P.J., Lohan, M.C., Ussher, S.J., and Bowie, A.R. (2014). Determination of dissolved iron in seawater: A historical review. Marine Chemistry *166*, 25-35.

Wu, J.F., Boyle, E., Sunda, W., and Wen, L.S. (2001). Soluble and colloidal iron in the oligotrophic North Atlantic and North Pacific. Science *293*, 847-849.

APPENDIX A:

THE FERROJAN HORSE HYPOTHESIS: IRON-VIRUS INTERACTIONS IN THE OCEAN

This appendix was published in:

Bonnain, C., Breitbart, M., & Buck, K. N. (2016). The Ferrojan Horse Hypothesis: Iron-virus interactions in the ocean. Frontiers in Marine Science, 3, 82.

frontiers in Marine Science

HYPOTHESIS AND THEORY
published: 08 June 2016
doi: 10.3389/fmars.2016.00082

The Ferrojan Horse Hypothesis: Iron-Virus Interactions in the Ocean

*Chelsea Bonnain, Mya Breitbart and Kristen N. Buck**

College of Marine Science, University of South Florida, St. Petersburg, FL, USA

Iron is an essential nutrient and the sub-nanomolar concentrations of iron in open ocean surface waters are often insufficient to support optimal biological activity. More than 99.9% of dissolved iron in these waters is bound to organic ligands, yet determining the identity of these ligands in seawater remains a major challenge. Among the potential dissolved organic ligands in the colloidal fraction captured between a 0.02 and a 0.2 μm filter persists an extremely abundant biological candidate: viruses, most of which are phages (viruses that infect bacteria). Recent work in non-marine model systems has revealed the presence of iron ions within the tails of diverse phages infecting *Escherichia coli*. Based on these findings and the presence of conserved protein motifs in marine phages, here we present several lines of evidence to support the hypothesis that phages are organic iron-binding ligands in the oceans. With average concentrations of 10^7 phages per milliliter surface seawater, we predict that phages could contain up to 0.7 pM iron, a value equivalent to as much as 70% of the colloidal fraction of organically complexed dissolved iron in the surface ocean. Additionally, the production and uptake of siderophores, a strategy that bacteria have developed for assimilating iron, renders cells vulnerable to phage infection due to the dual function of these cell surface receptors. Iron ions present in phage tails enable phages to exploit their bacterial host's iron-uptake mechanism via the "Ferrojan Horse Hypothesis" proposed herein, where the apparent gift of iron leads to cell lysis. Finally, if host iron stores are recycled during the assembly of progeny phages, as much as 14% of the cellular iron released into the water column upon lysis would already be incorporated into new phage tails. The potential role of phages as iron-binding ligands has significant implications for both oceanic trace metal biogeochemistry and marine phage-host interactions.

Keywords: iron, ligand, phage, marine, virus, siderophore, infection, bacteria

OPEN ACCESS

Edited by:
Toshi Nagata,
The University of Tokyo, Japan

Reviewed by:
Arvind Singh,
Physical Research Laboratory, India
Elvira Pulido-Villena,
Mediterranean Institute of Oceanography, France
Dave Kirchman,
University of Delaware, USA

****Correspondence:***
Kristen N. Buck
kristenbuck@usf.edu

Specialty section:
This article was submitted to Marine Biogeochemistry, a section of the journal Frontiers in Marine Science

Received: *16 February 2016*
Accepted: *17 May 2016*
Published: *08 June 2016*

Citation:
Bonnain C, Breitbart M and Buck KN (2016) The Ferrojan Horse Hypothesis: Iron-Virus Interactions in the Ocean. Front. Mar. Sci. 3:82. doi: 10.3389/fmars.2016.00082

THE FERROJAN HORSE HYPOTHESIS

Iron is an essential micronutrient for microbial life. To thrive in the ocean, where iron concentrations are astonishingly low (Gordon et al., 1982), bacteria have evolved specialized iron-acquisition strategies, such as the production of siderophores (Neilands, 1957; Sandy and Butler, 2009). Siderophores are exceedingly strong organic iron-binding ligands produced by bacteria to outcompete other ligands for the binding and uptake of iron via a specific "trap door" receptor on the cell surface (Pawelek et al., 2006; Sandy and Butler, 2009; Vraspir and Butler, 2009; Hider and Kong, 2010). In non-marine systems, it has long been demonstrated that bacteriophages (phages; viruses that infect bacteria) take advantage of their bacterial hosts' vulnerabilities by utilizing the

siderophore-bound iron receptors on the bacterial cell surface membrane for infection, directly competing with siderophore-bound iron uptake (Neilands, 1979; Braun, 2009). These siderophore-bound iron receptors, collectively referred to as TonB-dependent receptors, are essential for bacterial iron acquisition (Luria and Delbruck, 1943; Braun et al., 1973; Hantke and Braun, 1975; Luckey et al., 1975; Braun and Endriss, 2007). Mutations in critical regions of these surface-exposed receptors are therefore selected against, providing an advantage to phages in the ongoing phage-host evolutionary arms race (Van Valen, 1973; Stern and Sorek, 2011; Samson et al., 2013).

A series of recent studies demonstrating the presence of iron ions in the tail proteins of several well-studied phages that infect enteric bacteria (Bartual et al., 2010; **Figure 1**) leads us to propose the "Ferrojan Horse Hypothesis" (*Ferrum* = Latin for iron; **Figure 2**). If marine phages, which are present at concentrations of ∼10 million colloidal-sized (0.02–0.2 μm) particles per milliliter of surface seawater, contain similar amounts of iron, then a significant amount of the dissolved iron in the oceans could be complexed within phages. In this model, phages use the essential micronutrient iron in the manner of a Trojan horse: iron within the phage tail fibers is recognized by the host siderophore-bound iron receptor, enabling the phage to attach to the bacterial cell, puncture the cell membrane and inject its nucleic acid into the host for infection (**Figure 2**). Furthermore, we hypothesize that cellular iron stocks are recycled for incorporation into the tail fibers of new phage progeny during phage protein synthesis and assembly, which occurs inside the host cell prior to lysis (King, 1968; Chuprov-Netochin et al., 2010; Rohwer et al., 2014). Following cell lysis, host cell materials are remineralized via the viral shunt and new phages (containing a substantial fraction of the cellular iron) are released into the environment where they proceed to infect new hosts. Here we present the lines of evidence that support the plausibility for phages to act as organically complexed dissolved iron in the oceans and discuss the implications on oceanic biogeochemistry and phage-host interactions.

OCEANIC IRON BIOGEOCHEMISTRY

Bioavailable iron is scarce in open ocean surface waters due to its low solubility in oxic seawater at a pH of 8 and the vast distance from continental iron sources (Kuma et al., 1996; Johnson et al., 1997). This poses a challenge for marine microbes, since iron is essential for multiple biological functions, including the production of enzymes necessary for photosynthesis and respiration (Raven et al., 1999). As such, the iron quotas (Fe:C) for these cells are high relative to the requirements for any other trace metal (Bruland et al., 1991; Tortell et al., 1999; Morel and Price, 2003; Twining and Baines, 2013). In order to satisfy such a high iron requirement, marine bacteria have developed specialized mechanisms for iron acquisition. The synthesis and uptake of siderophores, which are high-affinity iron-chelating compounds, is a common strategy that bacteria use to secure iron from the marine environment (Butler, 2005). The process of organic complexation protects dissolved iron from precipitation (Kuma et al., 1996), stabilizing the pool of bioavailable dissolved iron so that bacteria may then take up the entire complex via a siderophore-bound iron receptor (Sandy and Butler, 2009; Shaked and Lis, 2012). Furthermore, some bacteria have developed strategies to acquire the iron bound to siderophores produced by other bacteria, called "xenosiderophores" (Matzanke et al., 1997; Sandy and Butler, 2009; Cornelis, 2010; Gauglitz et al., 2014).

Iron bioavailability serves as a bottom-up control on primary productivity in much of the modern surface ocean, making characterization of iron speciation of vital importance to understanding the carbon cycle and global climate (e.g., Martin et al., 1989). The concentration of dissolved iron in seawater is largely regulated by organic complexation, with >99.9% of dissolved iron complexed by organic iron-binding ligands as measured by competitive ligand exchange-adsorptive cathodic stripping voltammetry (CLE-ACSV: Gledhill and van den Berg, 1994; Rue and Bruland, 1995). Most recently, applications of CLE-ACSV to basin-scale surveys of the Atlantic Ocean as part of the GEOTRACES program have reported widespread organic complexation, with iron-binding ligands present in excess of dissolved iron concentrations through most of the Atlantic water column (Buck et al., 2015; Gerringa et al., 2015).

Numerous studies have sought to identify the organic iron-binding ligands measured by CLE-ACSV throughout the oceans. The strongest known iron-binding ligands are siderophores, which are typically small, soluble molecules (<10 kDa or <0.02 μm), though some marine siderophores are colloidal in size (>0.02 μm but <0.2 μm) due to long fatty acid chains presumably used to tether the ligand to the bacterial cell that produced it (Martinez et al., 2003). Siderophores are the best-characterized strong iron-binding ligand class, yet the concentration of siderophores measured in the Atlantic Ocean is only 3–20 pM (Mawji et al., 2008)—though this is likely an underestimate due to the challenges of isolating siderophores from seawater (Vraspir and Butler, 2009; Gledhill and Buck, 2012). Iron-binding humic substances have been increasingly recognized as an important component of a weaker iron-binding ligand pool in the oceans, particularly in the deep sea and in coastal environments (Laglera et al., 2007, 2011; Laglera and van den Berg, 2009). Similar to humic substances, other weaker iron-binding ligands most likely also originate from the remineralization of organic matter in the oceans (Hunter and Boyd, 2007; Boyd and Ellwood, 2010; Boyd et al., 2010). These may include exopolymeric substances, transparent exopolymers, nanofibrils, and even the biotoxin domoic acid (**Figure 3**; Rue and Bruland, 2001; Mancuso Nichols et al., 2004; Stolpe and Hassellov, 2010; Hassler et al., 2011).

To date, few studies have combined size fractionation with iron-binding ligand measurements (Cullen et al., 2006; Thuroczy et al., 2010; Fitzsimmons et al., 2015). These studies have all measured the largest excess of strong iron-binding ligands within the soluble (<0.02 μm) size fraction, consistent with the traditional siderophore model. However, strong iron-binding

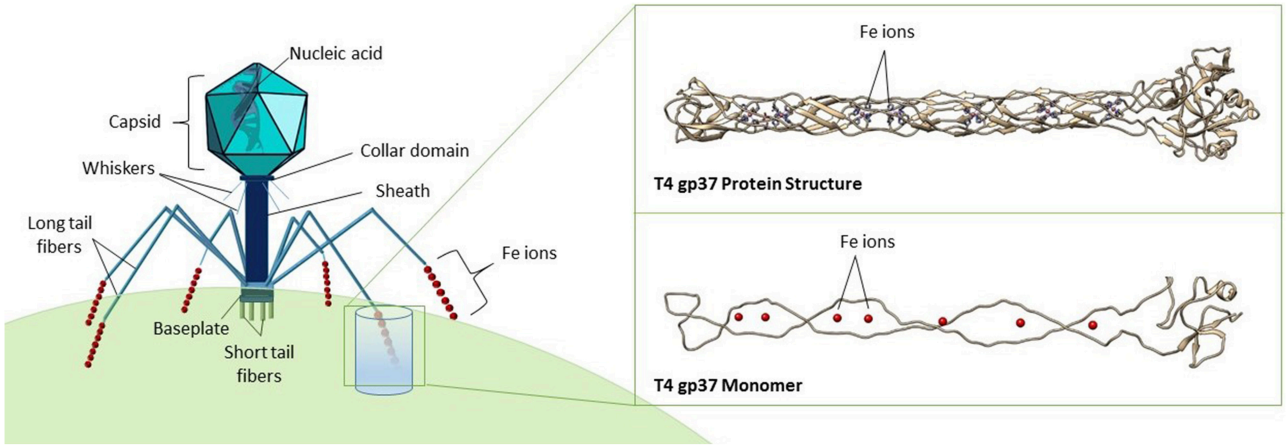

FIGURE 1 | Structure of a typical bacteriophage belonging to the *Myoviridae* family. The expanded inset shows a model of the gp37 tail fiber protein of phage T4 (PDB ID code 2XGF), visualized in Chimera (Pettersen et al., 2004), and VMD (Humphrey et al., 1996). Seven iron ions (red spheres) are coordinated octahedrally by histidine residues, forming a trimer as shown in the top image, while the bottom image shows a gp37 monomer.

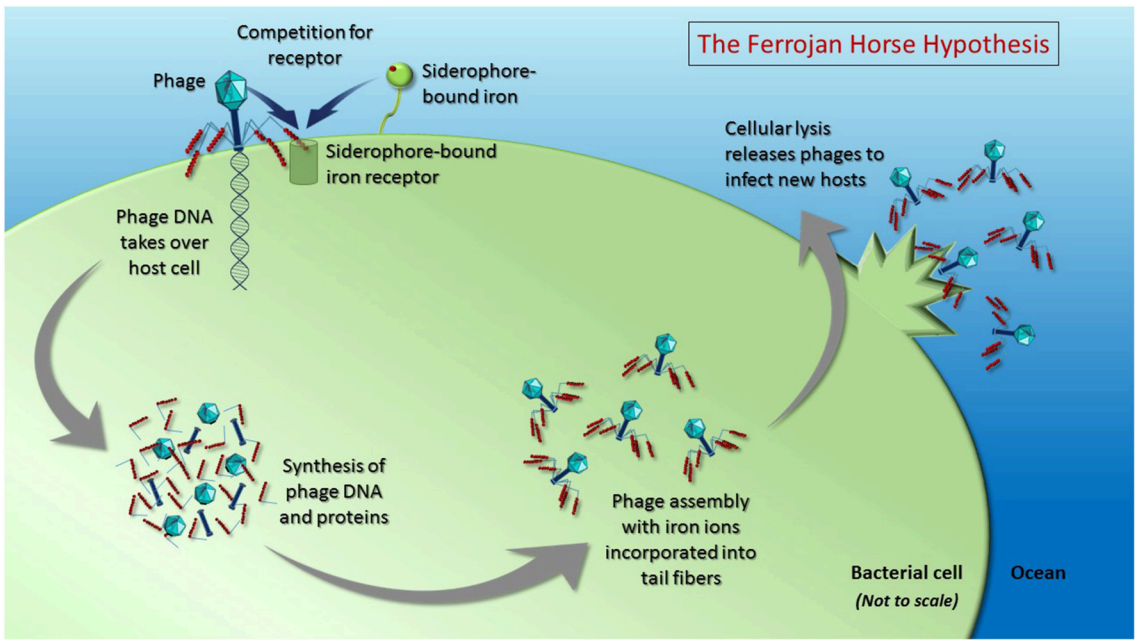

FIGURE 2 | *The Ferrojan Horse Hypothesis* depicts the use of iron ions (red spheres) within phage tail fibers to compete with siderophore-bound iron for access to the same receptor on the surface of the host cell. Once a phage docks on the cell surface, it can pierce the cell membrane and inject its nucleic acid, which takes over the host cell, instructing the cell to produce phage DNA and proteins. Cellular mechanisms are used to fold the proteins and assemble them into progeny phages, with iron from within the cell incorporated into the tail fibers. Upon cell lysis, new phages are released to infect hosts using the iron that has been pre-packaged within their tail fibers. This proposed recycling of cellular iron during phage production results in a depletion of the amount of iron available for remineralization upon lysis (i.e., via the viral shunt). Figure is not drawn to scale.

ligands were also detected within the colloidal fraction (0.02–0.2 μm), though at concentrations closer to that of dissolved iron with little to no excess ligands found in this size fraction (Cullen et al., 2006; Thuroczy et al., 2010; Fitzsimmons et al., 2015). Since measuring organic ligands that are already saturated with iron is particularly challenging by CLE-ACSV (e.g., Gledhill and Buck, 2012), the persistence of colloidal iron in these studies was suggested to result from recent dust deposition of inorganic colloidal iron or an unknown but organically-stabilized colloidal iron complex. Size fractionation studies of dust dissolution from aerosols in the Atlantic Ocean have shown that iron in dust proceeds from particulate to colloidal to soluble size fractions

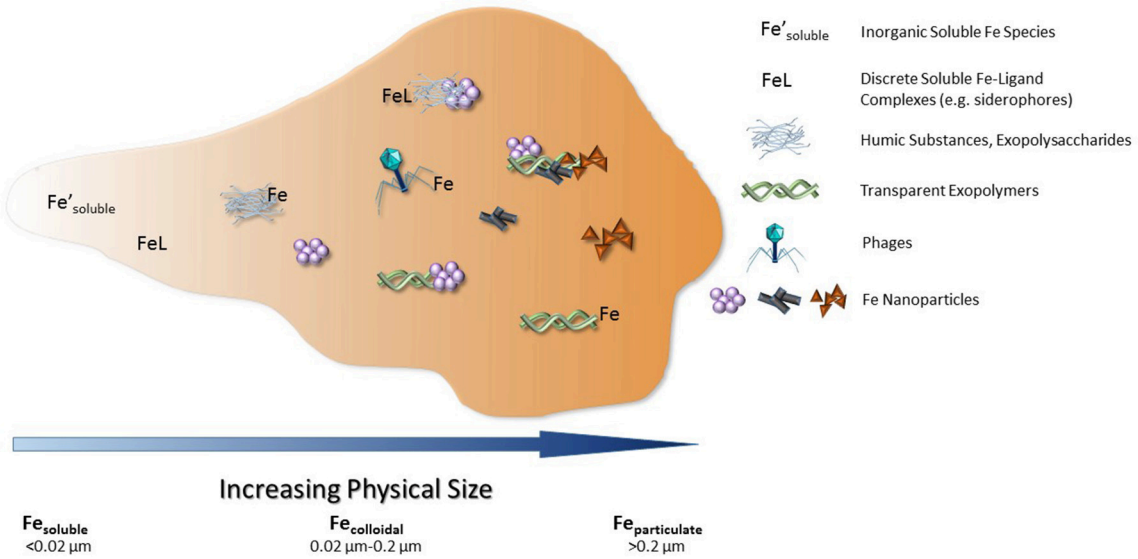

FIGURE 3 | Current dissolved iron-binding ligands identified within seawater, with the addition of phages within the colloidal size range. Figure modified from Gledhill and Buck (2012).

in the presence of strong organic iron-binding ligands like siderophores (Aguilar-Islas et al., 2010; Fishwick et al., 2014). In the absence of strong ligands, on the other hand, the iron remains in the colloidal size fraction, re-aggregates and is lost (Aguilar-Islas et al., 2010; Fishwick et al., 2014). The same may be expected of other particulate iron sources such as hydrothermal vents or shelf sediments, and the inorganic colloidal iron remains difficult to characterize. Recently, the ability of iron-oxidizing bacteria to produce iron oxides from hydrothermal vents has been proposed to contribute to the dissolved iron pool as a source of inorganic iron colloids (Emerson, 2016). While these studies highlight the complexity of iron speciation in seawater and the likelihood that inorganic iron colloids are an important dissolved iron species upon iron addition, the majority of the dissolved iron pool in the oceans is still thought to be organically complexed. Indeed, UV oxidation of seawater samples is commonly employed to release ligand-bound iron in seawater samples (Rue and Bruland, 1997; van den Berg, 2005; Biller and Bruland, 2012). Intriguingly, UV oxidation also reduces the infectivity of viruses and has been shown to destroy viral particles (Wilhelm et al., 1998); such treatment of phages in seawater would presumably also release any iron sequestered in phage tails.

The contribution of biologically sequestered iron to the organically complexed dissolved iron fraction has been largely ignored to date. The "biogenic" iron incorporated into the cells of phytoplankton and bacteria (typically >0.2 µm in diameter) can be a substantial portion of total (unfiltered) iron in the oceans, and when the fraction of dissolved iron is operationally defined as <0.45 µm, many marine bacteria may contribute to the dissolved iron pool (Tortell et al., 1999). However, to our knowledge, no studies have explored the potential for viruses, the most abundant biological entities in the ocean, to contribute to the iron-binding ligand pool in seawater, where they may account for a significant proportion of dissolved, and specifically colloidal (0.02–0.2 µm), organically complexed iron.

MARINE VIRUSES

With average concentrations of 10 million particles per milliliter, viruses (the majority of which are phages that infect bacteria) are the most abundant biological entities in the oceans (Wommack and Colwell, 2000; Breitbart, 2012). The impact of viruses on ocean biogeochemistry is often evoked purely through the act of host lysis (Fuhrman, 1999; Suttle, 2007), but very few studies have considered the chemical contributions of the viral particles themselves. Recent modeling work suggests that marine virus particles contain a significant amount of macronutrients (carbon, nitrogen, and phosphorus), and that the stoichiometric mismatch (i.e., the relative difference in elemental contents) between phages and their bacterial hosts has the potential to drive the differential release of nutrients upon cell lysis (Jover et al., 2014). However, no studies have considered the potential impact of trace elements within the structure of marine viral particles. If viruses contain or interact with trace metals such as iron, their small size and sheer abundance in the oceans would translate into a major influence for biogeochemical cycling of this vital micronutrient. Since phages dominate marine viral communities and the field of marine viral ecology is relatively young compared to the century of knowledge of phage biology (Rohwer and Segall, 2015; Salmond and Fineran, 2015), here we present the lines of evidence from non-marine model systems that suggest critical linkages may exist between phages and oceanic iron cycling.

EVIDENCE FROM NON-MARINE MODEL SYSTEMS

Iron within Phages Contributes to Colloidal Organically Complexed Dissolved Iron

Phage particles are composed of nucleic acids contained within a protein shell (capsid) with or without a proteinaceous tail, and occasionally surrounded by a lipid membrane (**Figure 1**; Hershey and Chase, 1952; Rohwer et al., 2014). A recent X-ray crystallography study demonstrated the presence of seven iron ions within the receptor-binding tip of each of the six long tail fibers (gp37) of phage T4, one of the most extensively studied *Escherichia coli* phages (Bartual et al., 2010). These iron ions, assumed to be Fe^{2+}, are coordinated through paired histidine residues (HxH domains) in the phage's long tail fiber protein (**Figure 1**; Bartual et al., 2010). The octahedral coordination of iron ions by the paired histidine residues in phage tails suggests that the iron ions are a stable part of the phage particle which would contribute to the colloidal organically complexed iron pool (i.e., FeL). This is consistent with recent evidence that colloidal and particulate Fe(II) is more abundant in the oceans than previously considered and that the majority of this Fe(II) is associated with organic carbon (von der Heyden et al., 2014). The HxH domains (PFAM 03335; **Figure 4**) are present in the tail fibers of several model phages that infect *E. coli* such as T4 (family *Myoviridae*) and lambda (family *Siphoviridae*), where they are repeated a variable number of times (Finn et al., 2014). From the marine environment, we used BLAST similarity to T4 gp37 to identify HxH domains in putative tail fibers from several cyanophages infecting *Prochlorococcus* (phage P-SSM2) and *Synechococcus* (phages ACG2014f_1 and KBS-2A), as well as in an uncultured phage with an unknown host from the Mediterranean Sea (uvMED; **Figure 4**). The conservation of HxH motifs known to facilitate iron binding in the putative tail fibers of several marine phages suggests that these pathways documented in well-studied phages infecting *E. coli* may also occur within diverse phages in the oceans. Although the receptors for the vast majority of marine phages are yet unknown (Breitbart, 2012; Silva et al., 2016), if some marine phages also utilize siderophore-bound iron receptors for host infection, this mechanism would have major implications for our current understanding of marine phage-host interactions in the iron-limited surface ocean.

In addition to the tail fibers, conserved HxH domains within other phage structural proteins have also been shown to bind iron ions. For example, the baseplate assembly proteins of phages P2 and Φ92 (family *Myoviridae*), which form a membrane piercing spike, have recently been shown to contain iron ions coordinated octahedrally by paired histidine residues (Yamashita et al., 2011; Browning et al., 2012). Although the P2 and Φ92 proteins share conserved HxH motifs and the same function, the proteins that comprise the structure only share 19% amino acid identity. Since most phages with contractile tails (*Myoviridae*) utilize the same cell-puncturing mechanism (Leiman and Shneider, 2012), it is likely that distantly related *Myoviridae* may also contain iron-loaded tail spikes, even if these proteins cannot be identified through sequence homology. In addition, the tail tip protein (gpL) of phage N15, a member of the *Siphoviridae* family of phages with non-contractile tails, binds an iron-sulfur cluster (Tam et al., 2013). While the function of this cluster remains unknown, it has been speculated to play a role in stabilizing the tail tip protein or in conformational changes that this protein undergoes during assembly or DNA injection (Tam et al., 2013), implying that the incorporation of metals into phage tails may broadly be utilized by diverse phages for strengthening and stabilizing host-piercing proteins.

In order to estimate the proportion of colloidal dissolved iron that could be bound within the tail fibers of oceanic phages, we calculated the number of iron atoms present in phage tail fibers based on knowledge from *E. coli* phage T4. According to Bartual et al. (2010), seven iron ions are coordinated within each of the six long tail fibers of phage T4 (Leiman et al., 2010), equaling 42 iron ions per phage. Using the average of 10^7 viruses per milliliter of seawater (Wommack and Colwell, 2000; Breitbart, 2012; Parsons et al., 2012; Wommack et al., 2015) and assuming all viruses are tailed phages containing the same number of iron ions as T4, there are potentially a total of 4.2×10^8 iron ions bound to phage tail fibers in a milliliter of seawater, accounting for up to 0.7 pM dissolved iron.

However, several caveats accompany these assumptions, which may significantly affect the relative impact of phages on dissolved iron concentrations. First, the presence of iron has not been demonstrated in any marine phage tails to date, so the numbers used here are based on well-studied model systems and the detection of conserved HxH motifs in marine phages. Since strong evolutionary relationships exist between marine and non-marine phages, with many phage proteins conserved across ecosystems, it is likely that successful infection strategies documented in non-marine model systems will also be present in the oceans (Rohwer et al., 2000; Sullivan et al., 2005). Second, the number of iron ions per phage tail fiber is likely to vary, as demonstrated by the variable number of HxH motifs seen in marine phage sequences (**Figure 4**). While our preliminary analyses have identified many HxH motifs among metagenomic sequences of uncultured marine viral communities (e.g., uvMED in **Figure 4** and additional data not shown), the limited database of marine phage genomes and limited levels of sequence similarity between phage tail proteins despite their conserved function makes a complete analysis of the prevalence and abundance of conserved iron-binding motifs in phage tail fibers challenging. Third, marine viral communities are extremely diverse, containing viruses with a myriad of particle sizes and morphologies that infect hosts across all domains of life (Breitbart et al., 2007; Suttle, 2007; Rohwer and Thurber, 2009; Breitbart, 2012; Wommack et al., 2015). While tailed phages are consistently present in the oceans, the proportion of the viral community that they comprise can vary widely (Brum et al., 2013) and still requires further evaluation. A quantitative transmission electron microscopy study performed across the world's oceans demonstrated that tailed phages comprised between 8 and 49% of the total viral communities sampled (Brum et al., 2013). Repeating the above calculations using the lower bound of 8% tailed phages, phage

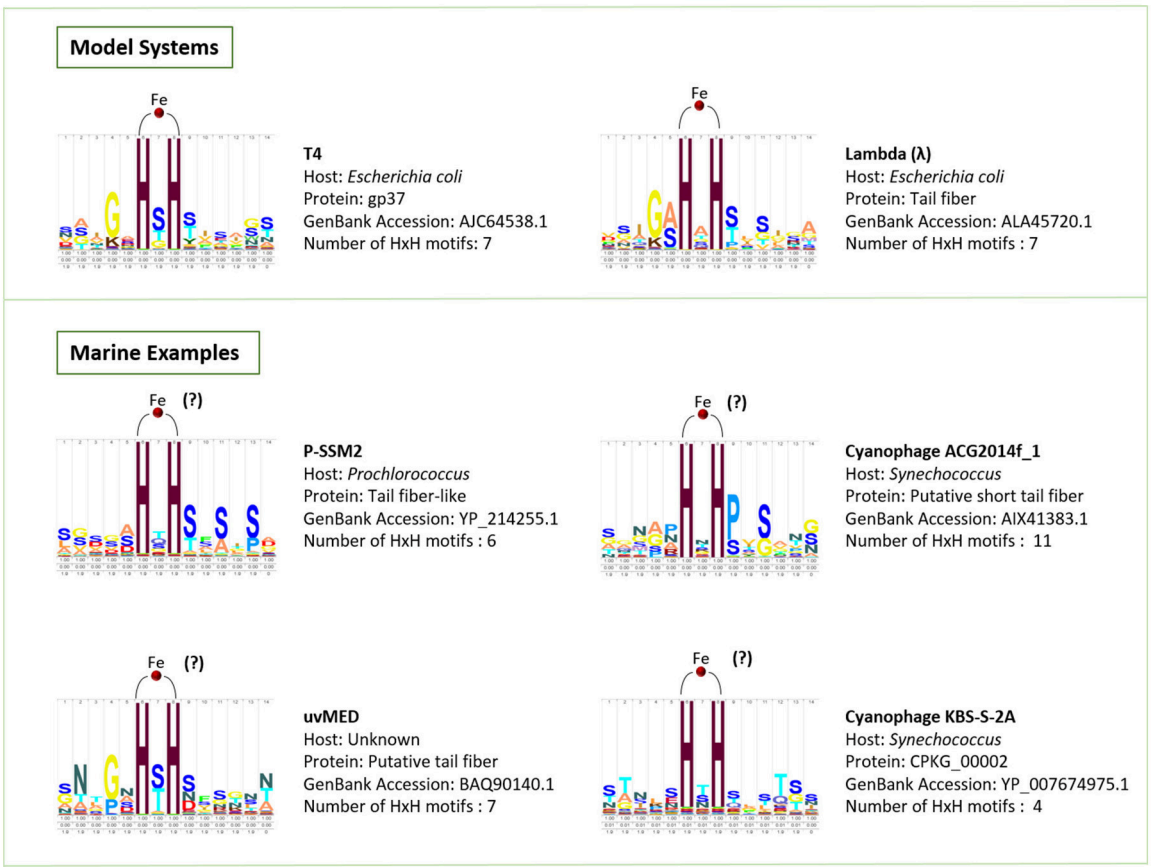

FIGURE 4 | HMM logos created using Skylign (Wheeler et al., 2014) for the HxH motifs that bind iron ions in the model phages T4 and lambda, as well as conserved HxH motifs identified here in the putative tail fiber proteins of marine phages, which we hypothesize play a role in binding iron.

tail fibers would account for 0.06 pM dissolved iron. In addition, phage tails may not be the only structural proteins that interact with iron. For example, Daughney et al. (2004) showed that iron could also adsorb to phage capsids, creating the possibility that non-tailed phages (and perhaps eukaryotic or archaeal viruses) could also play a role in iron cycling. Since these experiments used iron oxide concentrations far exceeding typical marine concentrations, future work is needed to explore the relevance of these studies to natural systems and test the ability of marine phage capsids to bind iron.

With average dissolved iron concentrations for open ocean surface waters of 0.01–0.2 nM (Johnson et al., 1997; Mawji et al., 2015) and the colloidal fraction accounting for 10–25% of the total dissolved iron at the surface (Nishioka et al., 2001; Bergquist et al., 2007; Fitzsimmons and Boyle, 2014), the proportion of iron bound to the tail fibers of phages in 1 ml of seawater could thus account for ∼5.6–70% of the colloidal fraction of dissolved iron, depending on the proportion of tailed phages. When considering that siderophore-bound iron concentrations in the Atlantic Ocean may comprise 0.2–4.6% (likely an underestimate) of the soluble fraction of dissolved iron (Mawji et al., 2008), phages potentially constitute a similarly substantial proportion of ligand-bound iron within the colloidal fraction.

Phage Utilization of Outer Membrane Siderophore-Bound Iron Receptors

In 1943, Luria and Delbruck launched the field of bacterial genetics with their seminal work identifying mutants of *E. coli* strain B that were resistant to infection by a specific phage (Luria and Delbruck, 1943). Although not named in the original study, the phage used was T1 and one of the resistant mutants was designated *tonA*. It wasn't until 1973 that researchers were able to ascribe the phage resistance to a single monomeric protein, TonA (named for *T one* resistance), which was also shown to bind phage T5 and colicin M (Braun et al., 1973). The exciting discovery in 1975 that TonA was capable of transporting iron bound to the siderophore ferrichrome (Hantke and Braun, 1975; Luckey et al., 1975) later prompted a change in the protein's name from TonA to FhuA (named for *f*erric *h*ydroxamate *u*ptake; Kadner et al., 1980). It is now known that the outer membrane protein FhuA functions as a receptor for numerous phages (T1, T5, Φ80, UC-1, H8; Lundrigan et al., 1983; Poon and Dhillon, 1987; Rabsch et al., 2007; Braun, 2009; Silva et al., 2016), as well as in the transport of ferrichrome, the peptide toxins colicin M, and microcin 25 (Braun et al., 1976), and the antibiotics albomycin and rifamycin CGP 4832 (which contain ferrichrome attached to an antimicrobial agent; Braun et al., 2001). Finally, the

broad host range phage H8 achieves infection via adsorption to a different siderophore-bound iron receptor, the outer membrane porin protein FepA, suggesting that utilizing TonB-dependent siderophore-bound iron receptors (including FhuA and FepA) is a highly effective infection strategy (Rabsch et al., 2007).

Iron is so critical for growth that bacteria must rely upon specialized systems for the uptake of siderophore-bound iron, even though these strategies render them vulnerable to phage infection (Neilands, 1979) This places bacterial host cells in a precarious position because mutations in critical regions of these surface-exposed receptors that could provide resistance against phage infection may compromise their ability to acquire the iron they need for growth (Rabsch et al., 2007), thus providing an advantage to phages in the ongoing phage-host evolutionary arms race (Van Valen, 1973; Stern and Sorek, 2011; Samson et al., 2013). Additionally, the dual function of these cell surface receptors in siderophore-bound iron uptake and phage infection creates competition for receptor binding. In early *in vitro* studies, several phages (T5, T1, Φ80, UC-1) were shown to compete with ferrichrome for the FhuA receptor on the outer membrane of *E. coli* (Luckey et al., 1975; Wayne and Neilands, 1975; Hantke and Braun, 1978; Lundrigan et al., 1983; Bonhivers et al., 1996). Likewise, addition of iron bound to the siderophore enterobactin inhibits the binding of phage H8 to its receptor FepA (Rabsch et al., 2007).

Iron Incorporated into Phage Particles Prior to Host Lysis

Marine heterotrophic bacteria, which are highly abundant and contain significantly more iron per unit biomass than eukaryotic phytoplankton, have been estimated to account for up to half of the total iron in the marine environment (Tortell et al., 1996, 1999). While grazing of bacteria transfers cellular contents to higher trophic levels, phage infection plays an important role in regeneration of carbon, nutrients, and other elements through the viral shunt (Fuhrman, 1999; Wilhelm and Suttle, 1999). A growing body of literature has documented the critical roles of viral activity on iron cycling and bioavailability in the surface oceans (Gobler et al., 1997; Poorvin et al., 2004; Mioni et al., 2005). Experimental studies have demonstrated that organic iron-ligand complexes generated through phage lysis of infected bacterial cells are highly bioavailable and rapidly assimilated by heterotrophic bacteria (Poorvin et al., 2004; Mioni et al., 2005). In high nutrient, low chlorophyll (HNLC) systems, iron regeneration via phage lysis is critical for recycling organically complexed iron and speculated to regenerate enough dissolved iron to support some phytoplankton growth (Poorvin et al., 2004).

Although the source of the iron in phage tails has not yet been experimentally determined in any system, the fact that phage progeny fully assemble within the host cell prior to lysis, combined with the much higher iron concentrations inside bacterial cells compared to seawater, suggests that iron reserves in bacterial cells are the most likely source of the iron in phage tails (King, 1968; Tortell et al., 1999; Chuprov-Netochin et al., 2010; Rohwer et al., 2014). The incorporation of iron into phage tails assembled within the bacterial cell has significant implications for understanding the biogeochemistry of dissolved organic matter and trace metals released as a result of bacterial host cell lysis. An average marine heterotrophic bacterial cell has an iron quota of 7.5 μmol Fe per mol C (Tortell et al., 1996, 1999). Using an estimate of 20 fg C per cell (Ducklow, 2000), this translates to 7518 iron ions per heterotrophic bacterial cell. If marine phages contain similar amounts of iron in their tails as phage T4 (42 iron irons/phage; Bartual et al., 2010), and assuming an average burst size (number of progeny phages released through a lysis event) of 25 phages per infection (Wommack and Colwell, 2000; Parada et al., 2006), then ∼14% of the bacterial iron previously assumed to be released into the water column as dissolved iron for remineralization would already be incorporated into new phage particles. The magnitude of this impact could vary widely as the calculations required several assumptions, including the iron quota of marine bacterial cells, which has been reported to range between 6.05 and 112 μmol Fe per mol C, depending on bioavailable iron concentrations (Brand, 1991; Tortell et al., 1996, 1999; Maldonado and Price, 1999; Boyd et al., 2010; Shire and Kustka, 2015), and the average burst size, which ranges from 10 to 500 for marine viruses (Wommack and Colwell, 2000; Parada et al., 2006). Nevertheless, if phage-bound iron originates from cellular iron reserves, this form of recycling and subsequent depletion of the iron available for remineralization upon lysis will be important to consider in modeling ocean biogeochemistry.

IMPLICATIONS AND FUTURE WORK

Here we have detailed several lines of evidence supporting the Ferrojan Horse Hypothesis. The three facets of this hypothesis are: (1) Phages constitute important iron-binding ligands in the marine environment, where they can account for a substantial portion of the colloidal fraction of organically complexed dissolved iron; (2) Marine phages compete with siderophore-bound iron for uptake receptors on the bacterial cell surface, effectively acting as a Trojan horse where the apparent gift of iron leads to cell lysis; (3) The iron incorporated into marine phage tails originates from bacterial cellular iron reserves, which reduces the amount of iron available for remineralization upon lysis. All the calculations described in this manuscript are based on knowledge from the structure of *E. coli* phage T4 as a model system (Bartual et al., 2010) and combined with average published values for viral abundance and dissolved iron concentrations within the surface oceans; therefore, a great deal of work still needs to be performed to validate this hypothesis and quantify its impact on ocean biogeochemistry and phage-host interactions. In addition, it is still unknown how strongly phages bind iron, or how this binding strength compares to known organic ligands such as siderophores within the marine environment. Yet if marine phages incorporate iron into their tail fibers as a mechanism to gain access to bacterial hosts through receptors developed for iron acquisition and uptake, as seen in the model system of *E. coli* and T4, this infection strategy could answer fundamental questions regarding marine

phage-host specificity and infection dynamics in the marine environment.

Notably, the competition for iron is not unique to the marine environment and the topics discussed here have broad implications for many ecosystems. For example, biomedical studies have demonstrated the importance of iron regulation within the human blood stream, with both pathogens and the human immune system manipulating iron as a tool for survival (Barasch and Mori, 2004; Drakesmith and Prentice, 2012; Barber and Elde, 2014). Analogous to the manner in which phages exploit bacterial siderophore-bound iron receptors, several mammalian viruses also utilize the cell-surface transferrin receptor for gaining entry to mammalian cells (Demogines et al., 2013). Additionally, although the mechanisms are largely unknown, recent phage therapy studies have demonstrated that the addition of iron-doped apatite nanoparticles to phages in solution enhances phage infection, resulting in an increase in the number of plaques forming on bacterial lawns by up to 128% (Andriolo et al., 2014). Given similarities in ionic strength and pH between seawater (Byrne and Breland, 1989) and blood (May et al., 1977), insights gained from human systems can aid in our understanding of the interactions between iron, bacteria, and viruses within the marine environment and vice versa.

Finally, although the Ferrojan Horse Hypothesis focuses on iron, the same concepts may be applicable to other essential nutrients found within the protein structure of phages, including metals like zinc and macronutrients like phosphorus. Zinc was found to be bound by histidines to one of the short tail fibers (gp12) of *E. coli* phage T4 in a manner similar to the iron ions in the T4 long tail fibers (Thomassen et al., 2003; Bartual et al., 2010). In addition, recent work by Jover et al. (2014) has estimated that viral particles can account for 0.01–24 nM of dissolved organic phosphorus in the oceans. Phages have a skewed C:N:P of ∼20:7:1 (Jover et al., 2014), which is highly enriched in phosphorous and nitrogen compared to the Redfield ratio of cellular life in the oceans, 106:16:1 (Redfield, 1958). This stoichiometric mismatch suggests that the chemical composition of phages should be further investigated to determine elements for which they can make disproportionately large contributions to marine chemistry.

Future research will test the Ferrojan Horse Hypothesis by documenting the ability of phages to act as iron-binding ligands within the oceans and exploring the role of iron exploitation in governing phage-host interactions. In the meantime, however, the linkages made in this manuscript clearly demonstrate the importance of considering the potential contributions of phages, as well as other biological entities, to the concentrations and biogeochemical cycling of dissolved trace metals and macronutrients in the ocean.

AUTHOR CONTRIBUTIONS

MB and KNB jointly conceived this hypothesis. CB took the lead in assembling evidence, compiling manuscript content, and creating graphics. All three authors contributed equally to writing the manuscript text and approved the manuscript for publication.

ACKNOWLEDGMENTS

The authors thank Dr. Leon Hardy at the University of South Florida Saint Petersburg for help visualizing the structure of phage T4 gp37 presented in **Figure 1** and Dr. Robert A. Edwards at San Diego State University for bioinformatics support. This work was supported by National Science Foundation grants from the Division of Integrative Organismal Systems (IOS-1456301) to MB and from the Division of Ocean Sciences (Chemical Oceanography, OCE-1446327) to KNB, as well as a donation from George H. Lorton. We thank three reviewers for their helpful contributions that improved this manuscript.

REFERENCES

Aguilar-Islas, A. M., Wu, J., Rember, R., Johansen, A. M., and Shank, L. M. (2010). Dissolution of aerosol-derived iron in seawater: leach solution chemistry, aerosol type, and colloidal iron fraction. *Mar. Chem.* 120, 25–33. doi: 10.1016/j.marchem.2009.01.011

Andriolo, J. M., Hensleigh, R. M., McConnell, C. A., Pedulla, M., Hailer, K., Kasinath, R., et al. (2014). Iron-doped apatite nanoparticles for improvement of phage therapy. *J. Vac. Sci. Technol. B* 32:06FD01. doi: 10.1116/1.4894460

Barasch, J., and Mori, K. (2004). Cell biology - iron thievery. *Nature* 432, 811–813. doi: 10.1038/432811a

Barber, M. F., and Elde, N. C. (2014). Escape from bacterial iron piracy through rapid evolution of transferrin. *Science* 346, 1362–1366. doi: 10.1126/science.1259329

Bartual, S. G., Otero, J. M., Garcia-Doval, C., Llamas-Saiz, A. L., Kahn, R., Fox, G. C., et al. (2010). Structure of the bacteriophage T4 long tail fiber receptor-binding tip. *Proc. Natl. Acad. Sci. U.S.A.* 107, 20287–20292. doi: 10.1073/pnas.1011218107

Bergquist, B. A., Wu, J., and Boyle, E. A. (2007). Variability in oceanic dissolved iron is dominated by the colloidal fraction. *Geochim. Cosmochim. Acta* 71, 2960–2974. doi: 10.1016/j.gca.2007.03.013

Biller, D. V., and Bruland, K. W. (2012). Analysis of Mn, Fe, Co, Ni, Cu, Zn, Cd, and Pb in seawater using the Nobias-chelate PA1 resin and magnetic sector inductively coupled plasma mass spectrometry (ICP-MS). *Mar. Chem.* 130, 12–20. doi: 10.1016/j.marchem.2011.12.001

Bonhivers, M., Ghazi, A., Boulanger, P., and Letellier, L. (1996). FhuA, a transporter of the *Escherichia coli* outer membrane, is converted into a channel upon binding of bacteriophage T5. *EMBO J.* 15, 1850–1856.

Boyd, P. W., and Ellwood, M. J. (2010). The biogeochemical cycle of iron in the ocean. *Nat. Geosci.* 3, 675–682. doi: 10.1038/ngeo964

Boyd, P. W., Ibisanmi, E., Sander, S. G., Hunter, K. A., and Jackson, G. A. (2010). Remineralization of upper ocean particles: implications for iron biogeochemistry. *Limnol. Oceanogr.* 55, 1271–1288. doi: 10.4319/lo.2010.55.3.1271

Brand, L. E. (1991). Minimum iron requirements of marine-phytoplankton and the implications for the biogeochemical control of new productuon. *Limnol. Oceanogr.* 36, 1756–1771.

Braun, V. (2009). FhuA (TonA), the career of a protein. *J. Bacteriol.* 191, 3431–3436. doi: 10.1128/JB.00106-09

Braun, V., Bos, C., Braun, M., and Killmann, H. (2001). Outer membrane channels and active transporters for the uptake of antibiotics. *J. Infect. Dis.* 183, S12–S16. doi: 10.1086/318840

Braun, V., and Endriss, F. (2007). Energy-coupled outer membrane transport proteins and regulatory proteins. *Biometals* 20, 219–231. doi: 10.1007/s10534-006-9072-5

Braun, V., Hancock, R. E. W., Hantke, K., and Hartmann, A. (1976). Functional organization of outer membrane of *Escherichia coli* - phage and colicin receptors as components of iron uptake systems. *J. Supramol. Struct.* 5, 37–58. doi: 10.1002/jss.400050105

Braun, V., Schaller, K., and Wolff, H. (1973). Common receptor protein for phage T5 and colicin M in outer membrane of *Escherichia coli B. Biochim. Biophys. Acta* 323, 87–97. doi: 10.1016/0005-2736(73)90433-1

Breitbart, M. (2012). Marine viruses: truth or dare. *Annu. Rev. Mar. Sci.* 4, 425–448. doi: 10.1146/annurev-marine-120709-142805

Breitbart, M., Thompson, L. R., Suttle, C. A., and Sullivan, M. B. (2007). Exploring the vast diversity of marine viruses. *Oceanography* 20, 135–139. doi: 10.5670/oceanog.2007.58

Browning, C., Shneider, M. M., Bowman, V. D., Schwarzer, D., and Leiman, P. G. (2012). Phage pierces the host cell membrane with the iron-loaded spike. *Structure* 20, 326–339. doi: 10.1016/j.str.2011.12.009

Bruland, K. W., Donat, J. R., and Hutchins, D. A. (1991). Interactive influences of bioactive trace-metals on biological production in oceanic waters. *Limnol. Oceanogr.* 36, 1555–1577. doi: 10.4319/lo.1991.36.8.1555

Brum, J. R., Schenck, R. O., and Sullivan, M. B. (2013). Global morphological analysis of marine viruses shows minimal regional variation and dominance of non-tailed viruses. *ISME J.* 7, 1738–1751. doi: 10.1038/ismej.2013.67

Buck, K. N., Sohst, B., and Sedwick, P. N. (2015). The organic complexation of dissolved iron along the US GEOTRACES (GA03) North Atlantic Section. *Deep-Sea Res. Part II-Top. Stud. Oceanogr.* 116, 152–165. doi: 10.1016/j.dsr2.2014.11.016

Butler, A. (2005). Marine siderophores and microbial iron mobilization. *Biometals* 18, 369–374. doi: 10.1007/s10534-005-3711-0

Byrne, R. H., and Breland, J. A. (1989). High- precision multiwavelength pH determinations in seawater using cresol red. *Deep-Sea Res. Part A-Oceanogr. Res. Pap.* 36, 803–810. doi: 10.1016/0198-0149(89)90152-0

Chuprov-Netochin, R. N., Faizullina, N. M., Sykilinda, N. N., Simakova, M. N., Mesyanzhinov, V. V., and Miroshnikov, K. A. (2010). The beta-helical domain of bacteriophage T4 controls the folding of the fragment of long tail fibers in a chimeric protein. *Russ. J. Bioorganic Chem.* 36, 172–178. doi: 10.1134/S1068162010020056

Cornelis, P. (2010). Iron uptake and metabolism in pseudomonads. *Appl. Microbiol. Biotechnol.* 86, 1637–1645. doi: 10.1007/s00253-010-2550-2

Cullen, J. T., Bergquist, B. A., and Moffett, J. W. (2006). Thermodynamic characterization of the partitioning of iron between soluble and colloidal species in the Atlantic Ocean. *Mar. Chem.* 98, 295–303. doi: 10.1016/j.marchem.2005.10.007

Daughney, C. J., Chatellier, X., Chan, A., Kenward, P., Fortin, D., Suttle, C. A., et al. (2004). Adsorption and precipitation of iron from seawater on a marine bacteriophage (PWH3A-P1). *Mar. Chem.* 91, 101–115. doi: 10.1016/j.marchem.2004.06.003

Demogines, A., Abraham, J., Choe, H., Farzan, M., and Sawyer, S. L. (2013). Dual host-virus arms races shape an essential housekeeping protein. *PLoS Biol.* 11:e1001571. doi: 10.1371/journal.pbio.1001571

Drakesmith, H., and Prentice, A. M. (2012). Hepcidin and the iron-infection axis. *Science* 338, 768–772. doi: 10.1126/science.1224577

Ducklow, H. (2000). "Bacterial production and biomass in the oceans," in *Microbial Ecology of the Oceans,* ed D. L. Kirchman (New York, NY: Wiley-Liss Inc.), 85–120.

Emerson, D. (2016). The irony of iron - biogenic iron oxides as an iron source to the ocean. *Front. Microbiol.* 6:1502. doi: 10.3389/fmicb.2015.01502

Finn, R. D., Bateman, A., Clements, J., Coggill, P., Eberhardt, R. Y., Eddy, S. R., et al. (2014). Pfam: the protein families database. *Nucleic Acids Res.* 42, D222–D230. doi: 10.1093/nar/gkt1223

Fishwick, M. P., Sedwick, P. N., Lohan, M. C., Worsfold, P. J., Buck, K. N., Church, T. M., et al. (2014). The impact of changing surface ocean conditions on the dissolution of aerosol iron. *Global Biogeochem. Cycles* 28, 1235–1250. doi: 10.1002/2014GB004921

Fitzsimmons, J. N., and Boyle, E. A. (2014). Both soluble and colloidal iron phases control dissolved iron variability in the tropical North Atlantic Ocean. *Geochim. Cosmochim. Acta* 125, 539–550. doi: 10.1016/j.gca.2013.10.032

Fitzsimmons, J. N., Bundy, R. M., Al-Subiai, S. N., Barbeau, K. A., and Boyle, E. A. (2015). The composition of dissolved iron in the dusty surface ocean: an exploration using size-fractionated iron-binding ligands. *Mar. Chem.* 173, 125–135. doi: 10.1016/j.marchem.2014.09.002

Fuhrman, J. (1999). Marine viruses: biogeochemical and ecological effects. *Nature* 399, 541–548. doi: 10.1038/21119

Gauglitz, J. M., Inishi, A., Ito, Y., and Butler, A. (2014). Microbial tailoring of acyl peptidic siderophores. *Biochemistry* 53, 2624–2631. doi: 10.1021/bi500266x

Gerringa, L. J. A., Rijkenberg, M. J. A., Schoemann, V., Laan, P., and de Baar, H. J. W. (2015). Organic complexation of iron in the West Atlantic Ocean. *Mar. Chem.* 177, 434–446. doi: 10.1016/j.marchem.2015.04.007

Gledhill, M., and Buck, K. N. (2012). The organic complexation of iron in the marine environment: a review. *Front. Microbiol.* 3:69. doi: 10.3389/fmicb.2012.00069

Gledhill, M., and van den Berg, C. M. G. (1994). Determination of complexation of iron (III) with natural organic complexing ligands in seawater using cathodic stripping voltammetry. *Mar. Chem.* 47, 41–54. doi: 10.1016/0304-4203(94)90012-4

Gobler, C. J., Hutchins, D. A., Fisher, N. S., Cosper, E. M., and Saňudo-Wilhelmy, S. A. (1997). Release and bioavailability of C, N, P Se, and Fe following viral lysis of a marine chrysophyte. *Limnol. Oceanogr.* 42, 1492–1504. doi: 10.4319/lo.1997.42.7.1492

Gordon, R. M., Martin, J. H., and Knauer, G. A. (1982). Iron in Northeast Pacific waters. *Nature* 299, 611–612. doi: 10.1038/299611a0

Hantke, K., and Braun, V. (1975). Membrane receptor dependent iron transport in *Escherichia coli*. *FEBS Lett.* 49, 301–305. doi: 10.1016/0014-5793(75)80771-X

Hantke, K., and Braun, V. (1978). Functional interaction of TonA-TonB receptor system in *Escherichia-coli*. *J. Bacteriol.* 135, 190–197.

Hassler, C. S., Alasonati, E., Nichols, C. A. M., and Slaveykova, V. I. (2011). Exopolysaccharides produced by bacteria isolated from the pelagic Southern Ocean - role in Fe binding, chemical reactivity, and bioavailability. *Mar. Chem.* 123, 88–98. doi: 10.1016/j.marchem.2010.10.003

Hershey, A. D., and Chase, M. (1952). Independent functions of viral protein and nucleic acid in growth of bacteriophage. *J. Gen. Physiol.* 36, 39–56. doi: 10.1085/jgp.36.1.39

Hider, R. C., and Kong, X. (2010). Chemistry and biology of siderophores. *Nat. Prod. Rep.* 27, 637–657. doi: 10.1039/b906679a

Humphrey, W., Dalke, A., and Schulten, K. (1996). VMD: visual molecular dynamics. *J. Mol. Graphics* 14, 33–38. doi: 10.1016/0263-7855(96)00018-5

Hunter, K. A., and Boyd, P. W. (2007). Iron-binding ligands and their role in the ocean biogeochemistry of iron. *Environ. Chem.* 4, 221–232. doi: 10.1071/EN07012

Johnson, K. S., Gordon, R. M., and Coale, K. H. (1997). What controls dissolved iron concentrations in the world ocean? *Mar. Chem.* 57, 137–161.

Jover, L. F., Effler, T. C., Buchan, A., Wilhelm, S. W., and Weitz, J. S. (2014). The elemental composition of virus particles: implications for marine biogeochemical cycles. *Nat. Rev. Microbiol.* 12, 519–528. doi: 10.1038/nrmicro3289

Kadner, R. J., Heller, K., Coulton, J. W., and Braun, V. (1980). Genetic control of hydroxamate-mediated iron uptake in *Escherichia coli*. *J. Bacteriol.* 143, 256–264.

King, J. (1968). Assembly of tail of bacteriophage T4. *J. Mol. Biol.* 32, 231–262. doi: 10.1016/0022-2836(68)90007-7

Kuma, K., Nishioka, J., and Matsunaga, K. (1996). Controls on iron(III) hydroxide solubility in seawater: the influence of pH and natural organic chelators. *Limnol. Oceanogr.* 41, 396–407. doi: 10.4319/lo.1996.41.3.0396

Laglera, L. M., Battaglia, G., and van den Berg, C. M. G. (2007). Determination of humic substances in natural waters by cathodic stripping voltammetry of their complexes with iron. *Anal. Chim. Acta* 599, 58–66. doi: 10.1016/j.aca.2007.07.059

Laglera, L. M., Battaglia, G., and van den Berg, C. M. G. (2011). Effect of humic substances on the iron speciation in natural waters by CLE/CSV. *Mar. Chem.* 127, 134–143. doi: 10.1016/j.marchem.2011.09.003

Laglera, L. M., and van den Berg, C. M. G. (2009). Evidence for geochemical control of iron by humic substances in seawater. *Limnol. Oceanogr.* 54, 610–619. doi: 10.4319/lo.2009.54.2.0610

Leiman, P. G., Arisaka, F., van Raaij, M. J., Kostyuchenko, V. A., Aksyuk, A. A., Kanamaru, S., et al. (2010). Morphogenesis of the T4 tail and tail fibers. *Virol. J.* 7, 1–28. doi: 10.1186/1743-422X-7-355

Leiman, P. G., and Shneider, M. M. (2012). Contractile tail machines of bacteriophages. *Viral Mol. Mach.* 726, 93–114. doi: 10.1007/978-1-4614-0980-9_5

Luckey, M., Wayne, R., and Neilands, J. B. (1975). *In vitro* competition between ferrichrome and phage for outer membrane T5 receptor complex of *Escherichia coli*. *Biochem. Biophys. Res. Commun.* 64, 687–693. doi: 10.1016/0006-291X(75)90375-7

Lundrigan, M. D., Lancaster, J. H., and Earhart, C. F. (1983). UC-1, a new bacteriophage that uses the TonA polypeptide as its receptor. *J. Virol.* 45, 700–707.

Luria, S. E., and Delbruck, M. (1943). Mutations of bacteria from virus sensitivity to virus resistance. *Genetics* 28, 491–511.

Maldonado, M. T., and Price, N. M. (1999). Utilization of iron bound to strong organic ligands by plankton communities in the subarctic Pacific Ocean. *Deep-Sea Res. Part II-Top. Stud. Oceanogr.* 46, 2447–2473. doi: 10.1016/S0967-0645(99)00071-5

Mancuso Nichols, C. A., Garon, S., Bowman, J. P., Raguenes, G., and Guezennec, J. (2004). Production of exopolysaccharides by Antarctic marine bacterial isolates. *J. Appl. Microbiol.* 96, 1057–1066. doi: 10.1111/j.1365-2672.2004.02216.x

Martin, J. H., Gordon, R. M., Fitzwater, S., and Broenkow, W. W. (1989). VERTEX - Phytoplankton iron studies in the Gulf of Alaska. *Deep-Sea Res. Part A-Oceanogr. Res. Pap.* 36, 649–680. doi: 10.1016/0198-0149(89)90144-1

Martinez, J. S., Carter-Franklin, J. N., Mann, E. L., Martin, J. D., Haygood, M. G., and Butler, A. (2003). Structure and membrane affinity of a suite of amphiphilic siderophores produced by a marine bacterium. *Proc. Natl. Acad. Sci. U.S.A.* 100, 3754–3759. doi: 10.1073/pnas.0637444100

Matzanke, B. F., Bohnke, R., Mollmann, U., Reissbrodt, R., Schunemann, V., and Trautwein, A. X. (1997). Iron uptake and intracellular metal transfer in mycobacteria mediated by xenosiderophores. *Biometals* 10, 193–203. doi: 10.1023/A:1018351728081

Mawji, E., Gledhill, M., Milton, J. A., Tarran, G. A., Ussher, S., Thompson, A., et al. (2008). Hydroxamate siderophores: occurrence and importance in the Atlantic Ocean. *Environ. Sci. Technol.* 42, 8675–8680. doi: 10.1021/es801884r

Mawji, E., Schlitzer, R., Dodas, E. M., Abadie, C., Abouchami, W., Anderson, R. F., et al. (2015). The GEOTRACES intermediate data product 2014. *Mar. Chem.* 177, 1–8. doi: 10.1016/j.marchem.2015.04.005

May, P. M., Linder, P. W., and Williams, D. R. (1977). Computer simulation of metal-ion equilibria in biofluids: models for the low-molecular-weight complex distribution of calcium(II), magnesium(II), manganese(II), iron(III), copper(II), zinc(II), and lead(II) ions in human blood plasma. *J. Chem. Soc. Dalton Trans.* 6, 588–595. doi: 10.1039/dt9770000588

Mioni, C. E., Poorvin, L., and Wilhelm, S. W. (2005). Virus and siderophore-mediated transfer of available Fe between heterotrophic bacteria: characterization using an Fe-specific bioreporter. *Aquat. Microb. Ecol.* 41, 233–245. doi: 10.3354/ame041233

Morel, F. M. M., and Price, N. M. (2003). The biogeochemical cycles of trace metals in the oceans. *Science* 300, 944–947. doi: 10.1126/science.1083545

Neilands, J. B. (1957). Some aspects of microbial metabolism. *Bacteriol. Rev.* 21, 101–111.

Neilands, J. B. (1979). Ironic function of bacteriophage receptors. *Trends Biochem. Sci.* 4, 115–118. doi: 10.1016/0968-0004(79)90396-7

Nishioka, J., Takeda, S., Wong, C. S., and Johnson, W. K. (2001). Size-fractionated iron concentrations in the northeast Pacific Ocean: distribution of soluble and small colloidal iron. *Mar. Chem.* 74, 157–179. doi: 10.1016/S0304-4203(01)00013-5

Parada, V., Herndl, G. J., and Weinbauer, M. G. (2006). Viral burst size of heterotrophic prokaryotes in aquatic systems. *J. Mar. Biol. Assoc. U.K.* 86, 613–621. doi: 10.1017/S002531540601352X

Parsons, R. J., Breitbart, M., Lomas, M. W., and Carlson, C. A. (2012). Ocean time-series reveals recurring seasonal patterns of virioplankton dynamics in the northwestern Sargasso Sea. *ISME J.* 6, 273–284. doi: 10.1038/ismej.2011.101

Pawelek, P. D., Croteau, N., Ng-Thow-Hing, C., Khursigara, C. M., Moiseeva, N., Allaire, M., et al. (2006). Structure of TonB in complex with FhuA, *E. coli outer membrane receptor*. *Science* 312, 1399–1402. doi: 10.1126/science.1128057

Pettersen, E. F., Goddard, T. D., Huang, C. C., Couch, G. S., Greenblatt, D. M., Meng, E. C., et al. (2004). UCSF chimera–a visualization system for exploratory research and analysis. *J. Comput. Chem.* 25, 1605–1612. doi: 10.1002/jcc.20084

Poon, A. P. W., and Dhillon, T. S. (1987). The attachment sites of T5-host range temperate coliphages. *Virology* 158, 431–434. doi: 10.1016/0042-6822(87)90215-7

Poorvin, L., Rinta-Kanto, J., Hutchins, D., and Wilhelm, S. (2004). Viral release of iron and its bioavailability to marine plankton. *Limnol. Oceanogr.* 49, 1734–1741. doi: 10.4319/lo.2004.49.5.1734

Rabsch, W., Ma, L., Wiley, G., Najar, F. Z., Kaserer, W., Schuerch, D. W., et al. (2007). FepA- and TonB-dependent bacteriophage H8: receptor binding and genomic sequence. *J. Bacteriol.* 189, 5658–5674. doi: 10.1128/JB.00437-07

Raven, J. A., Evans, M. C. W., and Korb, R. E. (1999). The role of trace metals in photosynthetic electron transport in O_2-evolving organisms. *Photosyn. Res.* 60, 111–149. doi: 10.1023/A:1006282714942

Redfield, A. C. (1958). The biological control of chemical factors in the environment. *Am. Sci.* 46, 205–221.

Rohwer, F., Segall, A., Steward, G., Seguritan, V., Breitbart, M., Wolven, F., et al. (2000). The complete genomic sequence of the marine phage Roseophage SIO1 shares homology with nonmarine phages. *Limnol. Oceanogr.* 45, 408–418. doi: 10.4319/lo.2000.45.2.0408

Rohwer, F., and Segall, A. M. (2015). In retrospect: a century of phage lessons. *Nature* 528, 46–48. doi: 10.1038/528046a

Rohwer, F., and Thurber, R. V. (2009). Viruses manipulate the marine environment. *Nature* 459, 207–212. doi: 10.1038/nature08060

Rohwer, F., Youle, M., Maughan, H., and Hisakawa, N. (2014). *Life in Our Phage World: A Centennial Field Guide to the Earth's Most Diverse Inhabitants*. San Diego, CA: Wholon.

Rue, E., and Bruland, K. (2001). Domoic acid binds iron and copper: a possible role for the toxin produced by the marine diatom *Pseudo-nitzschia*. *Mar. Chem.* 76, 127–134. doi: 10.1016/S0304-4203(01)00053-6

Rue, E. L., and Bruland, K. W. (1995). Complexation of iron(III) by natural organic-ligands in the central north Pacific as determined by a new competitive ligand equilibration adsorptive cathodic stripping voltammetric method. *Mar. Chem.* 50, 117–138. doi: 10.1016/0304-4203(95)00031-L

Rue, E. L., and Bruland, K. W. (1997). The role of organic complexation on ambient iron chemistry in the equatorial Pacific Ocean and the response of a mesoscale iron addition experiment. *Limnol. Oceanogr.* 42, 901–910. doi: 10.4319/lo.1997.42.5.0901

Salmond, G. P. C., and Fineran, P. C. (2015). A century of the phage: past, present and future. *Nat. Rev. Microbiol.* 13, 777–786. doi: 10.1038/nrmicro3564

Samson, J. E., Magadan, A. H., Sabri, M., and Moineau, S. (2013). Revenge of the phages: defeating bacterial defences. *Nat. Rev. Microbiol.* 11, 675–687. doi: 10.1038/nrmicro3096

Sandy, M., and Butler, A. (2009). Microbial iron acquisition: marine and terrestrial siderophores. *Chem. Rev.* 109, 4580–4595. doi: 10.1021/cr9002787

Shaked, Y., and Lis, H. (2012). Disassembling iron availability to phytoplankton. *Front. Microbiol.* 3:123. doi: 10.3389/fmicb.2012.00123

Shire, D. M., and Kustka, A. B. (2015). Luxury uptake, iron storage and ferritin abundance in *Prochlorococcus marinus* (Synechococcales) strain MED4. *Phycologia* 54, 398–406. doi: 10.2216/14-109.1

Silva, J. B., Storms, Z., and Sauvageau, D. (2016). Host receptors for bacteriophage adsorption. *FEMS Microbiol. Lett.* 363:fnw002. doi: 10.1093/femsle/fnw002

Stern, A., and Sorek, R. (2011). The phage-host arms race: shaping the evolution of microbes. *Bioessays* 33, 43–51. doi: 10.1002/bies.201000071

Stolpe, B., and Hassellov, M. (2010). Nanofibrils and other colloidal biopolymers binding trace elements in coastal seawater: significance for variations in element size distributions. *Limnol. Oceanogr.* 55, 187–202. doi: 10.4319/lo.2010.55.1.0187

Sullivan, M. B., Coleman, M. L., Weigele, P., Rohwer, F., and Chisholm, S. W. (2005). Three *Prochlorococcus* cyanophage genomes: signature features and ecological interpretations. *PLoS Biol.* 3:e144. doi: 10.1371/journal.pbio.0030144

Suttle, C. A. (2007). Marine viruses - major players in the global ecosystem. *Nat. Rev. Microbiol.* 5, 801–812. doi: 10.1038/nrmicro1750

Tam, W., Pell, L. G., Bona, D., Tsai, A., Dai, X. X., Edwards, A. M., et al. (2013). Tail tip proteins related to bacteriophage lambda gpL coordinate an iron-sulfur cluster. *J. Mol. Biol.* 425, 2450–2462. doi: 10.1016/j.jmb.2013.03.032

Thomassen, E., Gielen, G., Schutz, M., Schoehn, G., Abrahams, J. P., Miller, S., et al. (2003). The structure of the receptor-binding domain of the bacteriophage T4 short tail fibre reveals a knitted trimeric metal-binding fold. *J. Mol. Biol.* 331, 361–373. doi: 10.1016/S0022-2836(03)00755-1

Thuroczy, C. E., Gerringa, L. J. A., Klunder, M. B., Middag, R., Laan, P., Timmermans, K. R., et al. (2010). Speciation of Fe in the Eastern North Atlantic Ocean. *Deep-Sea Res. Part I-Oceanogr. Res. Pap.* 57, 1444–1453. doi: 10.1016/j.dsr.2010.08.004

Tortell, P. D., Maldonado, M. T., Granger, J., and Price, N. M. (1999). Marine bacteria and biogeochemical cycling of iron in the oceans. *FEMS Microbiol. Ecol.* 29, 1–11. doi: 10.1111/j.1574-6941.1999.tb00593.x

Tortell, P. D., Maldonado, M. T., and Price, N. M. (1996). The role of heterotrophic bacteria in iron-limited ocean ecosystems. *Nature* 383, 330–332. doi: 10.1038/383330a0

Twining, B. S., and Baines, S. B. (2013). The trace metal composition of marine phytoplankton. *Annu. Rev. Mar. Sci.* 5, 191–215. doi: 10.1146/annurev-marine-121211-172322

van den Berg, C. M. G. (2005). Organic iron complexation is real, the theory is used incorrectly. *Comment on 'Measuring marine iron(III) complexes by CLE-AdSV'. Environ. Chem.* 2, 88–89. doi: 10.1071/EN05029

Van Valen, L. (1973). A new evolutionary law. *Evol. Theor.* 1, 1–30.

von der Heyden, B. P., Hauser, E. J., Mishra, B., Martinez, G. A., Bowie, A. R., Tyliszczak, T., et al. (2014). Ubiquitous presence of Fe(II) in aquatic colloids and its association with organic carbon. *Environ. Sci. Technol. Lett.* 1, 387–392. doi: 10.1021/ez500164v

Vraspir, J. M., and Butler, A. (2009). Chemistry of marine ligands and siderophores. *Annu. Rev. Mar. Sci.* 1, 43–63. doi: 10.1146/annurev.marine.010908.163712

Wayne, R., and Neilands, J. B. (1975). Evidence for common binding-sites for ferrichrome compounds and bacteriophage Phi-80 in cell-envelope of *Escherichia coli*. *J. Bacteriol.* 121, 497–503.

Wheeler, T. J., Clements, J., and Finn, R. D. (2014). Skylign. *BMC Bioinform.* 15:7. doi: 10.1186/1471-2105-15-7

Wilhelm, S. W., and Suttle, C. A. (1999). Viruses and nutrient cycles in the sea. *Bioscience* 49, 781–783. doi: 10.2307/1313569

Wilhelm, S. W., Weinbauer, M. G., Suttle, C. A., and Jeffrey, W. H. (1998). The role of sunlight in the removal and repair of viruses in the sea. *Limnol. Oceanogr.* 43, 586–592. doi: 10.4319/lo.1998.43.4.0586

Wommack, K. E., and Colwell, R. R. (2000). Virioplankton: viruses in aquatic ecosystems. *Microbiol. Mol. Biol. Rev.* 64, 69–114. doi: 10.1128/MMBR.64.1.69-114.2000

Wommack, K. E., Nasko, D. J., Chopyk, J., and Sakowski, E. G. (2015). Counts and sequences, observations that continue to change our understanding of viruses in nature. *J. Microbiol.* 53, 181–192. doi: 10.1007/s12275-015-5068-6

Yamashita, E., Nakagawa, A., Takahashi, J., Tsunoda, K.-I., Yamada, S., and Takeda, S. (2011). The host-binding domain of the P2 phage tail spike reveals a trimeric iron-binding structure. *Acta Crystallogr. Sect. F Struct. Biol. Cryst. Commun.* 67, 837–841. doi: 10.1107/s1744309111005999

Conflict of Interest Statement: The authors declare that the research was conducted in the absence of any commercial or financial relationships that could be construed as a potential conflict of interest.